Application of Advanced Load-Frequency Control on Battery Energy Storage System in Islanded Microgrid

A thesis submitted in partial fulfillment
for the degree of Doctor of Philosophy

Graduate School of Engineering and Science
SHIBAURA INSTITUTE OF TECHNOLOGY

by
Sandro Sitompul
NA18502

Application of Advanced Load-Frequency Control on Battery Energy Storage System in Islanded Microgrid

Sandro Sitompul

Doctor of Philosophy

Graduate School of Engineering and Science
SHIBAURA INSTITUTE OF TECHNOLOGY

2021

Abstract

There are numerous remote islands globally, and among them, in small-scale systems independent from large-scale systems, electric power is supplied mainly by distributed energy resources (DER) or diesel generators using fossil fuel. In recent years, however, Renewable Energy Sources (RES) such as photovoltaics (PV) and wind turbines (WT) have been introduced due to problems such as global warming and depletion of fossil fuels. On the other hand, since the generated electric power of RES depends on the weather, the output wildly fluctuates in a short period, and it is feared that it causes lowering of electric power quality and solution row of generators. Moreover, a small independent system is easily affected by output fluctuation and load fluctuation of RES because of the small system capacity. A method to compensate for these fluctuations by installing a Battery Energy Storage (BES) system is proposed.

BES participation is made possible by utilizing load-frequency control (LFC). However, the traditional LFC has no frequency limitation, so it is still possible that the battery participation does not put the frequency in the allowed area. By using advanced LFC, the system frequency can be maintained in the desired range. It is possible because the proposed control uses three control areas, namely Region 1, Region 2, and Region 3.

Active participation makes the battery SoC more volatile. These fluctuations should be avoided as they can shorten the life of the battery. SoC control was introduced to solve this problem. This control adopts a droop reference shift based on the SoC level up to the LFC. Hence, BES can participate in the chili system while maintaining the SoC level of the battery. These controls are examples of advanced applications of advanced LFC.

In this thesis, a discussion of battery economics is also discussed. Advanced LFC has proven influence in BES (technical) operations. However, the applicability of this control can be seen if the proposed control influences the size and investment costs of the BES. In this study, the use of advanced LFC is proven to have a better impact than traditional LFC, both in terms of cost and system performance over frequency. However, the investigation shows that this control could not apply to all types of batteries. This study case confirms that this control is suitable only for high capacity batteries, which can operate until the end of the project lifetime.

Acknowledgments

Table of Contents

List of Tables

List of Figures

List of Abbreviations

Abbreviations are sorted according to the first appearance of the text. Some are also defined in the text. However, for a comprehensive definition, please refer to this section

AC	Alternating current
BES	Battery energy storage
CH_4	Methane
CO_2	Carbone dioxide
COP21	Conference of Parties 21
DC	Direct current
DER	Distributed energy sources
DoD	Depth of discharge
EDGAR	Emission Database for Global Atmospheric Research
ESS	Energy storage system
GHG	Greenhouse Gasses
HES	Hybrid electric systems
HFCs	High-fructose corn syrup
IEEE	Institute of Electrical and Electronics Engineers
INDC	Intended nationally determined contributions
IPCC	Intergovernmental Panel on Climate Change

LCS	Lower critical state
LFC	Load-frequency control
Li-ion	Lithium-ion
LL	Lower limit
LP	Linear programming
MIP	Mixed-integer programming
N_2O	Nitrous oxide
NaS	Sodium-sulfur
NDC	Nationally determined contributions
NiCd	Nickel-cadmium
NiMH	Nickel-metal-hydride
PCS	Power conditioning system
PFCs	Perfluorochemicals
PI	Proportional-integrator
PnP	Plug-and-play
PS	Power-sharing
PSO	Particle swarm optimization
PV	Photovoltaic
RES	Renewable energy source
RMS	Root mean square
SF_6	Sulfur hexafluoride
SoC	State-of-charge
UCS	Upper critical state

UL   Upper limit

UNFCCC   UN Conference on Environment and Development published the
          United Framework Convention on Climate Change

US   United States of America

VOLL   Value of lost load

VRB   Vanadium redox-flow battery

VSG   Virtual synchronous generator

WT   Wind turbine

List of Symbols

Symbol's definitions are sorted according to the first appearance of the text. Some symbols are also defined in the text. However, for a comprehensive definition, please refer to this section

Chapter 2

α	Phase difference
c, c_s	Capacitance
c_1, c_0	Positive and zero sequences capacitance
c_g	Ground capacitance
E	Sending-end voltage
f^0	Frequency reference
f^1	Frequency actual
f_{dh}	Grid frequency
f^{max}, f^{min}	LFC maximum and minimum frequency
f^{pu}	Nominal frequency
I^{rms}	Root mean square current
K	Diesel regulator gain
K_b	BES droop gain
K_{DER}	DER droop gain
K_{DER}^{pu}	DER droop gain in pu

K_P, K_i	Proportional and integral gain
l, l_s	Inductive
l_1, l_0	Positive and zero sequences capacitance
P	Active power
P_b'	BES power after in saturated frequency region
P_b^0	BES droop active power reference
P_{bdh}	BES power at each interval
P_g^0	Generator droop active power reference
P_g'	Generator output power after in saturated frequency region
P_{gidh}	Generator output power
P^{pu}	Nominal active power
r, r_s	resistance
R	Generator droop gain
Q	Reactive power
t	Time
T_d	Engine time delay
T_{min}, T_{max}	Maximum and minimum torque
T_1, T_2, T_3	Regulator time constant
T_4, T_5, T_6	Actuator time constant
V	Receiving-end voltage
V^{rms}	Root mean square voltage
X	Line reactance
x_L	Capacitive reactance

x_L	Inductive reactance
Δf	Frequency change
Δf^s	Deadband frequency area
ΔP	Active power change
θ	Phase angle
ω_{ref}	Angle speed reference

Chapter 3

E_b	BES energy capacity
f^{crmax}, f^{crmin}	Maximum and minimum shifted frequency
K_C	Portion that can be charged/discharged
P_b	BES power at each interval
K_{Psoc}, K_{isoc}	Proportional and integral gain for SoC control
$SoC^{initial}$	SoC initial state
SoC^{max1}, SoC^{max2}	First and second SoC upper bound
SoC^{min1}, SoC^{min2}	First and second SoC lower bound
SoC	State-of-charge
Δf^n	Frequency shift
η	BES efficiency

Chapter 4

d	Index for day.
h	Index for hour
i	Index for distributed generators
G	Set of generators
W	Set of renewable energy sources
a, b, c	Generator fuel cost coefficient
CE, CP	BES annualized energy and power capital cost
CM	BES annual operating and maintenance cost
CI	BES annualized installation cost
e	BES lifecycle
P_{Ldh}	Total load demand at day d, hour h
P_{ridh}	RES output power
Q	Fuel cost
V	Value of lost load
RD_i, RU_i	Ramp down and ramp-up rates
$\alpha_i^{max}, \alpha_i^{min}$	Maximum and minimum BES energy rating to power rating ratio
β	Maximum BES depth of discharge
η^{dch}, η^{ch}	BES discharge and charge efficiency
E_b^R, P_b^R	BES rated energy and rated power
E_{bdh}	Stored energy in BES at each interval
LL_{dh}	Lost load at each interval
$P_{bdh}^{dch}, P_{bdh}^{ch}$	BES discharge and charge power at each interval

Y	Fuel consumption function
u_{idh}	BES operating state
ζ_{idh}	BES cycle indicator
$\rho^{\max}, \rho^{\min}$	Generator power at LFC maximum and minimum frequency

Chapter 5

Chapter 1

1 Introduction

1.1 Research Background

1.1.1 Environmental Issues

Svante Arrhenius (1859 - 1927), a Swedish scientist, 1896 stated that burning fossil fuels might result in global warming. He explained his claim by introducing the relationship between atmospheric carbon dioxide concentration (CO_2) and temperature. Arrhenius found that the Earth's average surface temperature is around 15°C because of water vapor and CO_2 infrared absorption ability. He called this the greenhouse effect. Arrhenius suggests that doubling the concentration of CO_2 can trigger a temperature rise of 5°C [1].

For years, from Arrhenius's claims to the present day, humanity has been grappling with Greenhouse Gases' issue (GHG). The increasing temperature of the
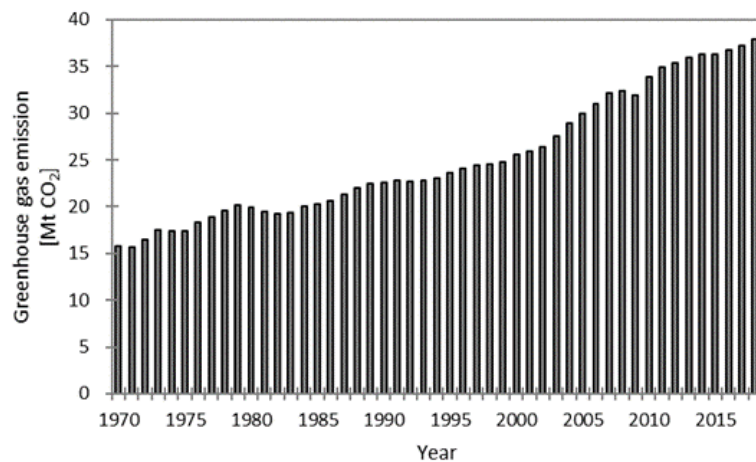
Figure 1.1 Total CO_2 emission in global [2]

Earth's surface, water availability changes, the number of species becoming extinct, rising sea levels are the consequences of this issue.

The world is now really trying to solve this problem to be prevented due to consequences caused by GHG. This concern is also supported by data compiled by the Emission Database for Global Atmospheric Research (EDGAR) that the world's total GHG has more than doubled in the last four decades since the data was available, which is shown in Figure 1.1. The latest data states that the three big countries contributing to GHG emissions are China, the United States, and the European Union [2].

If traced back to its history, this issue began to get international attention 30 years ago, starting with the US Academy of Sciences report on climate in 1983. Then continuing in the same year, the United Nations established the World Commission on Environment and Development, which in 1987 issued a report entitled "Our Common Future." This report has prompted increasing international attention to the issue of GHG. It has led to many conferences being held to discuss this issue. In 1988, it was discovered that world temperatures were warmer than at any time since 1880. The greenhouse gas effect theory emerged and established the Intergovernmental Panel on Climate Change (IPCC) by the United Nations Environmental Program and the World Meteorological Organization. The organization seeks to predict the greenhouse effect's impact based on available climate models and literary information. Since 1990, to continue monitoring CO_2 emission figures, IPCC has issued a climate change report every five years [3], [4].

Several attempts to reduce GHG emissions have been made. In Brazil, 1992, UN Conference on Environment and Development published the United Framework Convention on Climate Change (UNFCCC) with the primary objective to prevent further climate change to a dangerous state. Developed countries agreed in Kyoto Protocol to reduce their emission of GHGs (CO_2, CH_4, N_2O, HFCs, PFCs, and SF_6) by an average of 5.2% by 2008-2012 compared with the 1990 levels. In December 2015,

the Conference of Parties 21 (COP21) declared the Paris Agreement, increasing the global average temperature to below 2 degrees Celsius. All parties are invited to initiated domestic preparations by submitting their own intended nationally determined contributions (INDC) to the committee in COP21. These INDCs are considered as nationally determined contributions (NDC) after the Paris Agreement is concluded. In Japan, the INDC is a GHG emission reduction of 26.0% by fiscal year (FY) 2030. Until today, this issue forces the world to establish policies based on the environment. UN targets that global emissions must be cut by 45% by 2030 to limit the global temperature rise to an average of 1.5 degrees Celsius above pre-industrial levels [3]–[5].

Several efforts have been made to reduce CO_2 emissions, such as increasing non-carbon energy sources that are more environmentally friendly. Electricity generation still depends on carbon energy sources such as coal, oil, and natural gas. Here are some attempts to be made to achieve these targets. One of the efforts that has been made is to promote implementation of renewable energy resources (RESs).

RESs are resources that utilize natural power. Some examples of RES that are widely known in the social community are photovoltaic (PV), wind turbine (WT), ocean, hydro, biomass, geothermal, etc. Each energy source has different characteristics and operations. Moreover, the extent of the required location is a determinant of implementing technology. They cause the number of installations for each type of RES to be different.

In implementing RES, a technical potential becomes a benchmark for considering a technology. Generally, the technical potential concludes how much each technology can generate the gross output of electricity. Various energy researchers have completed their research on technical potential. It is concluded that solar PV has
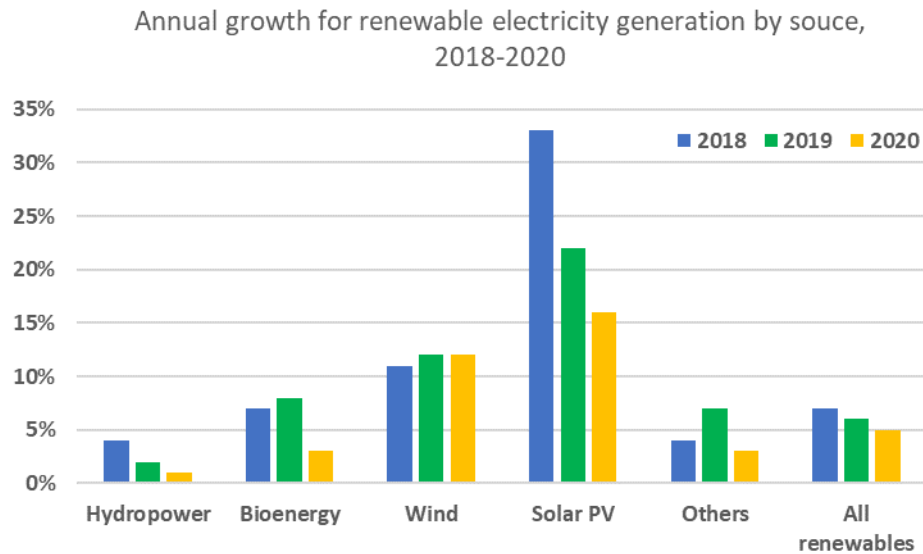
Figure 1.2 Annual growth for renewable energy sources, 2018-2020 [7]

a higher technical potential than other technologies. The reason is that PV materials are getting cheaper and more research is being carried out related to PV development [6].

The International Energy Agency (IEA) in April 2020 reported the annual growth for RES generation during the period 2018-2020, as shown by Figure 1.2. The report stated that solar PV has the fastest increase compared to all renewable energy sources in 2020. Due to a large number of PV panel installations, small-to-medium-sized enterprises on their roofs or business sites and increasing PV penetration for power systems in many locations. The report suggests that solar PV is still the most popular RES technology among all technologies and provides research opportunities [7].

1.1.2 Islanded Microgrid

Environmental issues have brought various changes to all sectors, including the energy sector, especially power systems. Nowadays, power systems are significantly changed both horizontally and vertically. Various techniques were developed to reduce

GHG emissions. However, the system's changes are not limited to reducing emissions and improving system reliability and power quality [8].

One of those changes is the widespread use of distributed energy sources (DERs). The use of DERs is increasingly widespread due to the ability to create hybrid electric systems (HES) supporting the creation of clean and economically affordable energy [9]. HES consist of several DERs, consumer, and energy storage units. An accretion of DERs forms a microgrid and supply to a regional area. Such systems are often called microgrids.

A microgrid is "a system that has clearly defined boundaries that consist of interconnected loads and distributed energy resources (DERs); acts as a single controllable entity concerning the grid; can operate independently and dependent from the utility grid [10]." According to this definition, DER installations could be considered as microgrid if comprised of three distinct characteristics: they must have electrical boundaries that are clearly defined, there must exist a master controller to control and operate DERs and loads as a single controllable entity, and the installed generation capacity must exceed the peak critical load thus it could be disconnected from the utility grid, i.e., the islanded mode, and seamlessly supply local critical loads.

Many benefits can be felt with the microgrid. These advantages include increased system reliability, reduced carbon gas emissions, economical operation due to reduced transmission and distribution costs, improved power quality due to load management. The microgrid distribution network can be classified as DC type and AC type microgrids. As most DERs generate DC power and the DC distribution has no power quality problems, research on the DC microgrid system is critical. However, most of the loads are operated in AC systems. Hence, the DC microgrid system may not be popular. On the other hand, microgrids are generally utilized in AC [8]–[10].
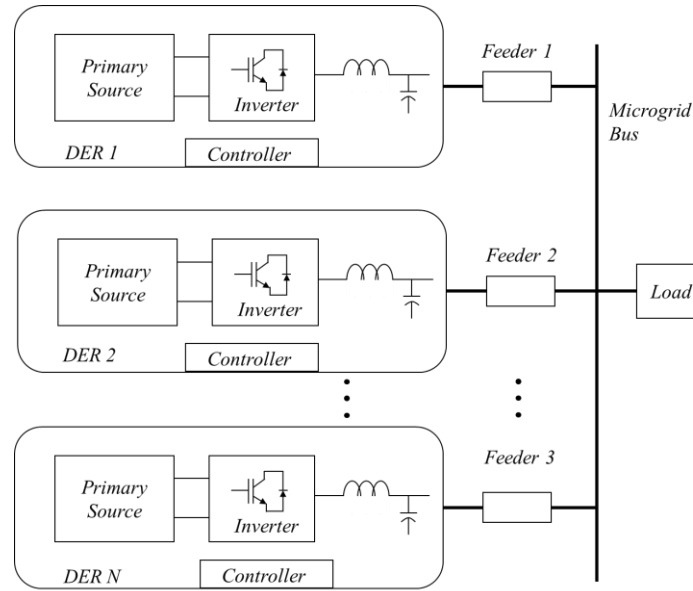
Figure 1.3 Example of islanded microgrid [11]

Microgrids' primary objective in islanded mode is to allow the system to operate even in adverse scenarios, such as faults in the primary grid, high prices of main grid's power, and supplying remote areas. Figure 1.3 is one of the islanded microgrid examples [11]. High priority loads, such as hospitals, transportation, and telecommunication facilities, must have their supply assured in an islanding case. This case is possible due to DERs penetration, including renewable, fossil, combined heat and power, and energy storage units. However, microgrids' operation in islanded mode requires more attention due to the higher outage risk since the power generation capacity is limited.

1.1.3 Microgrid Stability

Compared with the traditional grid's stability, the dynamic process of microgrid conventional grid stability, microgrid stability's dynamic approach is more complicated. An islanded microgrid system has small system inertia because it depends on installed DERs such as photovoltaic (PV), wind turbine (WT), fuel cells, microturbine. The

intermittent nature of the RESs on the system has a significant impact on microgrid operation. So the plan depends on the system's inertia for its stability [10]–[12].

Instability in the system occurs due to several factors. For microgrids, the prominent instability occurs due to variations in the load and energy source. The load on the microgrid tends to fluctuate. It is because, in the microgrid system, most types of loads are residential and office loads. Hence, any changes in the load on the microgrid are felt by the system. Likewise, most of the energy sources installed on the microgrid are renewable energy sources (RESs) for microgrid energy sources. The instability often occurs due to the intermittent character of the RESs. These characteristics have a significant impact on microgrid operation [13], [14].

When the microgrid is operated grid-connected, stability is maintained by the utility grid. The utility grid maintains the output voltage and frequency of a microgrid. Nevertheless, this is different from the islanded operation. According to the microgrid operating characteristics, the islanded microgrid stability mainly depends on the microgrid structure, the capacity of stored-energy DERs, the control strategy of DERs. The response speeds of primary energy sources like PV, wind power, micro gas turbines are slow. Still, the interfaced inverter adjusts the output power, and they are usually used along with stored-energy DERs. The stored-energy DERs have a significant effect on the stability when load fluctuation occurs. The dynamic process of stored-energy DERs is not similar to synchronous generators machinery rotating process, which involves rotor angle problems [15]–[17].

For islanded microgrids, the generation and system load should be maintained by themselves. Thus, islanded microgrid's transient behaviors to significant disturbance are much sensitive to the grid-connected microgrid. Many researchers have claimed that the influence of load fluctuation is more significant for islanded mode. System stability problems, such as frequency and voltage stability, are often encountered when variation in the system operation occurs. Frequency stability problems arise on islanded

microgrid systems when power imbalances arise. The system requires the availability of fast frequency response to resolve the stability problem [10], [18]–[20]; the system inability to perform the response could increase severe issues in operation and control of the islanded microgrid.

Several frequency stability issues related to islanded microgrid systems have been discussed. The reduction in inertia increases the system's frequency oscillations, as discussed in [15], [21]–[27]. A frequency control strategy based on dynamically high-power machines to reduce the load is proposed [15], [27]. The author in [23] discusses a virtual synchronous generator (VSG) control strategy by utilizing a self-adaptive damping control strategy. A decentralized control synthesis procedure for stabilizing the frequency that enables plug-and-play (PnP) operations is introduced [11]. The frequency-reactive control is proposed in [25], [28], [29]. Several studies have also started using an energy storage system (ESS) to solve frequency stability in the islanded microgrid system.

1.2   Battery Energy Storage System

Microgrid with ESS has become a promising component for future smart grid deployment. However, due to the intermittent characteristics of RESs and fluctuating load profiles, the power supply in the microgrid fails to mitigate the load demand and causes the frequency fluctuation. Efficient ESS management, power electronic interfaces, charging and discharging, conversion mechanism of power, reliability, and protection are the major issues for developing the ESS in microgrid applications.

One of the most widely used ESSs in microgrid systems is the battery. However, the battery does not stand up but has several supporting components to make it compatible with a microgrid called the battery energy storage (BES) system. BES system comprises mainly batteries, control, and power conditioning system (PCS) that
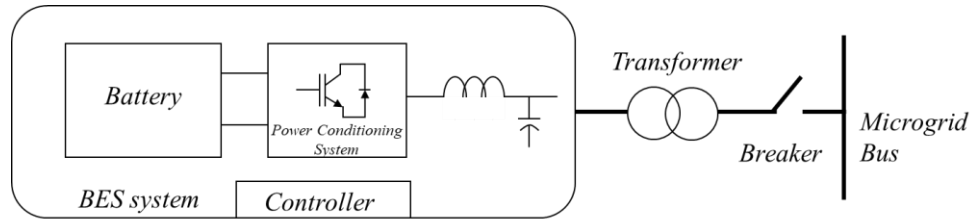
Figure 1.4 Battery energy storage system structure

shown in Figure 1.4. The battery and PCS are the major BES components, and each of these technologies is rapidly developing [30], [31].

The battery is made of an arrangement of cells that can generate electrical energy from chemical reactions and vice versa. The value of the battery voltage and current is obtained by arranging the cells in series and parallel. Regarding capacity, battery capacity is assessed based on its energy and power rating. For some types of batteries, energy capacity and power are independent of each other. In its application, several things must be considered in battery operation, such as efficiency, life span, operating temperature, depth of discharge, and self-discharge. Depth of discharge (DoD) refers to the extent to which they are discharged [30]–[32].

1.2.1 Battery Energy Storage Technology

Electrical energy must be used as soon as possible after being generated. Along with developing RESs, energy storage is designed as one of the intermittent energy countermeasures. The utilization of batteries in power system applications are deep cycle batteries with energy capacity ranging from 17 to 40 MWh and having efficiencies around 70 - 80%. Batteries currently in development include lead-acid, nickel-metal-hydride (NiMH), nickel-cadmium (NiCd) battery, lithium-ion (Li-ion), sodium-sulfur (NaS), and vanadium redox-flow batteries (VRBs). Each type of battery has different characteristics. Besides the price difference, each battery technology can be implemented into a power system due to its unique features and characteristics.
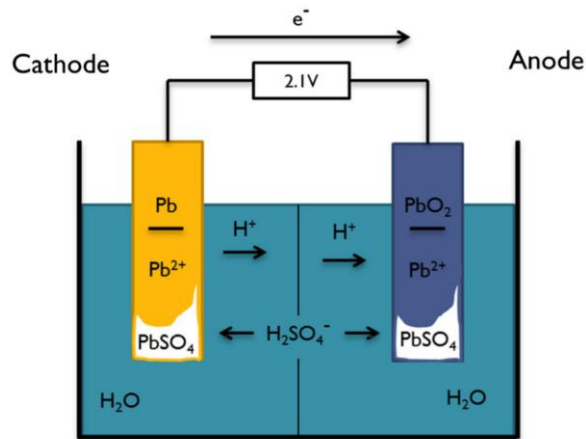
Figure 1.5 Schematic illustration of the lead-acid battery [33]

1. **Lead-acid battery**: A storage battery that uses lead dioxide for the positive electrode, lead for the negative electrode, and dilute sulfuric acid for the electrolytic solution. It is resistant to overcharging, has high output, and operates in a wide temperature range (5 °C to 50 °C) at room temperature. Another feature is that the price is relatively low, there is a wealth of experience in adoption, and a domestic recycling system has been established. On the other hand, when the state-of-charge (SOC) is placed in a low state, the deterioration of the electrodes progresses, and the capacity and input/output decrease, and the charge/discharge energy efficiency is lower than that of other batteries, staying at about 75% to 85%. The problem is that periodic SOC resets using commercial power must even out the voltage variations in the power storage system. Figure 1.5 shows the illustration of a lead-acid battery [33].

2. **NiMH/NiCd battery:** NiCd batteries have been the second type of rechargeable batteries introduced, being invented by the Swedish engineer Waldemar Jungner in 1899. The storage device uses a negative cadmium electrode, a nickel oxide-hydroxide positive electrode, a separator, and an electrolyte (usually potassium hydroxide). Given that NiCd batteries have a
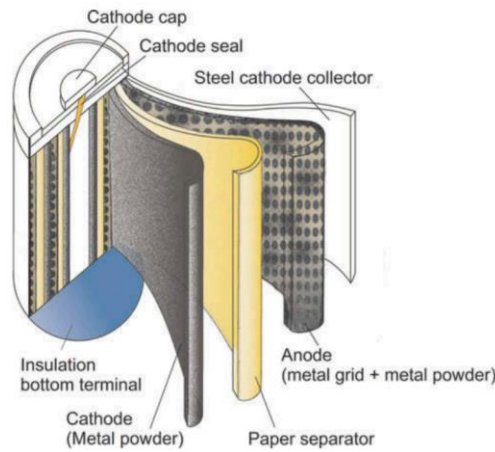
Figure 1.6 Illustration of NiMH battery [34]

lower energy density for applications varying from 1 kW to 0.5 MW and present some environmental hazards that require complex recycling procedures, NiMH batteries have replaced them. NiMH battery consists of a nickel-oxyhydroxide-based positive electrode, a metallic cadmium-based negative electrode, and an alkaline electrolyte (usually potassium hydroxide). This type of battery has higher power/energy density, realizes better environmental friendliness, and is less prone to undergo memory effect than NiCd battery. Nevertheless, it has several technical drawbacks, such as high self-discharge rate, limited cycle life, and low Coulombic efficiency (around 65%). Besides, it has a low ability to tolerate fast charging and overcharge. During fast charging, a massive amount of heat may be generated, and hydrogen buildup may cause cell rupture, leading to considerable capacity decay. Figure 1.6 shows the illustration of the NiMH battery [34].

3. **Li-ion battery:** Li-ion battery is a storage battery that uses a lithium-containing metal oxide (lithium cobalt oxide, in recent years, lithium nickel oxide, lithium manganate, and lithium iron olivine) as the positive electrode material, a carbon-based material as the negative electrode material, and an organic
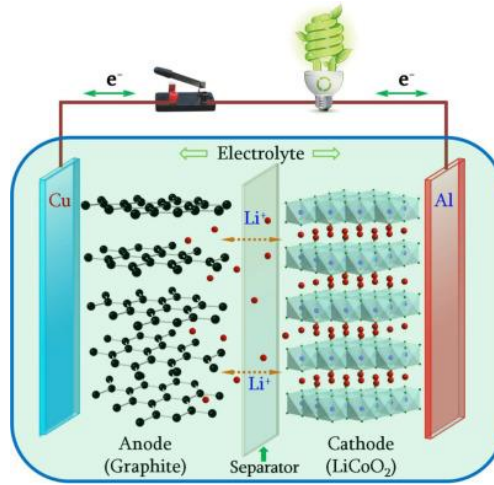
Figure 1.7 Illustration of Li-ion battery [35]

electrolyte as the electrolyte. It is characterized by high energy density and charge/discharge efficiency, small self-discharge, long life because it does not involve metal precipitation on the electrodes, and high-speed charge/discharge. On the other hand, since the organic electrolyte is used and there is a risk of ignition, safety measures have been taken. The disadvantages of the Li-ion battery are its cycle depth of discharge (DoD) and high cost. However, the cost of Li-ion cell is expected to decrease with large-scale production. Figure 1.7 shows the illustration of the Li-ion battery [35].

4. **NaS battery:** Sulfur is used for the positive electrode, sodium is used for the negative electrode, and solid electrolyte beta-alumina ceramics is used as the electrolyte. Since the sodium ion conduction of the solid electrolyte beta-alumina ceramics is used, heating must keep the operating temperature at about 300°C. It has a high energy density, can increase capacity, save space, and reduce costs through mass production because it does not use rare earth, has no self-discharge, has a wide SoC range to be used, and has high charge/discharge energy efficiency. Its high point also characterizes it. On the other hand, since the battery operates at a high temperature, a heater is heated at the start of
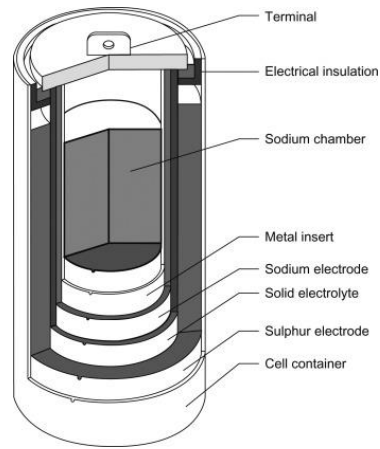
Figure 1.8 Illustration of NaS battery [36]

operation. Due to the use of flammable materials, care must be taken in handling and controlling heat dissipation. A potential device to implement in microgrid shows high efficiency, a long cycle of up to 15 years, and fast response (in milliseconds) during full charging and discharging operation. Figure 1.8 shows the illustration NaS battery [36].

5. **Redox Flow battery:** Flow technology has been first proposed in the 1970s, but the vanadium redox solution was developed by the Australian chemist Maria Skyllas-Kazacos in the 1980s. It utilizes the reaction that causes
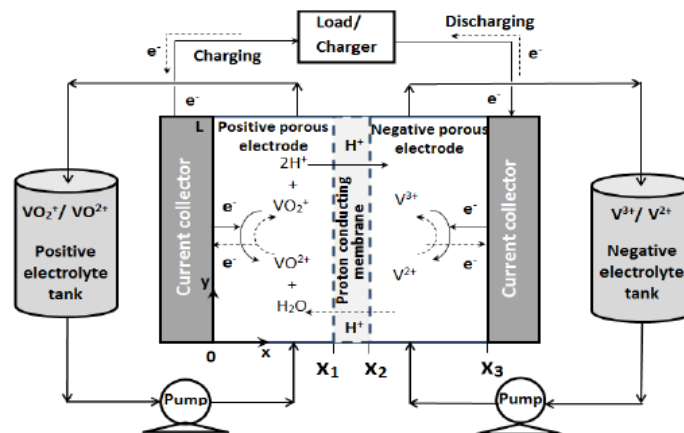
Figure 1.9 Illustration of VRB [37]

oxidation and reduces two types of redox-based active substances on the surface of the inert electrode. A redox flow battery consists of a distribution-type electrolytic cell that performs a battery reaction, a positive and negative electrode tank that stores a solution of active material (electrolytic solution), a pump for circulating the electrolytic solution from the tank to the cell, and piping. It has a long cycle life, is not affected by irregular charge/discharge operations, can be flexibly installed by separating the cell and tank, and can

(a)

(b)

(c)
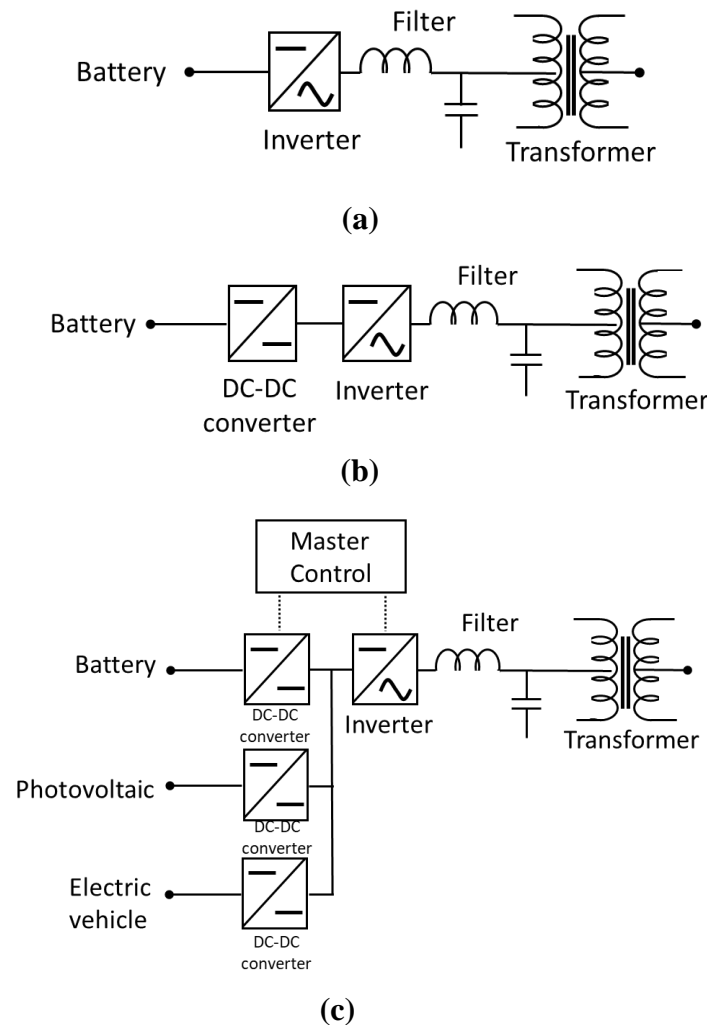
Figure 1.10 PCS Architecture; (a) Singe stage converter, (b) Multi-stage converter, (c) Multi-port, multi-stage converter [38]

easily monitor the SoC during operation. Also, since it has an instantaneous response to milliseconds, it can be used as a countermeasure against instantaneous power failure. On the other hand, the energy density is relatively low because the tank's volume is large. Another problem is that pump power is required to circulate the electrolyte, and current loss occurs through the electrolyte. Figure 1.9 shows the illustration of VRB [37].

1.2.2 Power Conditioning System (PCS)

Except for pumped hydro and compressed air, most energy storage devices employ a DC interface. Therefore, a PCS is required to integrate with the alternating current (AC) grid. The purpose of the PCS is to provide bi-directional conversion and electrical isolation. The PCS forms a vital part of the BES system. PCS consists of power electronic components, which are collected as power converters [38]. It interfaces the batteries to the loads (utility/end-user) and regulates the battery charge/discharge charging rate. The PCS cost is high, and it can be greater than 25% of the overall energy storage system. However, this technology is maturing rapidly due to the recent developments in renewable and distributed energy sources' power conditioning systems. The present research is being carried out to reduce the overall cost, improve reliability, and develop more efficient and better packaging of PCS [38].

There are several utilized power conversion architectures that are shown in Figure 1.10. One simple, single-stage converter has high efficiency. However, this architecture has the disadvantage that the DC voltage must be greater than 1.5 times the AC RMS voltage. This disadvantage results in constraints on the minimum battery string voltage. One that is quite popular to use is the multi-stage converter. This architecture goes from the storage device voltage to an intermediate DC voltage and then converts to AC. It provides more flexibility in the DC voltage range at the expense of increased conversion losses. The other type is a multi-port, multi-stage inverter. It enables energy storage to interface with other DC sources units sharing a common DC

bus. If the DC sources unit is connected on the common DC bus, this architecture is more efficient than coupling at the AC grid [38]–[40].

Generally, the BES system PCS is designed to use the BES to achieve many functions. To develop a multi-functional BES system, several investigators have suggested many control philosophies. Some of the studies design controls BES to improve the power system reliability and operation directly. Others are indirect applications (generally adding new features/providing more excellent capabilities to custom power devices).

Some of the development in designing the BES control can be mainly attributed to the rapid growth in power electronic devices. The BES control is designed for power system applications, especially islanded microgrid applications. However, most of the investigations neither attempt to quantify the benefits of the BES controls nor try to make any suggestions about the optimal size of BES for the present-day market-based systems. Although most of the investigators state that increasing BES capacity improves its capabilities and thereby power system performance, no suggestion has been made regarding choosing the optimal size/ capacity of BES.

1.2.3 Battery Energy Storage System Application

Battery energy storage system in microgrids is used to retain the power balance between the load demand and generation, ensuring frequency and grid voltage regulation. The selection of different battery energy storage units, each having distinguished characteristics in power and energy, depends on the nature of power required and delivered.

There are several BES applications in microgrids such as peak shaving, home energy management, load leveling, power fluctuations, transmission and distribution upgrade deferral, frequency regulation, low voltage ride through, and loss minimization. Peak shaving is the technique to reduce electricity consumption when the electricity

demand is at a peak, usually during the daytime in summers and the nighttime in winters. A battery energy storage is deployed in the houses to provide a power supply during power interruptions. The batteries are often used with an uninterruptable power supply (UPS) to protect the equipment during load leveling. It involves storing energy when the grid load is light and delivering back during high spikes of loads. Energy storage systems have effectively reduced fluctuations by shifting the load from the peak periods to off-peak periods. The electrical distribution system's radial structure has a large current to voltage ratio results in a high quantity of power losses in a distribution system [11], [38].

An efficient and optimum economic operation and electric power generation system planning have an essential position in the electric power industry. The classic problem is the economic dispatch of fossil-fired generation systems to achieve minimum cost. The increasing concern of environmental matters leads to the necessity of "economic dispatch" that includes minimizing pollutants and conserving various fuel forms. In the first instance, the power generation is centralized, and then the energy is transferred by using a transmission and distribution system to reach the customer.

Various control strategies for microgrids' economic operation are being developed recently, such as decentralized control, hierarchical optimization and control, predictive control, and intelligent control such as fuzzy logic and genetic algorithm. The control strategy's primary purpose is to achieve optimal operation strategy with minimum cost and balanced condition. The complexity of the control depends on several controlled variables and objectives.

1.3 Problem Statements

As discussed earlier, the islanded microgrid must be able to maintain its power quality. It is because no utility grid can meet all the deficiencies that occur in the system. Several attempts have been made to keep the islanded microgrid system's stability to

maintain system stability. One solution that is often used is the installation of BES on an islanded microgrid system. However, in the installation of BES, several issues are of concern in this study.

In this thesis, the BES operations problems in the islanded microgrid are divided into two main points. **The first problem is how to regulate the grid frequency when the BES is implemented into the systems.** The frequency regulation function is starting to increase because of the need for BES to help maintain system stability while reducing the impact of pollution generated by generators. Not only that, an advanced control that can amplify the BES function must be considered.

The second problem is how the proposed control affects BES optimization. BES installation is a solution that is often used to solve several issues on the islanded microgrid system. The frequency control function allows BES to contribute more to any changes to the system. This contribution has an impact on the advanced LFC effects against microgrid operation in economic view.

When discussing BES contribution to the system, the BES size is a factor that must be addressed in the study. It is because the size of the BES affects the investment costs that must be incurred. Of course, this cost also affects the operating costs of the microgrid. Installing the BES into the system causes changes in the operational costs of the microgrid. Among all energy storage devices, batteries have the highest equipment costs. When the battery's investment cost depends on the BES size, it is necessary to determine the BES's size accordingly. The sizing is done so that the investment cost of BES remains cheap but does not neglect the power quality system.

1.4 Study Contributions

Study contributions arranged by chapters are shown as follows:

- **Chapter 2: Advanced Load-Frequency Control in Battery Energy Storage**

This chapter proposes an advanced load-frequency control (LFC) in battery energy storage. The main contributions consist of the proposed frequency limitations in this control. The restrictions put the BES always to regulate its power. Hence the system frequency can be maintained at the prescribed range. It can happen because, in an islanded microgrid system, the frequency depends on the generator's output power. The main idea is to maintain the generator's power output by continuously regulating the battery output power, which results in supported frequency.

Journal:

1. S. Sitompul, Y. Hanawa, V. Bupphaves, and G. Fujita, "State of Charge Control Integrated with Load Frequency Control for BESS in Islanded Microgrid," *Energies*, vol. 13, no. 18, pp 4657, Sep. 2020**.**

International Conference:

1. S. Sitompul, G. Fujita, "Reducing Self-discharge Rates Effects of Flywheel Energy Storage System in Power System Application," *13th South East Asian Technical University Consortium (SEATUC),* Hanoi, Vietnam, February 2019.

- **Chapter 3: State-of-Charge Control on Advanced Load-Frequency Control**

In this chapter, a state-of-charge control is proposed. The control is integrated with the proposed LFC in chapter 2, contributing not only to the active power-frequency regulation but also to keep the SoC within the prescribed range. A shift-

droop control is offered for the proposed method. This method allows a change of BES output power according to the SoC status.

Journal:

1. S. Sitompul, Y. Hanawa, V. Bupphaves, and G. Fujita, "State of Charge Control Integrated with Load Frequency Control for BESS in Islanded Microgrid," *Energies*, vol. 13, no. 18, pp 4657, Sep. 2020**.**

International Conference:

1. S. Sitompul, G. Fujita, "Implementation of Shifted-Droop Method as State-of-Charge Control on Battery Energy Storage System Load-Frequency Control," *15th South East Asian Technical University Consortium (SEATUC)*, Bandung, Indonesia, February 2021.

2. S. Sitompul, G. Fujita, "Implementation of BESS Load-Frequency Control in Islanded Microgrid by Considering State-of-Charge," *IEEE PES Innovative Smart Grid Technology (ISGT) Europe,* The Haag, Netherlands, 2020.

3. S. Sitompul, G. Fujita, "Sizing of Battery Energy Storage System in Islanded Microgrid by Considering a Short-term operation," *14th South East Asian Technical University Consortium (SEATUC),* Bangkok, Thailand, February 2020.

- **Chapter 4: Optimal Battery Energy Storage Sizing with Advanced Load-Frequency Control**

This chapter presents a contribution of the proposed LFC to BES size. The proposed active power-frequency control can keep the generator output in a particular range. It causes the fuel used by the generator to be limited in that range. Thus, this

control indirectly impacts the generator operation and makes it cheaper. By applying the suitable battery capacity, you can get a cheap battery and can also solve the problem of frequency stability.

Journal:

1. S. Sitompul, G. Fujita, "Impact of Advanced Load-Frequency Control on Optimal Size of Battery Energy Storage in Islanded Microgrid System," *Energies,* vol. 14, no.8, pp 2213, April 2021.

International Conference:

1. S. Sitompul, G. Fujita, "Impact of State-of-Charge Control Integrated with Load-Frequency Control on Battery Energy Storage System in Islanded Microgrid System," *Energy Conversion Congress and Exposition – Asia (ECCE Asia) 2021*, Singapore, May 2021.

1.5 Thesis Outline

In order to answer the questions stated in the problem statement, this research is divided into topics arranged in a chapter format. The followings are the outline of this thesis.

- **Chapter 1: Introduction**

This chapter includes the background and motivation of this research. Here, the concept of islanded microgrid and battery energy storage are also described.

- **Chapter 2: Advanced Load-Frequency Control in Battery Energy Storage**

The main objective of this chapter is to design an advanced load-frequency control for BES. The proposed control is used to regulate the grid frequency by doing

load-sharing between source units. This chapter starts with the problem statement together with the literature review. Section 2.3 shows the design of the proposed control, which begins with the curve and calculation. The implementation and results are shown in Section 2.5, in which the results are achieved from the simulation.

- **Chapter 3: State-of-Charge Control on Advanced Load-Frequency Control**

  This chapter presents a further application of the proposed control. A state-of-charge (SoC) control is proposed in the proposed control by applying shift-reference droop control. The chapter begins with the problem statement, introducing the importance of SoC for the BES life. Details are followed by the literature review of the SoC control. Also, section 3.3 shows the details of the proposed SoC control and fundamental analysis.

- **Chapter 4: Optimal Battery Energy Storage Sizing with Advanced Load-Frequency Control**

  The main context of this chapter is to present how the advanced load-frequency control affects the BES size. The proposed control shows it can minimize the investment cost without violating any frequency limitation. The chapter starts with section 4.1 for the problem statement. This section includes the issue of the BES sizing. The chapter continues with the literature review of BES sizing. For result comparison, several scenarios are presented in section 4.3. The optimization and results are shown in section 4.4

- **Chapter 5: Conclusion**

  This chapter presents the thesis conclusion and future works. Section 5.1 concludes the studies and contribution to this thesis. The main future works include the extension works of the advanced load-frequency control are shown in section 5.2.

Chapter 2

2 Advanced Load-Frequency Control in Battery Energy Storage

2.1 Chapter Introduction

The islanded microgrid system is a unique electric power system. Usually, these systems consist of small energy sources or DER and are close to the consumer. Apart from being a small source unit, DER usually consists of renewable energy sources. On the one hand, having DER is environmentally friendly and relatively cheap due to its size. However, some drawbacks have a significant impact on the system. Namely, the microgrid system has relatively small system inertia. Most of the installed generators are energy sources with little or no inertia (for collision energy). This issue makes the islanded microgrid system vulnerable to changes in load and changes in weather. Many studies have tried to summarize this system's weaknesses and reveal that the islanded microgrid system is susceptible to alteration/disturbance. That said, stability has always been a hot issue in the islanded microgrid system.

The issue of frequency stability is a fundamental topic in the islanded microgrid system. The frequency is one of the main factors a system can run or not, whether the connected equipment can operate. Several attempts have been made to address this issue. One solution that is often taken is the use of energy storage devices, especially batteries. At first, power operators widely used batteries to smooth the output of renewable energy sources. The fluctuating renewable energy sources (RES) output impacts the system so that the battery functions as a buffer. Now the battery began to

be required to participate in system operation actively. Not only as a buffer or load leveling but also as a grid frequency regulator. [10], [27]

There has been much-published work on the function of the BES frequency regulator. Author [41] proposed control on the BES to keep the grid frequency at the threshold required. Similar methodology and experiments are published in [42]. The authors propose the use of droop control on BES to activate the frequency regulation function. There is also a study that proposed the use of a decentralized frequency system on BES [26]. Most of the work is done under different names, but this refers to one type of control, namely active power-frequency control or what is commonly called load-frequency control (LFC).

This chapter's main objective is to propose a new load-frequency control with a frequency limiter for the system. This control consists of three work areas, namely Region 1, Region 2, and Region 3, determined based on the actual system frequency. Each region has its function and determines how the BES participates in the system when changes occur. A further objective is to evaluate the performance of the controls proposed in the system. The expected results are in the form of BES participation that changes according to changes in frequency.

2.2 Load-Frequency Control

LFC is generally a centralized active power-frequency control concept for all energy sources installed in the system. This control has the primary function: to ensure that each source regulates its fluctuation and contributes to system frequency control [43]. However, there is another approach that is taken namely decentralized LFC. By using the droop control method, the contribution of each source can be determined based on the droop slope gain of the source [9], [44]. Then, it can be concluded that the LFC on a system with multiple sources is a collection of droop controls. In larger systems, these controls may be differentiated by area.
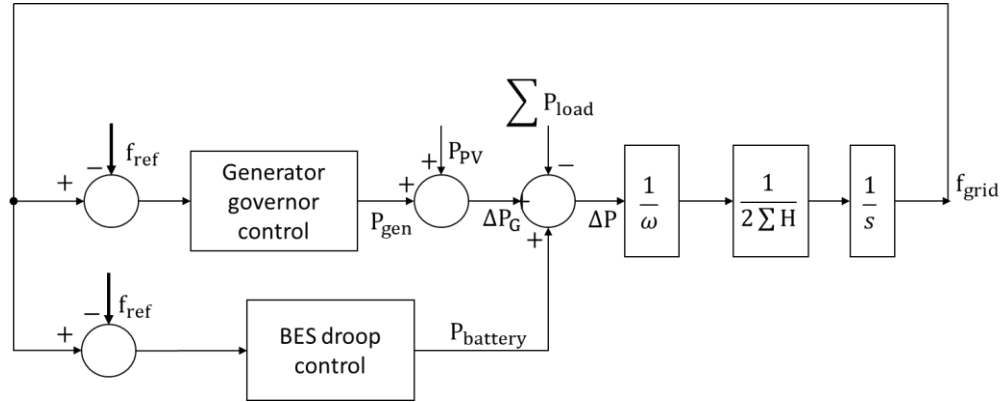
Figure 2.1 Load-frequency control with BES

LFC applies to sources that have inertia and applies to RES sources that are interfaced with the inverter. The LFC configuration between conventional generator (inertial source) and RES inverter is described and confirmed in [45], [46]. Those studies explain the LFC concept, focusing on the discussion on frequency-active power control in RES inverters. A similar approach is also carried out in this thesis that shown in Figure 2.1. The LFC concept offered is a control between sources without a communication line that determine active power for each source unit through droop control. The grid frequency is determined based on swing equation of the synchronous generator. Thus, it becomes the system backbone. However, the discussion that was carried out was centered on the BES control.

Load-frequency control controls active power-frequency to suppress the power deviation and frequency deviation within a specified range [47]. LFC has a long history, starting from being applied to traditional thermal power generation systems and hydropower generation systems until now applied to systems that are now developing. Generally, LFC consists of droop control. In BES applications, LFC does not only consist of droop control but also has a deadband area. In this section, the general LFC framework and what are the drawbacks of the widely used LFC are discussed.

2.2.1 Droop control

The stability of the microgrid system is supported by DERs, as discussing further islanded microgrid system operation. Sometimes, in one system, the system stability is supported by only one unit. This condition is encountered because, in its construction, the system initially consists of only one generator unit, usually a diesel generator. The addition of DER units is carried out to reduce generator fuel costs and the generator's pollution. This condition causes many droop control implementations to be used on these generators because the system can avoid the effects of generator oscillations caused by fluctuating loads. When the microgrid is connected to the primary grid, the DER can maintain a constant output power regardless of the load variation due to the utility grid presence. However, during islanded operation, DERs must follow the load demand strictly.
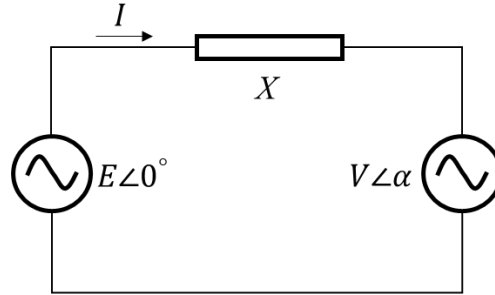
Figure 2.2 Simple AC circuit

There are two widely used droop controls, in theory, namely active power-frequency droop and reactive power-voltage droop. These two controls derive from the calculation of active and reactive power. Assume an investigation is conducted on a simple power circuit consists of two generators on both sides shown in Figure 2.2. In an inductive system, the active and reactive power can be expressed as follows [48]:

$$P = \frac{EV \sin \alpha}{X} \text{ Watt} \qquad (2.1)$$

$$Q = \frac{EV\cos\alpha - V^2}{X}\,\text{VAr} \qquad (2.2)$$

where E dan V are the amplitudes of the output voltage and common bus voltage, respectively, α is the power angle, and X is the output reactance. Based on equation (2.1) and (2.2) and assumed slight power angle, the active power is predominantly influenced by the power angle (or the grid frequency), and the reactive power is strongly dependent on the amplitude difference between E and V. It becomes the origin of the droop control. The main advantage of the droop control technique is its avoidance of critical communication links among parallel-connected DERs. The absence of communication links between them provides significant flexibility and high reliability. However, there are several drawbacks, such as an inherent trade-off between voltage regulation and load-sharing, line impedance mismatch, and poor harmonic load-sharing [49].

An active power versus frequency (P-f) droop control has been adopted for DER load-sharing methods. This control utilizes the grid's frequency as a common signal among the DERs to balance the system's active power generation. The active power-frequency droop-based power controllers have proven robust and adaptive to
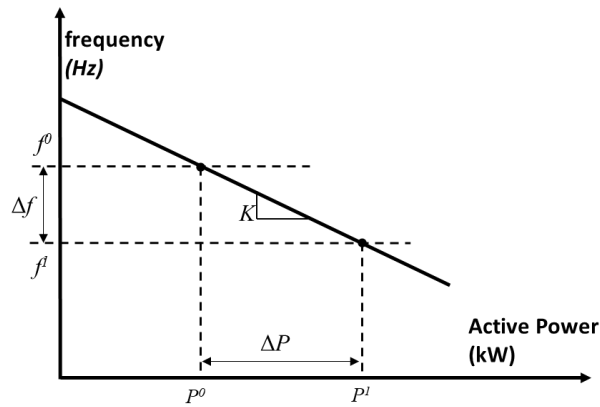
Figure 2.3 Active power – frequency droop curve

variation in the power system operational conditions. Moreover, this control is a wireless control that a communication network is not necessary. From the equation (2.1), the relationship between the frequency f and the DER output power in Figure 2.3 can be expressed as:

$$f^1 - f^0 = K\left(P^1 - P^0\right) \text{Hz}$$
(2.3)

where K is the droop gain in Hz/kW, f and P are the frequency in Hz and DER output at a new operating point in kW, Δf is the deviation of the frequency, and f^0 and P^0 are the nominal values, respectively in Hz and kW. Equation (2.3) also can be written in:

$$\frac{f^1 - f^0}{f^{pu}} = K^{pu}\left(\frac{P^1 - P^0}{P^{pu}}\right) \text{Hz}$$
(2.4)

Where f^{pu} is the rated frequency (in Hz) of the unit, P^{pu} is the base power, and K^{pu} is the gain droop per unit. From equation (2.4), we can simplify the equation into changing the frequency concerning the change in power. The new equation can be written as:

$$\Delta f = K^{pu}\frac{f^{pu}}{P^{pu}}\Delta P \text{ Hz}$$
(2.5)

where Δf is the change in frequency that occurs, and ΔP is the change in generator power.

When N dispatchable DER units operate parallel on the system, their speed-droop characteristics determine how load changes are apportioned among them in the steady-state. Assume the N units are synchronously operating at a given frequency when the load changes by ΔP kilowatts. The corresponding changes in the outputs of the units are given by Equation (2.5) as follows:

$$\text{DER unit 1: } \Delta P_{DER1} = \frac{P^{pu}}{K^{pu}_{DER1}} \frac{\Delta f}{f^{pu}} \text{ kW} \tag{2.6}$$

$$\vdots$$

$$\text{DER unit } i: \Delta P_{DERi} = \frac{P^{pu}}{K^{pu}_{DERi}} \frac{\Delta f}{f^{pu}} \text{ kW} \tag{2.7}$$

$$\vdots$$

$$\text{DER unit } N: \Delta P_{DERN} = \frac{P^{pu}}{K^{pu}_{DERN}} \frac{\Delta f}{f^{pu}} \text{ kW} \tag{2.8}$$

Adding these equations together gives the total change in output

$$\Delta P = \left(\frac{1}{K^{pu}_{DER1}} + \cdots + \frac{1}{K^{pu}_{DERi}} + \cdots + \frac{1}{K^{pu}_{DERN}} \right) \frac{P^{pu} \Delta f}{f^{pu}} \tag{2.9}$$

Hence, the frequency change can be written as:

$$\frac{\Delta f}{f^{pu}} = \frac{\Delta P}{P^{pu} \left(\dfrac{1}{K^{pu}_{DER1}} + \cdots + \dfrac{1}{K^{pu}_{DERi}} + \cdots + \dfrac{1}{K^{pu}_{DERN}} \right)} \text{ per unit} \tag{2.10}$$

By substituting equation (2.10) with equation (2.7), the change in power ΔP_{DERi} in the DER i unit can be written as:

$$\Delta P_{DERi} = \frac{\Delta P}{K^{pu}_{DERi} \left(\dfrac{1}{K^{pu}_{DER1}} + \cdots + \dfrac{1}{K^{pu}_{DERi}} + \cdots + \dfrac{1}{K^{pu}_{DERN}} \right)} \text{ kW} \tag{2.11}$$

Thus, equation (2.11) is the change in power for unit *i* when the overall load changes. This equation can be used for any generator installed in parallel as long as it has the same base power and the same base frequency for each generator.
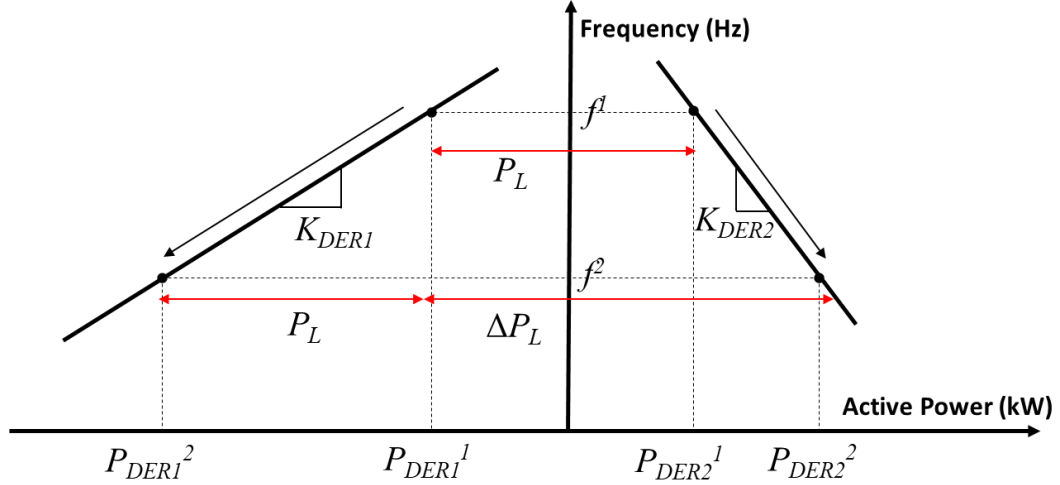
Figure 2.4 Droop operation for multi-DER

Figure 2.4 shows two source units having droop control. When there is only one source, the grid frequency tends to be very fluctuating. However, when two sources have droop control, they supply each other the load they operate on the common frequency. The load-sharing mechanism can keep the grid frequency not too high or too low from nominal frequency by applying the sources' droop control. This operation is the key to sources operating with droop control. From the equation (2.10), the system frequency change in Figure 2.4 can be calculated to be:

$$\frac{\Delta f}{f^{pu}} = \frac{\Delta P_L}{P^{pu}\left(\dfrac{1}{K_1^{pu}} + \dfrac{1}{K_2^{pu}}\right)} \text{ per unit} \tag{2.12}$$

with changes for each generator, it becomes:

$$\Delta P_{DER1} = \frac{\Delta P_L}{K_{DER1}^{pu}\left(\dfrac{1}{K_{DER1}^{pu}} + \dfrac{1}{K_{DER2}^{pu}}\right)}\ \text{kW} \tag{2.13}$$

$$\Delta P_{DER2} = \frac{\Delta P_L}{K_{DER2}^{pu}\left(\dfrac{1}{K_{DER1}^{pu}} + \dfrac{1}{K_{DER2}^{pu}}\right)}\ \text{kW} \tag{2.14}$$

From equations (2.13) and (2.14), it can be concluded that the generator supplies the load for each applicable load according to its droop gain.

2.2.2 Deadband area

Now many studies are developing that droop has a significant effect on the work of the system. However, many argue that the battery only needs to work when the frequency is far from the system's nominal frequency. It leads to the use of deadband areas for droop control. The deadband area allows the battery not to operate in particular areas. In battery implementations, the deadband area is applied at a frequency very close to the nominal frequency. This idea originated because the battery turns off when the system works at the nominal frequency. Below that, the battery discharges, and above the nominal frequency, the battery carries out the charging mechanism.

The deadband concept is when the system operates at a frequency close to the nominal frequency. In this state, the battery tends to switch between charging and discharging, as shown in Figure 2.5 (a). It leads to the life cycle of the battery and the lifespan of the battery itself. Thus, it is necessary to expand the area for the battery to stop working, so that battery participation becomes clearer for one load at a time. The deadband concept was introduced to address this problem, as shown in Figure 2.5 (b).
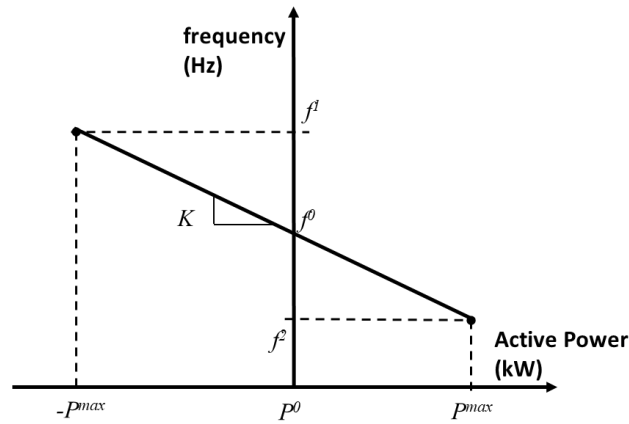
(a)
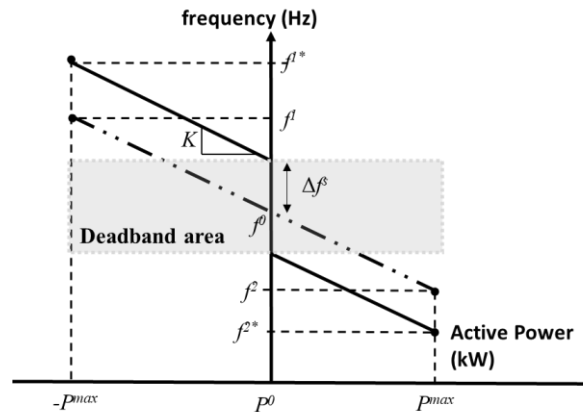
(b)

Figure 2.5 Droop control type; (a) conventional droop, (b) deadband droop

Figure 2.5 shows the difference when only the droop curve is used and when the deadband is added to the droop curve. If it is assumed that f^1 is the value of the frequency when BES operates at $-P_{max}$, and f^2, BES operates at P_{max}, the frequency shifts slightly when the deadband is applied. It can be seen in Figure 2.5 (b), which compares before and after the deadband area is included. Thus, it can be seen that the deadband area shifts the maximum value and the minimum value frequency when the battery is operating at its rated value. Also, the deadband control in Figure 2.5 (b) is a control that is widely used in BES active power-frequency control studies. It can also

be said that the control is a traditional LFC, where the end of the droop curve is the BES power rating, and after that, the BES supplies the rating for whatever frequency value is read. Given the deadband area, the droop equation (2.3) can be written as:

$$f^1 - \left(f^0 \pm \Delta f^s\right) = K\left(P^1 - P^0\right) \text{Hz} \tag{2.15}$$

Hence, if there is a multi-generator that works in parallel, the change in system frequency can be written as:

$$\frac{\Delta f \pm \Delta f^s}{f^{pu}} = \frac{\Delta P}{P^{pu}\left(\dfrac{1}{K_{DER1}^{pu}} + \cdots + \dfrac{1}{K_{DERi}^{pu}} + \cdots + \dfrac{1}{K_{DERN}^{pu}}\right)} \text{per unit} \tag{2.16}$$

The deadband concept has confirmed evidence of the contribution of batteries to microgrid systems. However, the control used is often limited to the droop deaband control and is only limited by the battery charge rating. A grid-connected microgrid system where the frequency control is carried out by the utility grid and the battery contribution to the frequency is insignificant. But there is a clear gap that in islanded microgrid systems that have not enough dispatchable units, the battery must contribute to the system. If the control is implemented in the islanded microgrid system, the system frequency does not have a clear limit. Indeed, this is trying to be solved, but the frequency limit contained in the battery control only limits the battery power output and forces other units to compensate.

If this concept is implemented, the frequency fluctuation problem rearises. Another solution that has been carried out is to give limitations to other units. This concept can be done when there is access to change or modify other source controls. One unit with another unit comes from a different manufacturer where there is no access to modify further controls in an implementation. One of the options you have to keep the frequency in the desired range is to modify the battery controls and make it

"as if" the battery pack controls another unit's output power. If this is done, then keeping the grid frequency in the desired range can be realized.

2.3 Advanced Load-Frequency Control

In the implementation of battery control in the system, load-frequency control (LFC) is widely utilized. LFC is an active-frequency power control designed to suppress power and frequency deviations within a specified range. This control is realized as LFC utilizes droop control as the basis of control. Also, this control is the reason that the battery actively participates in the system. The proposed control, namely advanced LFC, is an LFC that features an additional function of droop control which functions as a frequency limiter. The proposed LFC as the primary control configures P -f characteristics into multi-region curves shown in Figure 2.6. By using these additional features, the grid frequency is maintained between f^{max} and f^{min} by maximizing the battery output power from -$P_b{}^R$ to $P_b{}^R$, which is the battery power rating.
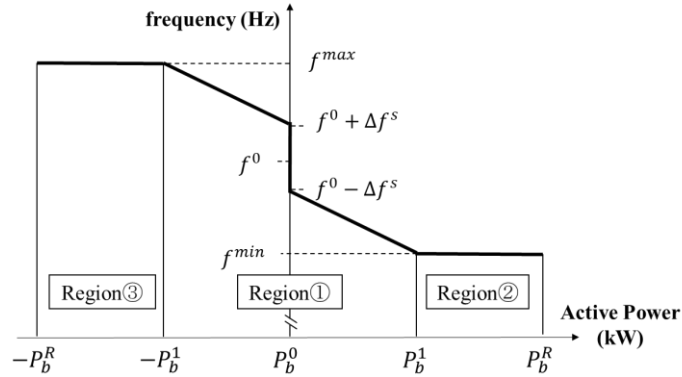
Figure 2.6 Advanced load-frequency control

The control is separated into three regions named Region 1, Region 2, and Region 3, that each of the regions determines the BES operation. In Region 1, the BES acts according to the droop curve for charging and discharging modes with a deadband area. The deadband area allows the BES to enter a standby mode (inactive) that stops

BES operation. In Region 2 and Region 3, the flat regions, the BESS supplies power according to the flat line while the frequency maintains at f^{max} and f^{min}.

2.3.1 Region 1 (deadband droop control)

The droop control is applied in Region 1. This control allows the BES power according to the droop equation expressed in (1)[50]:

$$f_{dh} - f^0 = K_b(P_{bdh} - P_b^0)$$

(2.17)

where f_{dh} is the grid frequency, f^0 represents the nominal frequency that acts as the droop reference, K_b represents the BES droop gain, P_{bdh} indicates the BES output power, and P_b^0 represents the BES power at nominal frequency.

The droop gain is determined based on the frequency limit allowed by the system. The IEEE released a standard regarding microgrid operation to use this guide in this study [51]. The guidelines state that the upper and lower limits of frequency allowed are ±0.5 Hz from the nominal value. For 60 Hz systems, the allowable limits are 60.5 Hz and 59.5 Hz. For a 50 Hz system, the limits are 50.5 Hz and 49.5 Hz. By referring to equation 2, the droop gain for the battery can be calculated based on the power limit used. The equation can be expressed as:

$$K_b = \frac{f_{dh} - f^0}{P_{bdh} - P_b^0}$$

(2.18)

the droop gain is obtained by entering f_{dh} and P_{dh} as the limit value of the frequency and battery power capacity. In some references, equation 2 with output power limitation is called the traditional LFC[11], [26], [28], [47], [52], [53].

In this region, a deadband area (Δf^s) is introduced, as shown in Figure 3. BES does not exchange power in the deadband area. Otherwise, it operates when the grid frequency is higher than $f^0 + \Delta f^s$ and $f^0 - \Delta f^s$ the BES power can be expressed as:

$$f_{dh} - (f^0 \pm \Delta f^s) = K_b(P_{bdh} - P_b^0) \tag{2.19}$$

which the deadband area f^s is included in the droop curve. There are two possibilities in equation (4). When the BES turns into charging mode, the nominal frequency acting as droop reference deviates into $f^0 + \Delta f^s$. On the other hand, the droop reference shifts into $f^0 - \Delta f^s$ when the BES turns into discharging mode. Deadband selection has no strict definition. Each study has its reference for determining the deadband [41], [42]. However, all studies generally determine that the deadband area is the normal operating area of the system, so that it is not necessary to have BES participation. In other words, the deadband area is the range in which the system can operate normally, even though under the load disturbance or unavailability of the source.

2.3.2 Region 2 (Lower Frequency Saturation)

This region is utilized to hold the system operating at the f^{min} frequency. This control departs from the parallel calculation between the battery and the generator. Figure 2.7 shows the movement of the battery power transition from traditional LFC to advanced LFC. Assume the load demand is P_L (purple line), causing the system to operate at f where f is lower than f^{min}. In this condition, BES supplies P_b (blue line), and
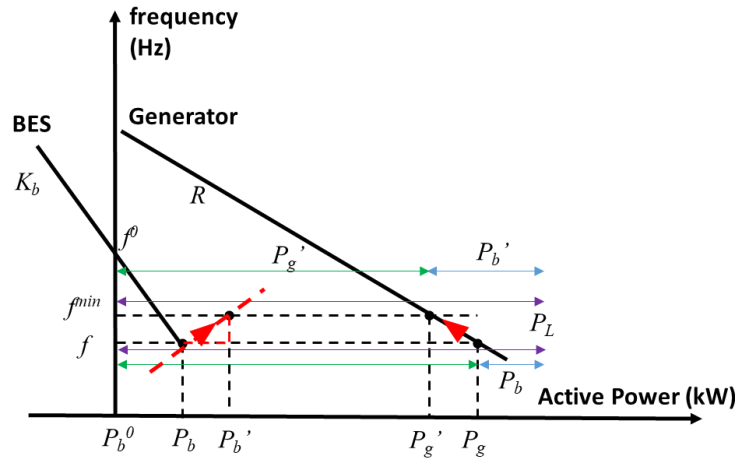
Figure 2.7 Region 2 (lower frequency saturation) scheme

the generator supplies P_g (green line). The proposed control serves to avoid the system operating below the frequency f. When the P_L load is applied, and the system has to operate in f^{min}, the power supplied by each source unit changes. For the system to operate at the desired frequency, the generator unit must supply P_g'. This operation causes the battery to supply the remaining load, become P_b'.

The dashed red line in Figure 2.7 shows the change in battery power that occurs. The line has the same slope as the generator slope or the droop gain. So, the red line can be written as:

$$R = \frac{f - f^{\min}}{P_b - P_b'} \text{ Hz/kW} \tag{2.20}$$

Equation (2.20) can also be written as:

$$P_b' = P_b + \left(\frac{f^{\min} - f}{R} \right) \text{kW} \tag{2.21}$$

we know that equation (2.3) can be used to find the value of P_b before changing to P_b'. If this is substituted, the equation that is just written becomes:

$$P_b' = \frac{f - f^0}{K_b} + P_b^0 + \left(\frac{f^{\min} - f}{R} \right) \text{kW} \tag{2.22}$$

when referring to the use of deadband in Region 1, the equation for Region 2 is written as:

$$P_{bdh}' = \frac{f_{dh} - \left(f^0 - \Delta f^s \right)}{K_b} + \left(\frac{f^{\min} - f_{dh}}{R} \right) + P_b^0 \text{ kW} \tag{2.23}$$

Equation (2.23) shows that in this region, BES functions to regulate the frequency in f^{min} by supplying power to the rating P_b^R. What needs to be understood is

that it is still used to keep the frequency value at the f^{min} value in implementing PI control. Moreover, control these regions if the system's steady-state frequency is below the desired value.

2.3.3 Region 3 (Upper-Frequency Saturation)
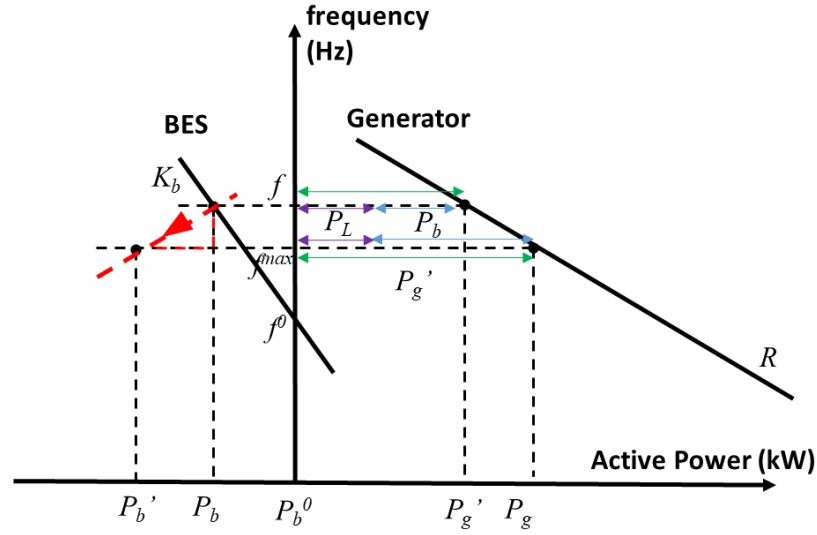
Figure 2.8 Region 3 (upper frequency saturation) scheme

In Region 3, similar to Region 2, the BESS regulates its output power at flat frequency f^{max}. This region's mechanism also has something in common with Region 2, shown in Figure 2.8. This figure shows the movement of the battery power transition from traditional LFC to advanced LFC. Assume the load demand is P_L (purple line), causing the system to operate at f where f is lower than f^{max}. In this condition, BES supplies P_b (blue line), and the generator supplies P_g (green line). The proposed control serves to avoid the system operating below the frequency f. When the P_L load is applied and the system has to operate in f^{max}, the power supplied by each source unit changes. For the system to operate at the desired frequency, the generator unit must supply P_g'. This operation causes the battery to supply the remaining load, become P_b'.

The dashed red line in Figure 2.8 shows the change in battery power that occurs. The line has the same slope as the generator slope or the droop gain. So, the red line can be written as:

$$R = \frac{f - f^{\max}}{P_b - P_b^{'}} \text{ Hz/kW}$$

(2.24)

Equation (2.24) can also be written as:

$$P_b^{'} = P_b + \left(\frac{f^{\max} - f}{R} \right) \text{kW}$$

(2.25)

We know that equation (2.3) can be used to find the value of P_b before changing to P_b'. If this is substituted, the equation that is just written becomes:

$$P_b^{'} = \frac{f - f^{0}}{K_b} + P_b^{0} + \left(\frac{f^{\max} - f}{R} \right) \text{kW}$$

(2.26)

when referring to the use of deadband in Region 1, the equation for Region 2 is written as:

$$P_{bdh}^{'} = \frac{f_{dh} - \left(f^{0} + \Delta f^{s} \right)}{K_b} + \left(\frac{f^{\max} - f_{dh}}{R} \right) + P_b^{0} \text{kW}$$

(2.27)

Equation (2.27) shows that in this region, BES functions to regulate the frequency in f^{max} by supplying power to the rating $-P_b{}^R$. What needs to be understood is that it is still used to keep the frequency value at the f^{max} value in implementing PI control. Moreover, control these regions if the system's steady-state frequency is below the desired value.

2.3.4 Advanced Load-Frequency Control Regions

Previously all the operation regions that describe their operation have been discussed. By combining all the LFC regions, the BES power P_{bdh} is determined based on the frequency value that is written as:

$$
P_{bdh} = \begin{cases}
\dfrac{f_{dh} - \left(f^{0} + \Delta f^{s}\right)}{K_b} + \left(\dfrac{f^{max} - f_{dh}}{R}\right) + P_b^0; & f_{dh} \geq f^{max} \\[4mm]
\dfrac{f_{dh} - \left(f^{0} + \Delta f^{s}\right)}{K_b} + P_b^0; & f^{0} + \Delta f^{s} \leq f_{dh} < f^{max} \\[4mm]
0; & f^{0} - \Delta f^{s} < f_{dh} < f^{0} + \Delta f^{s} \\[4mm]
\dfrac{f_{dh} - \left(f^{0} - \Delta f^{s}\right)}{K_b} + P_b^0; & f^{min} < f_{dh} \leq f^{0} - \Delta f^{s} \\[4mm]
\dfrac{f_{dh} - \left(f^{0} - \Delta f^{s}\right)}{K_b} + \left(\dfrac{f^{min} - f_{dh}}{R}\right) + P_b^0; & f_{dh} \leq f^{min}
\end{cases}
\tag{2.28}
$$

Equation (2.28) shows that the BES power P_{bdh} is calculated based on the system frequency. At the deadband area, the BES is at standby mode ($P_b = 0$). This area shows any variations in the system compensated for by other sources. At the droop area ($f^{min} < f_{dh} \leq f^{0} - \Delta f^{s}$ or $f^{0} + \Delta f^{s} \leq f_{dh} < f^{max}$), the BES adjusts its power according to the load-sharing between the generator and BES. When the system operates at Region 2 or
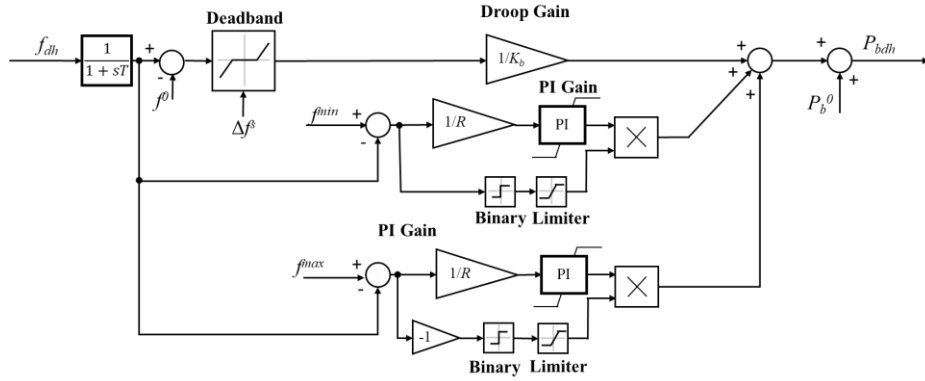
Figure 2.9 Advanced LFC block diagram

Region 3 ($f_{dh} \leq f^{min}$ or $f_{dh} \geq f^{max}$), the PI droop control is performed that makes BES regulates its power to maintain the generator power at specified points. Equation (7) can be represented in a block diagram control shown in Figure 2.9.

The block diagram is divided into three parts (upper, middle, and lower). The upper part describes the Region 1 control consisting of the droop control with deadband area, the middle part describes the Region 2 control consisting of the PI droop control for f^{min}, and the lower part describes the Region 3 control consisting of the PI droop control for f^{max}.

The proposed control has several non-linear components, including a limiter and a binary option which causes the control to have a non-linear characteristic. Then, this control output is connected to the generator swing equation, which is linear. Hence, there is a relationship between non-linear and linear systems in one loop of the control loop. Referring to Figure 2.9 and equation (2.28), mathematically advanced LFC consists of discontinuous equations. This relationship causes oscillations to occur when there is a change in the linear system side due to the determination of the work area contained in the advanced LFC. Such oscillations can cause instability in the proposed control. Therefore, the stability of the control must be guaranteed.

The stability of non-linear systems can be ascertained by several methods, such as describing function analysis, Lyapunov stability, and limit circle theory. One approach that is popular in its implementation is describing function analysis. The method is based on quasi-linearization, which approximates the non-linear system under investigation by a linear time-invariant (LTI) transfer function [54]. As previously explained, changes in the linear (frequency) side directly affect the non-linear system input. This relation causes operating changes that can generate oscillations. This method attempts to predict the characteristics of those oscillations by assuming a slow linear system with a low-pass filter centered on one frequency point

only. We can assume that the combined systems form a quasi-linear system with similar characteristics to the linear system but changes shape due to the non-linear system [55].

In this study, the stability of the control can be ensured if the control is a cascade with a sluggish linear system. In this case, the generator system is mathematically a linear system that can secure stability. Furthermore, with the generator's inertial response to changes, oscillations between advanced LFC work areas can be avoided. This response is closely related to the amount of inertia applied to the generator. However, there is a possibility that the generator inertia may not be large enough to reduce dampening the oscillations. Hence, additional controls such as virtual inertia on the inverter could be an additional solution.

2.4 Islanded Microgrid System Model

The microgrid system model used in this study refers to [20]. According to the reference, the study modeled the microgrid system in the Philippines. Both source capacity and load size were obtained. It is assumed that the system mainly relies on diesel power generation, which implies high generation and operational costs due to varying fuel costs and transport costs. The system also implements a solar PV penetration of more than 50% due to the geographical location advantage.

The load demand used in the study is based on the average load profile obtained from the actual data of 22 islands in the country. From these data, it is known that the load is never below 50% of the peak load. However, this study tries to demand a lower load than that obtained because the load characteristics are rural consumers. So, there is still a possibility that the load request is lower than the data obtained. The data also states that the peak load is defined as 50% of the installed power generation capacity without a battery [56].

In order to investigate LFC's advanced performance, an islanded microgrid system having BES is used, which is represented in Figure 2.10. The system is modeled

in MATLAB/Simulink R2019 software. The system is assumed to be a small system consisting of one generator, PV, and BES connected to the consumer. The installed synchronous generator acts as the backbone of the system. The system's frequency stability rests on the generator operation. The PV unit is also used as one of the RES installed in the system. Between the source and the load, a distribution channel is assumed to be very short so that the system is kept small.

The proposed BES control performance is examined on an islanded microgrid composed of a synchronous generator unit (diesel generator), consumer, PV, and BES. Each unit is connected to the AC bus microgrid. The generator with a capacity of 390 kW and having a droop control on its governor acts as the system backbone. The installed PV is assumed to be able to deliver up to 200 kW. The installed BESS has a capacity of 2.5 Ah with a PCS efficiency of 95%. The generator, PV, and BESS are network-integrated via a 0.4/13.2 kV step-up transformer. On the high voltage side, the transformer is connected to a 2 km long transmission line. At the end of the transmission line, a 13.2 kV/380 V step-down transformer connects the transmission to the load. Lastly, the load is assumed 295 kW as its peak.
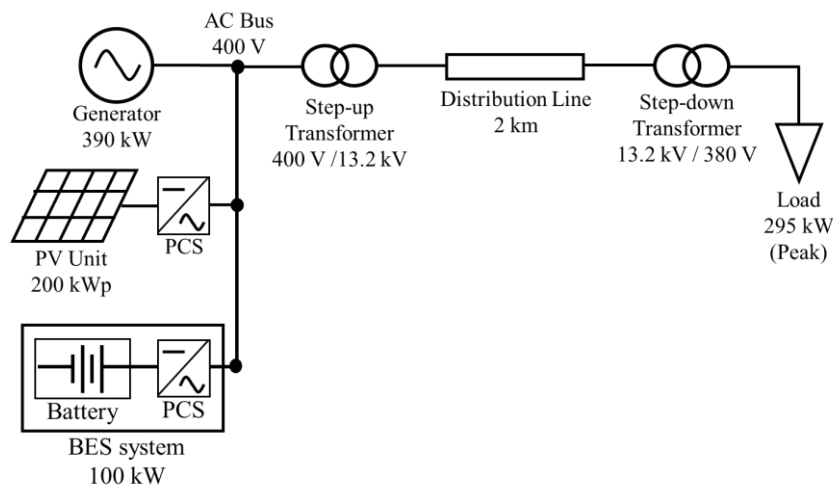
Figure 2.10 System model scheme

2.4.1 Diesel Generator

In this paper, a diesel generator is applied as the inertia source. Modeled in a simple first-order at the engine output, the engine model describes the level of fuel consumption in a function of speed and mechanical power. The model connects fuel consumption with engine mechanical power. A generator has a governor system whose engine speed is controlled automatically by connecting the fuel intake. The system, which is defined as a mechanical or electromechanical device, has several types in its implementation, such as mechanical-hydraulic direct mechanical, electrohydraulic, and microprocessor-based governor. Figure 2.11 illustrates the governor model used in this study. By implementing droop control, the variation in engine output power is directly proportional to the droop frequency. R physical unit, which is the regulator feedback parameter's physical significance, is Hz/kW and is always considered positive [57].
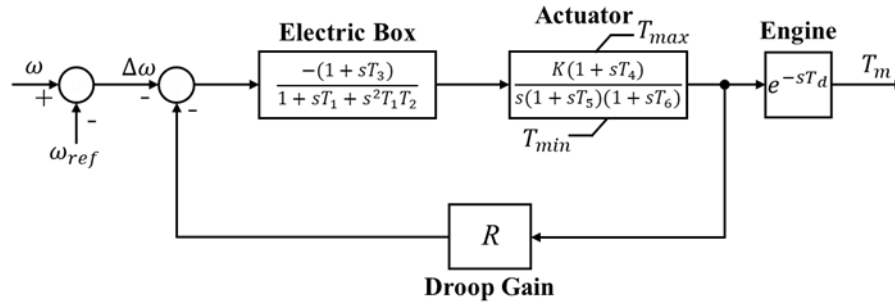
Figure 2.11 Diesel droop governor [57]

The author [58] develops a diesel generator computer model that acts as an emergency generator. However, this model only applies when the system works at a fixed frequency value. Conversely, the governor model used on this system is the governor model, which allows the frequency value to vary (droop control). Therefore, the governor model used is the governor model developed from a model [58], the DEGOV1 model from [59]. Both models are modeling governor systems adapted from well-known Woodward diesel governors [60]. The difference between those two is that

the model in [58] functions to maintain the frequency at its nominal value, while the DEGOV 1 model functions to variate the frequency based on the *R*-value.

The DEGOV1 model used in this system is shown in Figure 2.11. It is employed to simulate torque produced by the diesel engine based on the governor's speed signal. This model consists of an electric control box, an actuator, and a diesel engine in which all the used parameters are stated [59]. The parameter values used in this study are shown in Table 2.1and Table 2.2. The typical inertia for the diesel generator is 0.817 pu.

Table 2.1 Diesel governor parameter [60]

Regulator gain	Regulator time constant (s)		Actuator time constants (s)				Torque limits (pu)		Engine time delay (s)
K	T_1	T_2	T_3	T_4	T_5	T_6	T_{min}	T_{max}	T_d
9	0.022	0.002	0.1	0.25	0.009	0.0384	0	1.1	0.024

Table 2.2 Diesel droop parameter

Droop gain (pu)	Droop frequency reference (rad/s)	Droop power reference (kW)
R	f_f^0	P_g^0
0.03	60	100

Table 2.2 shows the droop parameters used in diesel generators. However, the diesel governor model used only angular speed, so the actual frequency must first be converted to the angular speed. The equation for angular velocity can be written as:

$$\omega = 2\pi f \text{ rad/s} \qquad (2.29)$$

In order to calculate the reference angular velocity, ω_{ref} can be written as:

$$\omega_{ref} = 2\pi f^0 \text{ rad/s} \qquad (2.30)$$

$$\omega_{ref} = 376.98 \text{ rad/s} \qquad (2.31)$$

2.4.2 Photovoltaic Array

Photovoltaic has dynamic performance depending on the weather condition. It is vital to understand how PV operates. In fundamental, PV can generate electricity using the photon from sunlight. As the photon knocks the electron inside the Silicon layers inside the PV cell, the electric field pushes the electron out of the Silicon junction. The generated power from the PV has a proportional relationship to the solar irradiation
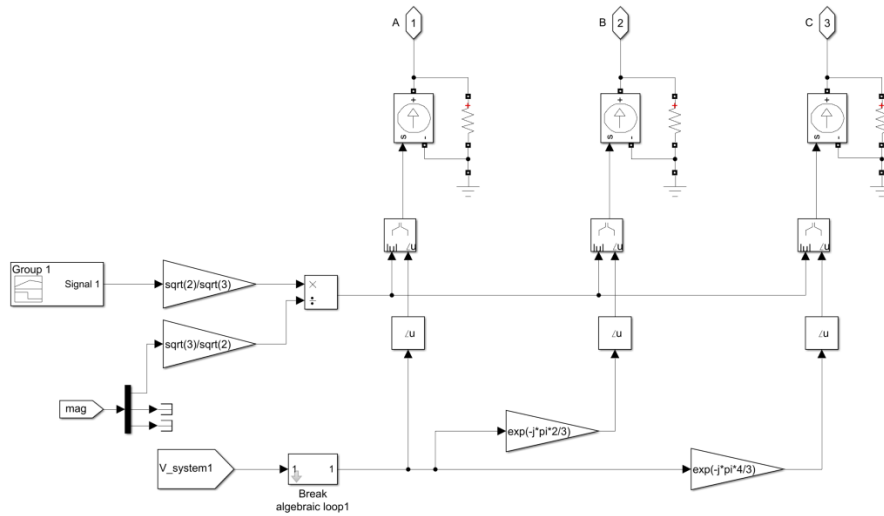
Figure 2.12 PV model

level; the more irradiation incidents to the PV cell, the higher the generated power can achieve.

To simplify calculations and speed up simulation time, the PV model is simplified into a current source that can be output regulated shown in Figure 2.12. This current source has been modeled into an AC source. The PV input is the value of the power to be supplied. This modeling is intended to make the PV a source disconnected from any power control and highly volatile.

2.4.3 Distribution Line

The line model used is the Three-Phase PI Section Line from the MATLAB / Simulink R2019 software [61] shown in Figure 2.13.
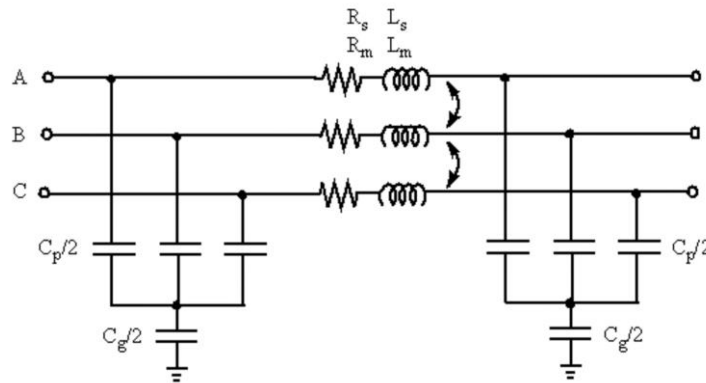
Figure 2.13 Distribution line model [61]

Since the distribution voltage is 13.2 kV and the assumed maximum load is 295 kW. However, the maximum current flowing through the system is assumed when the load reached 300 kW. From the three-phase power formula, where P is the three-phase power, V^{rms} is the line voltage, and I^{rms} is the line current, the current can be calculated into:

$$I^{rms} = \frac{P}{\sqrt{3}V^{rms}\cos\theta}\text{ A} \tag{2.32}$$

Assuming the power factor of 1.0, the line current is:

$$I^{rms} = \frac{P}{\sqrt{3}V^{rms}} \, \text{A}$$

$$= \frac{300 \times 10^3}{\sqrt{3} \times 13.2 \times 10^3} \, \text{A}$$

$$= 13.12 \, \text{A}$$

The resistance r per unit length, inductive reactance x_L, and capacitive reactance x_C can be obtained from the obtained maximum current. However, the nominal frequency uses the commercial frequency of 60 Hz. As 1 km = 3,280 ft, the resistance and inductive reactance can be written as:

$$r = 0.819 \, \Omega/1000\text{ft} \tag{2.33}$$

$$\approx 2.687 \, \Omega/\text{km}$$

$$\equiv r_s$$

$$x_L = 0.1465 \, \Omega/1000\text{ft} \tag{2.34}$$

$$\approx 0.4807 \, \Omega/\text{km}$$

Hence, the inductance can be written as:

$$l = \frac{x_L}{2\pi f} \, \text{mH/km} \tag{2.35}$$

$$= \frac{0.4807}{2\pi 60} \, \Omega/\text{km}$$

$$\equiv 1.275 \, \text{mH/km}$$

$$\equiv l_s$$

$$x_C = 0.7511 \times 10^6 \, \Omega/1000\text{ft} \qquad (2.36)$$

$$\approx 2.464 \times 10^6 \, \Omega/\text{km}$$

Also, the capacitance c per unit length can be written as:

$$C = \frac{1}{2\pi f x_C} \, \text{F} \qquad (2.37)$$

$$= 1.077 \, \text{nF}$$

$$\equiv c_s$$

In addition, if the distribution line is 2 km and the transmission loss is taken into consideration, the receiving end voltage can be calculated as follows:

$$V^r = V^{rms} - (I^{rms} \times r_s \times 2) \, \text{kV} \qquad (2.38)$$

$$= 13.13 \, \text{kV}$$

Therefore, the data adaptation in reference is consistent, the data in reference is used. Table 2.3 shows the line parameter.

$$r_s = \frac{2r_1 + r_0}{3} \ \Omega/\text{km} \tag{2.39}$$

$$l_s = \frac{2l_1 + l_0}{3} \ \text{H/km} \tag{2.40}$$

$$c_g = \frac{3c_1c_0}{c_1 - c_0} \ \text{F/km} \tag{2.41}$$

$$c_s = c_0 \tag{2.42}$$

$$\frac{1}{c_s} = \frac{1}{c_p} + \frac{3}{c_g} \tag{2.43}$$

$$c_p = c_1 \tag{2.44}$$

Table 2.3 Distribution line parameter

Positive-sequence resistances	Zero-sequence resistances	Positive-sequence inductances	Zero-sequence inductances	Positive-sequence capacitances	Zero-sequence capacitances
r_1	r_0	l_1	l_0	c_1	c_0
(Ω/km)	(Ω/km)	(mH/km)	(mH/km)	(nF/km)	(nF/km)
1.612	4.836	0.7650	2.295	0.3590	1.077

2.4.4 Battery Energy Storage Model

In modeling energy storage, several categories of models can be used: dynamic models, energy flow models, physics-based models, and black-box models. Each model has a different function and purpose. In this study, to model BES that focuses on performance over small-time scales, milliseconds to a minute, a dynamic model is the right choice. The battery model used in this study is a battery model that can calculate the SoC and energy capacity of the battery [38], [62]. However, the relationship between battery voltage and SoC is omitted. This assumption is used due to the scope of the study. The study is focused on the effect of battery power contribution on frequency. Thus, the voltage relationship with the battery SoC is neglected.

In the operation of the inverter, there are two types of inverter roles, namely grid-forming inverter and grid-following inverter. The grid-forming inverter is a converter that can create a reference voltage and frequency. Usually, this role has been covered by the inertial generator (e.g., synchronous generator). The grid-following
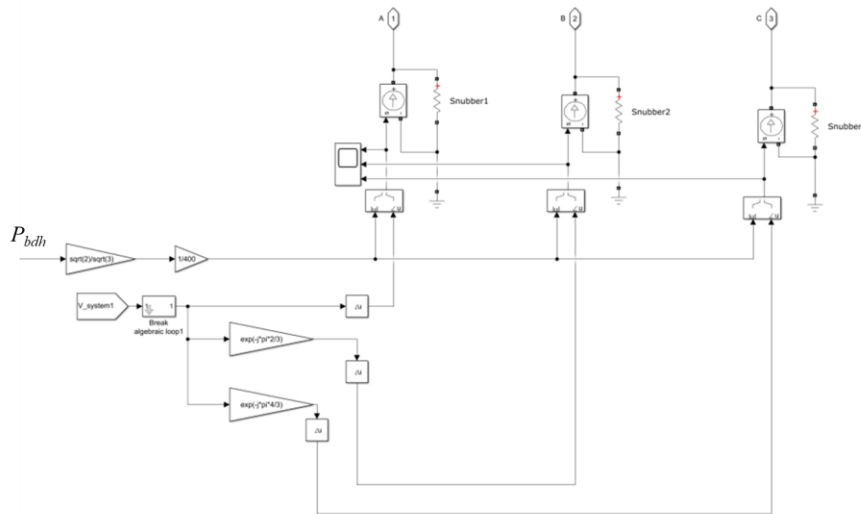
Figure 2.14 Battery Model

inverter regulates its output power by measuring the system frequency using a phase-locked loop (PLL) [63].

In this thesis, the study focuses on the battery's contribution to the system's frequency by regulating its output power. This contribution lays down the role of the battery in the microgrid system as grid-following through the installed inverter. Thus, the role only follows the measured voltage and frequency and regulates its output power. Due to the grid-following inverter characteristic, this type of inverter is modeled by a current source. It delivers the amount of current to the system to define supplied output power. Hence, the current source inverter model is used to enable the role of a grid-following inverter. Therefore, the battery contributes to the grid frequency by regulating its output power.

The dynamic model used in this study is a three phase AC source model. In this model, the entire battery mechanism up to the inverter output is simplified to become a current source. Thus, when using the proposed control, the control output is directly passed to the current source model. This model's choice focuses on the LFC's impact on generator performance and shortens the simulation time. The model is adopted from the MATLAB / Simulink library, which can be found [64].

Table 2. 4 BES control parameter

Description	Parameter	Value
Frequency operation limit	f_{max}	60.3 Hz
	f_{min}	59.7 Hz
Frequency deadband	Δf^δ	0.1 Hz
BESS droop gain	K_b	0.05 pu
LFC proportional gain	K_P	5
LFC integrator gain	K_I	0.02

Figure 2.14 shows the BES used in this study. The BES model used consists of the conversion from active power to the BES output current. In this model, to simplify computer calculations, the inverter and switching calculations are neglected. The input

of the model is the active battery power sent from the control. The phase angle for the BES output current is obtained from the voltage phase angle of the generator.

2.5 Results and Discussion

The proposed control verification is done using MATLAB/Simulink R2019 software. This software was chosen because it has proven capability to simulate electric power systems. Control verification is done by comparing the results of the traditional LFC with the advanced LFC. The two types of controls were compared to show significant differences in the proposed control. Load variations are applied to the model system to investigate the performance of the two controls. This variation is the load that continues to increase, and the load continues to fall. In addition, the variations that are applied are gradual. Hence, the battery operating conditions can be known for each applied load demand. For the proposed control, operation in each region is confirmed based on the prevailing load conditions.

2.5.1 Case 1 – Load increasing

In this case, the load is gradually increasing from 200 to 295 kW. First, the system is initiated at 60 Hz with the load demand of 200 kW, which puts BESS in standby mode. Figure 2.15 (a),(b),(c),(d) illustrates the BES active power, system frequency results, diesel generator active power, and diesel active power for different inertia, respectively. However, due to the installed distribution line, the grid starts operating at 59.97 Hz.

At t = 15 s, the load increases to 220 kW. It causes the frequency to drop as the generator tries to stabilize the system. The drop in the system frequency causes the battery to start operating and participating in the system. BESS's participation creates a load-sharing point that the BESS and generator must meet due to power imbalance. The point is reached at 59.93 Hz, the deadband area that caused BESS to in standby mode. This operation shows Region 1 advanced LFC at operation.

At t = 25 s, the load increases to 240 kW. The same event is repeated wherein the BESS and generator have to reach the load sharing point reached at 59.86 Hz. Based on the BESS control design, now the battery works on Region 1 droop side. In this region, the BESS delivers 4.741kW while the generator supplies 233.8 kW.
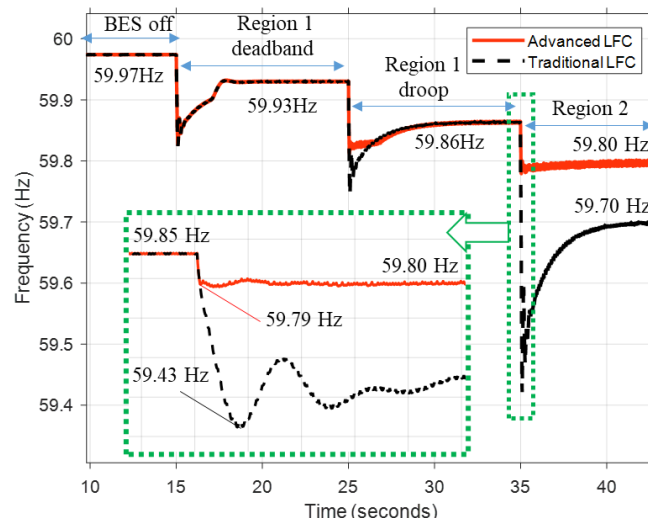
(a)
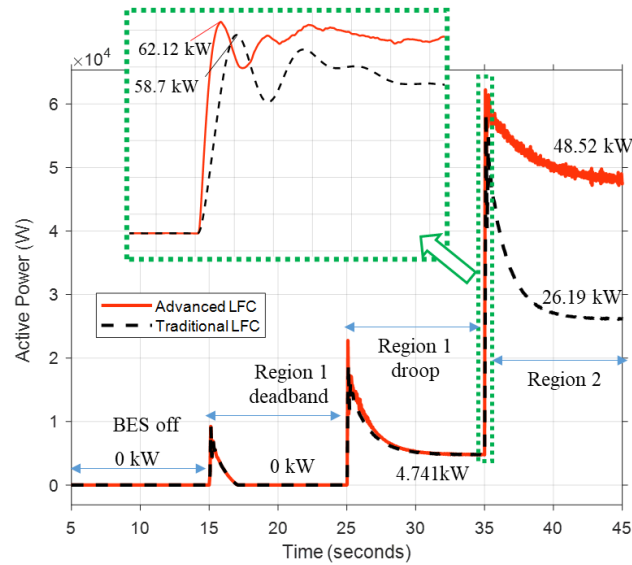
(b)
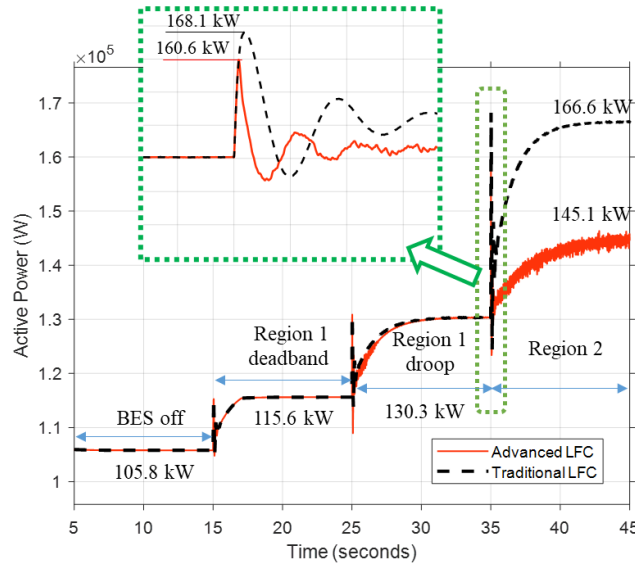
(c)

(d)

Figure 2.15 Load increasing case result; (a) frequency, (b) BES output power, (c) diesel generator output power, (d) inertia comparison

Finally, the load increases to 295 kW at t=35 s. Using the traditional LFC, the system operates at 59.7 Hz, which causes the generator to supply 166.6 kW of power and the BES to supply 26.19 kW. However, with the advanced LFC, BES tries to supply more power to reduce the portion of power that the generator must provide.

Thus, this operation causes the power supplied by BES to be 48.52 kW and the power supplied by the generator to 145.1 kW. In this condition, the system operates at 59.8 Hz. This operation shows that the proposed control can change the battery participation so that the system frequency is constant at 59.8 Hz. These results indicate that the LFC settles the generator output at the desired value by continuously regulating the BES output power.

Figure 2.15 (d) shows the power of the diesel generator when the load changes at t = 35 s by comparing the inertia of different engines. The inertia 1x is stated as the smallest inertia, while the inertia of 50x is stated as the enormous inertia. The least inertia is the inertia that can be applied to diesel engines. In the case of an increase in load, it is seen that each inertia gives a similar transient reaction. Generally, when an increase occurs, the generator will react first so that the output power increases sharply. The inertia of 1x or the smallest causes a faster reaction so that the generator reaches its highest and lowest values in a fast time. In contrast to the inertia 50x or the largest gives a little time for the generator to change its power. In this case, inertia causes a difference in the transient response of the generator but does not affect the operation of the proposed control.

2.5.2 Case 2 – Load decreasing

In this case, the load decreases gradually from 200 to 110 kW. The system is initiated at 60 Hz with the load demand of 200 kW, which puts BESS in standby mode. Figure 2.16(a),(b),(c),(d) illustrates the grid frequency, active power of BES, generator, and generator active power for different inertia respectively. However, due to the installed distribution line, the grid starts operating at 60.02 Hz.

At t = 15 s, the load changes to 185 kW. This event causes the frequency to rise as the generator is trying to stabilize the system. The rise in the system frequency causes the battery to start operating and participating in the system. BESS's participation

creates a load-sharing point that the BESS and generator must satisfy due to the power imbalance. The point is reached at 60.06 Hz, and the deadband area puts the BESS in standby mode. This condition states that the proposed control Region 1 deadband area.

At t = 25s, the load decreases to 165 kW. The same event is repeated as the battery, and the generator must find another load sharing point that reached 60.13 Hz
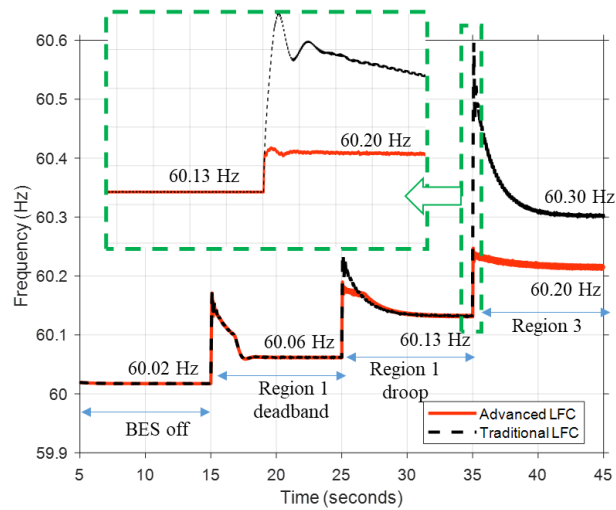
(a)

(b)
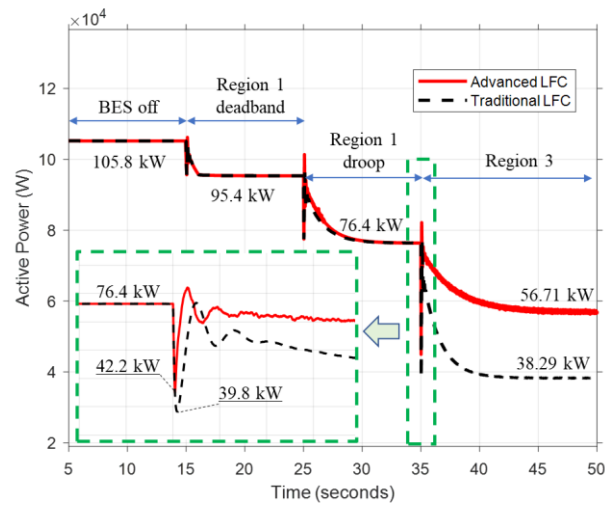
(c)

(d)

Figure 2.16 Load decreasing case result; (a) frequency, (b) BES output power, (c) diesel generator output power, (d) inertia comparison

(Region 1 droop side). In this region, the generator delivers 70.54 kW, and the battery delivers –4.22 kW.

Finally, the load decreases to 110 kW at t=35 s. Using the traditional LFC, the system operates at 60.3 Hz, which causes the generator to supply 33.32 kW of power and BES to supply –26.57 kW. However, with the advanced LFC, BES tries to absorb more power so that the portion of power that the generator must provide becomes more. This effort is made to reduce the frequency according to the control target. Thus, this operation causes the power supplied by BES to be –46.92 kW and the power supplied by the generator to 52.92 kW. In this condition, the system operates at 60.2 Hz. This operation shows that the proposed control can change the battery participation so that the system frequency is constant at 60.2 Hz. These results indicate that the LFC settles the generator output at the desired value by continuously regulating the BESS output power.

Figure 2.16 (d) shows the power of the diesel generator when the load changes at t=35 s by comparing the inertia of different engines. The inertia 1x is the smallest inertia applied to the engine, while the inertia 50x is the enormous inertia applied. These results indicate that the engine inertia affects the transient response of the generator. The smaller the inertia of the engine, the faster the generator will reach a steady value. However, small inertia causes a rapid change in generator power from the minimum to the maximum. This change may affect the stability of the system. On the other hand, large inertia affects the time to steady-state and the overshoot value. These results indicate that the difference in inertia does not affect the proposed control operation.

2.5.3 Case 3 – PV output increasing

In this case, the PV output increases gradually from 100 to 190 kW. The system is initiated at 60 Hz with the load demand of 200 kW and PV output 100 kW, which puts BESS in standby mode. Figure 2.17 (a),(b),(c),(d) illustrates the grid frequency, active power of BES, generator, and generator active power for different inertia

respectively. However, due to the installed distribution line, the grid starts operating at 59.97 Hz.
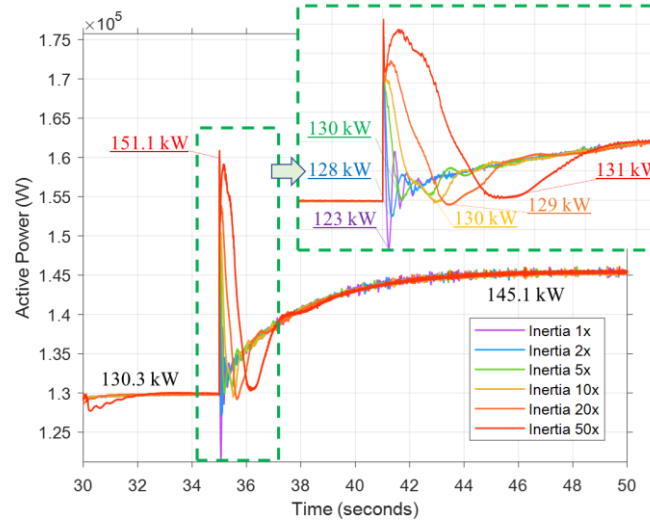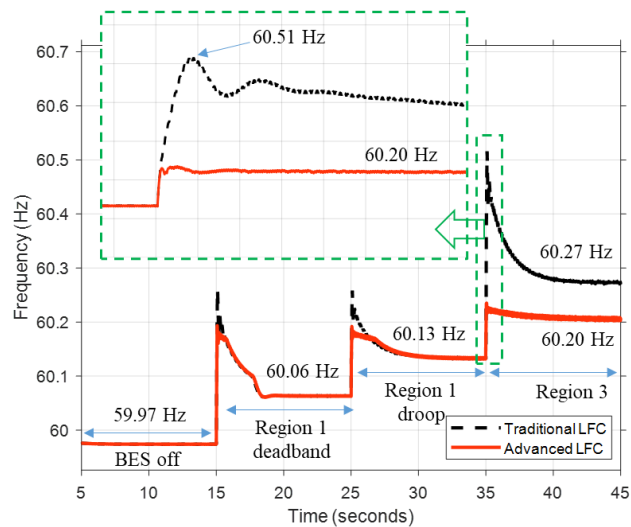

(a)
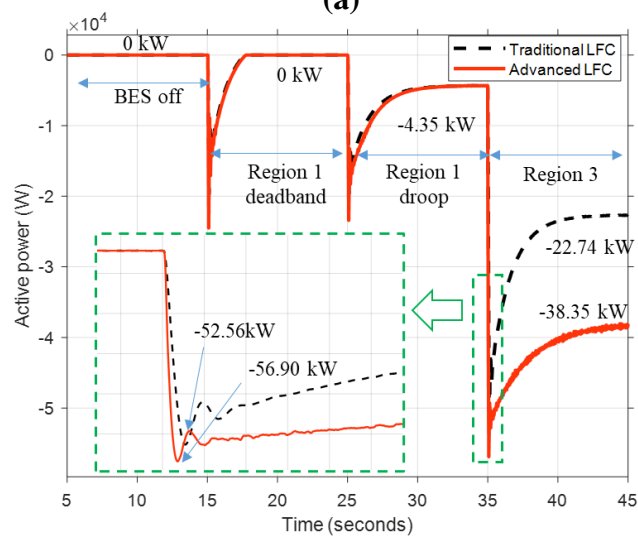
(b)
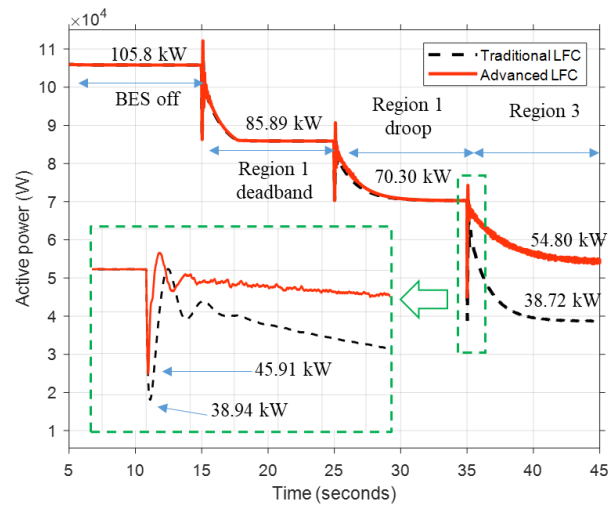
(c)
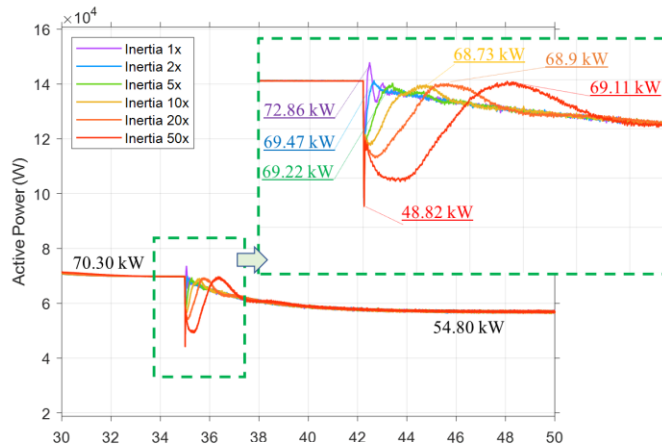
(d)

Figure 2.17 PV output increasing case result; (a) frequency, (b) BES output power, (c) diesel generator output power, (d) inertia comparison

At t = 15 s, PV delivers 120 kW. This incident caused the system to overload resources, causing generators and BES to swing and seek new operating points. The load-sharing point was reached at 60.06 Hz, causing BES to be in the Region 1 deadband area and the generator to supply 85.59 kW.

Then the PV power increases again to 140 kW at t = 25 s. The generator and battery continue to find the load-sharing points. The load sharing point was reached at 60.13 Hz, causing the generator to supply 70.30 kW and BES to supply -4.35 kW. It means that in this operation, the PV absorbs excess power from the system. It can be seen in this operation Region 1 droop is actively working.

Finally, the PV power reaches 190 kW. With the same load, the system is under excess power. Using the traditional LFC, the system operates at 60.27 Hz, which causes the generator to supply 38.72 kW of power and BES to supply –22.74 kW. However, with the advanced LFC, BES tries to absorb more power so that the portion of power that the generator must provide becomes higher. This effort is made to reduce the frequency according to the control target. Thus, this operation causes the power supplied by BES to be –38.35 kW and the power supplied by the generator to 54.80 kW. In this condition, the system operates at 60.2 Hz. This operation shows that the proposed control can change the battery participation so that the system frequency is constant at 60.2 Hz.

Figure 2.17 (d) shows the diesel power when the PV power increases at t=35 s by comparing the inertia of different engines. The results show that small inertia gives the fastest response so that the generator reaches a steady state. However, the time between the lowest and highest power is relatively fast. This change can affect the stability of the system. On the other hand, large inertia affects the time to steady-state and the generator power overshoot value. The results show that inertia does not affect the proposed control operation in this case.

2.5.4 Case 4 – PV output decreasing

In this case, the PV output decreases gradually from 100 to 30 kW. The system is initiated at 60 Hz with the load demand of 200 kW and PV output of 100 kW, which puts BESS in standby mode. Figure 2.18 (a),(b),(c),(d) illustrates the grid frequency,

active power of BES, generator, and generator active power for different inertia respectively. However, due to the installed distribution line, the grid starts operating at 59.97 Hz.
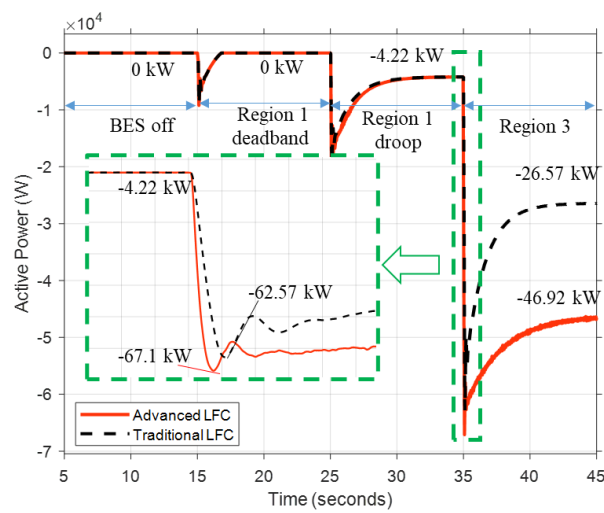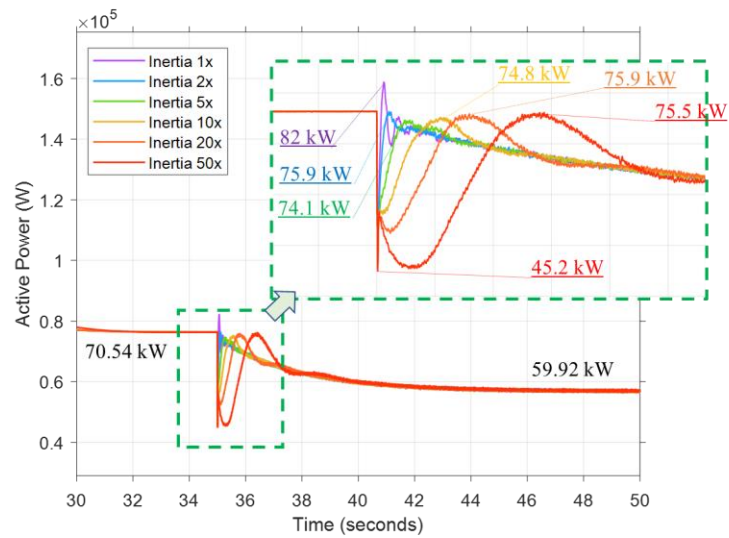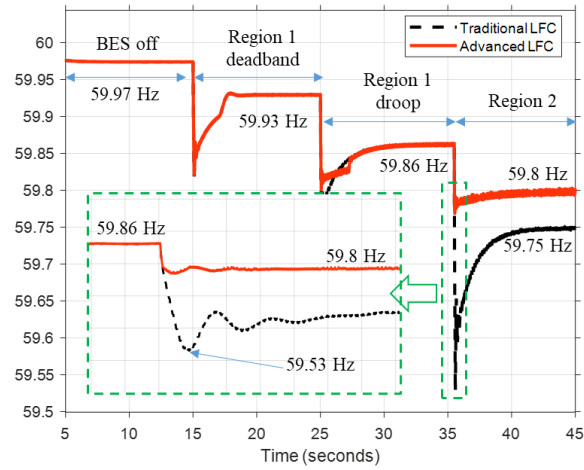

(a)
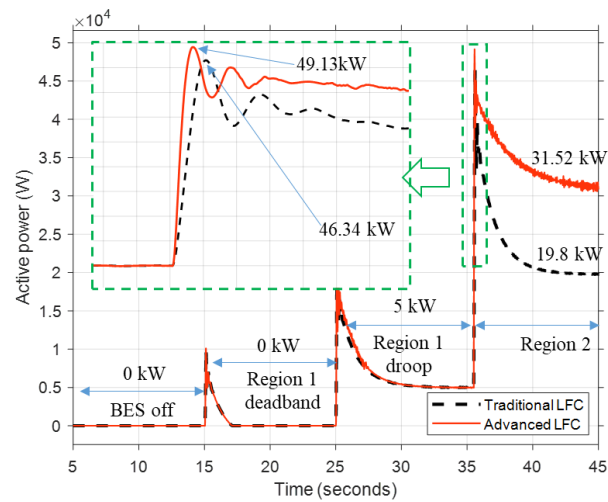
(b)
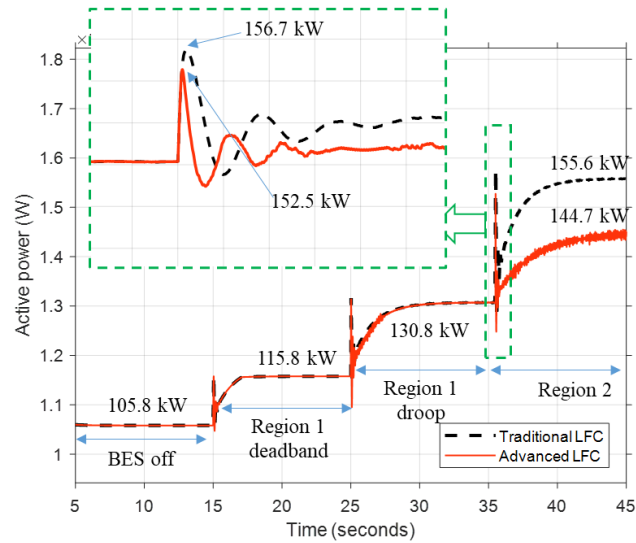
(c)
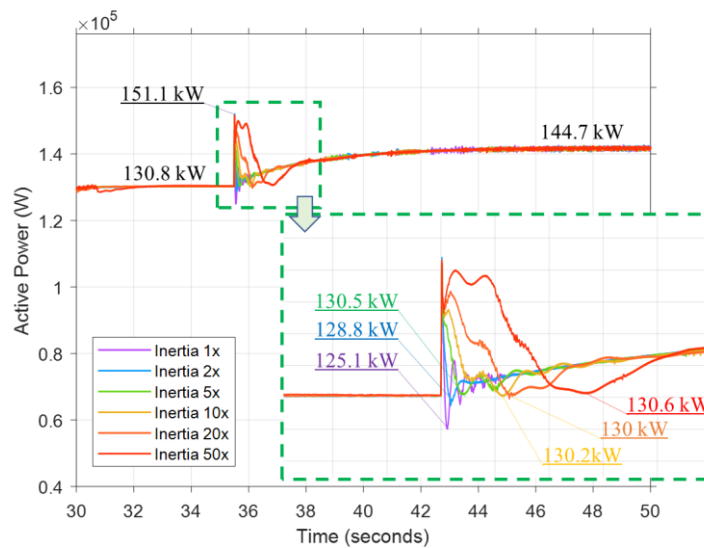
(d)

Figure 2. 18 PV output decreasing case result; (a) frequency, (b) BES output power, (c) diesel generator output power, (d) inertia comparison

At t = 15 s, PV delivers 90 kW. This incident caused the system to suddenly run out of power, causing the generator and BES to swing and look for new operating points.

The load-sharing point reaches 59.9. Hz, causing BES to be in Region 1 deadband area and the generator to supply 115.8 kW.

Then the PV power drops again to 70 kW at t = 25 s. The load sharing point is reached at 59.86 Hz, causing the generator to supply 130.8 kW and BES to supply 5 kW. It can be seen in this operation, Region 1 droop is actively working.

Finally, the PV power reaches 30 kW. With the same load, the system experiences a power shortage. Using the traditional LFC, the system operates at 59.75 Hz, which causes the generator to supply 155.6 kW of power and BES to supply 19.8 kW. However, with the advanced LFC, BES tries to deliver more power so that the portion of power that the generator must provide becomes lower. This effort is made to keep the frequency according to the control target. Thus, this operation causes the power supplied by BES to be 31.52 kW and the power supplied by the generator to 144.7 kW. In this condition, the system operates at 59.8 Hz. This operation shows that the proposed control can change the battery participation so that the system frequency is constant at 59.8 Hz.

Figure 2.18 (d) shows the diesel power when the PV power decreases at t=35 s by comparing the inertia of different engines. The results show that small inertia gives the fastest response so that the generator reaches a steady value. However, the time between the lowest and highest power is relatively fast, so it can affect the system's stability. On the other hand, large inertia affects the time to steady-state and the generator power overshoot value. The results show that inertia does not affect the proposed control operation in this case.

2.6 Conclusion

An advanced load-frequency control that utilizes battery capabilities to keep frequencies in a specific range is introduced. Region 1 functions to carry out the load-sharing mechanism between the diesel generator and the battery. Region 2 and Region

3 function to maintain the system frequency in the desired range. By changing the load installed on the system and PV output power, the proposed control's performance can be verified. The results show when in Region 2 or Region 3, BES changes its output power so that the frequency returns to the desired value. Moreover, the inertia comparison study confirms whether the proposed control is working on different inertia values.

Chapter 3

3 State-of-charge Control on Advanced Load-Frequency Control

3.1 Chapter Introduction

Previously, we discussed the structure of an advanced LFC. The proposed control allows active participation of the BES based on the control work areas. In terms of frequency, advanced LFC successfully answers problems and can help maintain frequency stability. However, keep in mind that the islanded microgrid system's operation is very volatile, both the load demand and the energy source for RES. By operating BES using advanced LFC, BES operations may fluctuate over time. This operation triggers BES degradation and causes short battery life.

When the battery has reached its age and cannot operate anymore, it must be replaced. Replacement of this component may be very detrimental to the operator, as the operator has to pay for battery replacement during a project period. Indeed, this cost is usually considered if the replacement is made in the middle of the project period. However, this replacement is very costly and makes the planning costs of battery usage very expensive.

Battery life is mainly caused by calendric aging and cyclic aging factors. Calendar aging occurs due to the nature of the BES itself. Aging is unavoidable but predictable and has entered into manufacturing calculations. Other factors are determined based on the operation of the BES during use. This factor is primarily due

to the depth of discharge of the BES and the number of cycles. The cycles must be taken into account so that the installation of advanced BES can still guarantee BES operation without considering the replacement of BES.

One of the simplest ways to preserve battery life is to keep the number of BES cycles minimum. Several studies suggest that by minimizing the depth of discharge of a battery, the number of cycles that can be performed is more significant. The greater the number of cycles, it extends the life of the battery. Thus, many studies on state-of-charge (SoC) control have been carried out to keep battery depth of discharge (DoD) to a minimum. However, for the implementation of BES in the islanded microgrid system, this is quite the opposite. BES is needed to regulate frequency, but on the one hand, DoD must be kept low so that battery life can be extended.

This chapter aims to propose SoC control on batteries. The proposed control is not an SoC control but an advanced LFC control which has a different function. Therefore, the proposed control is integrated with advanced LFC. Furthermore, the proposed control utilizes the shifting droop reference to alter the battery output control. This shift occurs based on the battery SoC information, which then changes the BES output. These changes eventually led to a change in the battery SoC. This phenomenon makes BES "as if" it has an SoC control in its control system. This control adopts a control strategy which is divided into five strategic scenarios. This strategy regulates how BES participates in the system based on the level of SoC currently held. Thus, BES's participation is not "blind" participation, but participation paid attention to other conditions.

3.2 State-of-charge (SoC)

One of the components that must be considered when discussing battery energy storage (BES) applications is the state-of-charge. SoC is static battery availability to operate. Usually, this status is represented as a percent (%) and counts zero to one

hundred. If the level is 100%, it shows the cell is said to be fully charged. Some batteries have limitations on their operation. However, it all depends on the type of battery used because a battery SoC is closely related to the battery life cycle and battery life.

The energy stored in the storage device is expressed as follows [48], [65]–[67]. If P_b is the battery output power, on charging mode ($P_b(t) < 0$), the power limitation and SoC calculation are written as:

$$-\eta P_b(t)\Delta t \le K_C E_b \tag{3.1}$$

$$SoC(t+1) = SoC(t) - \eta P_b(t)\Delta t \tag{3.2}$$

on the contrary, the power limitation and the SOC calculation when the BESS is in discharging mode ($P_b(t) > 0$) are respectively expressed as:

$$\frac{P_b(t)\Delta t}{\eta} \le K_C E_b \tag{3.3}$$

$$SoC(t+1) = SoC(t) - \frac{P_b(t)\Delta t}{\eta} \tag{3.4}$$

where η is the BES efficiency, K_c is the maximum portion of the rated capacity that can be added and released in an hour which determines the relation between the battery power and energy, E_b is the rated maximum stored energy, and Δt is the scheduling interval used in the study [66].

In a droop-based LFC, the output power of the generator is proportional to the system frequency. Without any control changes, the generator continues to supply power according to the predetermined ratio. However, the droop curve shift can create changes in the generator output power [25]. On the other hand, the BESS output power determines the SoC BESS at one time. For the SoC to be maintained within a

predetermined range, BES must change its output power. Therefore, by applying a droop-based LFC to the BES, droop shifting allows the BES to change its output power while operating thus, allowing the SoC BES to remain at the desired limits.

3.3 Integrated State-of-charge control with advanced LFC

Islanded microgrids share the same issue with stand-alone systems, namely satisfying the load balance and regulate the system microgrid voltage and frequency.

SoC (%)

100

SoC^{max2}

| Upper Critical State (UCS) |
| - Stop operating |

| Upper Limit (UL) |
| - Gradually decrease charging power |
| - Keep regulating system frequency |

SoC^{max1}

| Power Sharing (PS) |
| - Share the load power with other units |
| - Supply deficit power |
| - Absorb exceed power |

SoC^{min1}

| Lower Limit (LL) |
| - Gradually decrease discharging power |
| - Keep regulating system frequency |

SoC^{min2}

| Lower Critical State (LCS) |
| - Stop operating |

0

Figure 3.1 Five scenarios control strategy

In both cases, the control strategy should consider the SoC limits and the battery capacity [68]. An SoC control strategy that determines the BES operation for each region is discussed in this subsection.

The proposed SoC control strategy is shown in Figure 3.1. This strategy is divided into five control scenarios according to the SoC condition. These scenarios are upper critical state (UCS), upper limit (UL), power sharing (PS), lower limit (LL), and lower critical state (LCS). The proposed strategy can be performed by implementing a

shifting droop control as the battery SoC control. The colored lines in Figure 3.2 show the BES LFC with the SoC control effect. If we recall again from the previous chapter, the deadband droop equation can be written as:

$$f_{dh} - (f^0 \pm \Delta f^s) = K_b(P_{bdh} - P_b^0) \tag{3.5}$$

Thus, by applying the droop equation (3.5), the colored curve shift can be expressed as:

$$f_{dh} - \left(f^0 \pm \Delta f^s + \Delta f^n\right) = K_b\left(P_{bdh} - P_b^0\right) \tag{3.6}$$

where Δf^n is frequency shift. The frequency shift is determined based on the control scenario. Later in this section, Δf^n will be defined. When the SoC level is between SoC^{max1} and SoC^{min1}, the BES operates on PS shown by the green line. There is no frequency shift applied in this scenario. Thus, Δf^n equals zero. This operation aims to satisfy the power balance by regulating output power to satisfy the power balance and keep the frequency within f^{max} and f^{min}. Assume a load demand P_L^1 is applied, the
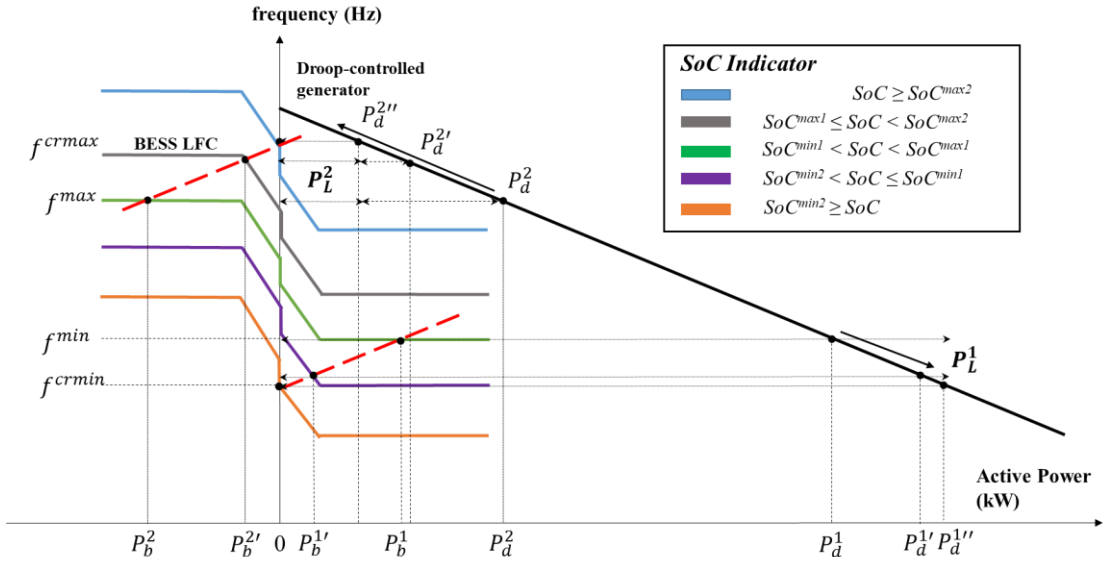
Figure 3.2 Proposed state-of-charge (SOC) control scheme

battery delivers $P_b{}^1$ while the generator delivers $P_d{}^1$. If the load demand $P_L{}^2$ is applied, the BESS delivers $P_b{}^2$ while the generator delivers $P_d{}^2$.

By operating the battery at $SoC^{max1} \leq SoC < SoC^{max2}$, the scenario changes to UL, illustrated by the grey line. This scenario allows the LFC curve (green line) to shift by Δf^n. It affects the nominal frequency of BES to shift to $f^0 + \Delta f^s + \Delta f^n$ where Δf^n can be written as:

$$\Delta f^n = f^{crmax} - f^{max} \tag{3.7}$$

This operation shifts the maximum frequency to be f^{crmax}. By changing the nominal frequency, the operation point of BES and generator are changed. Assume the load $P_L{}^2$ is applied while BES charges its energy. In this case, the BES delivers $P_b{}^{2'}$ and the generator output changes to $P_d{}^{2'}$. This operation makes the BES and the generator establish a new operating point. By substituting equation (3.7) to equation (3.6), the curve can be expressed as:

$$f_{dh} - \left[f^0 + \Delta f^s + \left(f^{crmax} - f^{max} \right) \right] = K_b \left(P_{bdh} - P_b^0 \right) \tag{3.8}$$

On the other hand, LL is activated when $SoC^{min2} < SoC \leq SoC^{min1}$, illustrated by the purple line. This scenario allows the LFC curve (green line) to shift by Δf^s. It affects the nominal frequency of BES shifting to $f^0 - \Delta f^s + \Delta f^n$ where Δf^n can be written as:

$$\Delta f^n = f^{crmin} - f^{min} \tag{3.9}$$

This operation allows the minimum frequency to be f^{crmin}. By changing its frequency limitation, the operation point of BES and generator are changed. Assume the load demand $P_L{}^1$ is applied. The BES delivers $P_b{}^{1'}$ while the generator delivers $P_d{}^{1'}$. By substituting equation (3.9) to equation (3.6), the curve can be expressed as:

$$f_{dh} - \left[f^0 - \Delta f^s + \left(f^{\text{crmin}} - f^{\text{min}} \right) \right] = K_b \left(P_{bdh} - P_b^0 \right) \qquad (3.10)$$

The UCS is activated when the SoC level is over SoC^{max2}. In this scenario, the BES stops its operation that brings the SoC to remain at this level. Assuming that the load P_L^2 is applied, the BES power becomes zero. Hence, the generator satisfies the load demand by delivering P_d^{2}". On the contrary, the LCS illustrated by the orange line actively operates if the SoC level is below SoC^{min2}. Assuming that the load P_L^1 is applied, the BES stops its operation. It causes the generator to meet all load demands by delivering P_d^{1}".

In this control, the SoC level has a significant impact on the amount of battery output power, so the battery power continuously varies according to the SoC level. From P_b^1 to zero or from P_b^2 to zero, all those variations can be correlated using a straight line illustrated by the dashed red line in Figure 3.2. This line describes BES power's movement in the presence of the droop reference shift due to SoC. The red line shows the relation between frequency shift Δf^n and power changes ΔP_b^n. The line has an identical slope as the generator droop curve. Thus, the relation between frequency shift and power changes written as:

$$\Delta P_b^n = \Delta f^n \times \frac{1}{R} \qquad (3.11)$$

where ΔP_b^n is the BES power changes, Δf^n is the frequency shift, and R is the generator droop gain. When the battery enters the critical state, both UCS and LCS, the droop reference shifts according to the generator droop's slope level described in equation (3.11). This shift causes the battery output to zero, so it can be written as:

$$0 - P_{bdh} = \Delta f^n \times \frac{1}{R}$$

Hence, it can be simplified into Equation (3.12).

$$-P_{bdh} \times R = \Delta f^{n} \tag{3.12}$$

Thus, by substituting equation (3.12) into equation (3.6), the Region 1 advanced LFC can be written as:

$$f_{dh} - \left[f^{0} \pm \Delta f^{s} + \left(-P_{bdh} \times R \right) \right] = K_{b} \left(P_{bdh} - P_{b}^{0} \right) \tag{3.13}$$

It can be concluded that a frequency shift is applied to the BES LFC curve in every scenario. Thus, the frequency shift Δf^{n} is written as in equation (3.14).

$$\Delta f^{n} = \begin{cases} -P_{bdh} \times R; & SoC \geq SoC^{\max 2} \\ f^{crmax} - f^{\max}; & SoC^{\max 1} \leq SoC < SoC^{\max 2} \\ 0; & SoC^{\min 1} < SoC < SoC^{\max 1} \\ f^{crmin} - f^{\min}; & SoC^{\min 2} < SoC \leq SoC^{\min 1} \\ -P_{bdh} \times R; & SoC \leq SoC^{\min 2} \end{cases} \tag{3.14}$$

Every shift in equation (3.14) is substituted into the LFC equation (2.28) so that the reference shift applies in each region. Finally, the LFC curve that includes the SOC control is shown below:

$$P_{bdh} = \begin{cases} \dfrac{f_{dh} - \left(f^{0} + \Delta f^{s} + \Delta f^{n} \right)}{K_{b}} + \left(\dfrac{f^{\max} - f_{dh} + \Delta f^{n}}{R} \right) + P_{b}^{0}; & f_{dh} \geq f^{\max} + \Delta f^{n} \\[4mm] \dfrac{f_{dh} - \left(f^{0} + \Delta f^{s} + \Delta f^{n} \right)}{K_{b}} + P_{b}^{0}; & f^{0} + \Delta f^{s} + \Delta f^{n} \leq f_{dh} < f^{\max} + \Delta f^{n} \\[4mm] 0; & f^{0} - \Delta f^{s} + \Delta f^{n} < f_{dh} < f^{0} + \Delta f^{s} + \Delta f^{n} \\[4mm] \dfrac{f_{dh} - \left(f^{0} - \Delta f^{s} + \Delta f^{n} \right)}{K_{b}} + P_{b}^{0}; & f^{\min} + \Delta f^{n} < f_{dh} \leq f^{0} - \Delta f^{s} + \Delta f^{n} \\[4mm] \dfrac{f_{dh} - \left(f^{0} - \Delta f^{s} + \Delta f^{n} \right)}{K_{b}} + \left(\dfrac{f^{\min} - f_{dh} + \Delta f^{n}}{R} \right) + P_{b}^{0}; & f_{dh} \leq f^{\min} + \Delta f^{n} \end{cases} \tag{3.15}$$
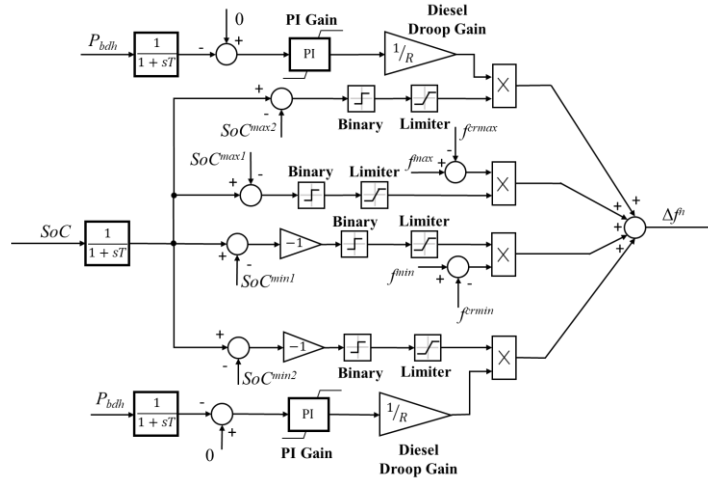
Figure 3.3 SoC control block diagram

Equation (3.15) shows the completed LFC with SoC control. This control allows a load-sharing mechanism in BES that monitors its SoC at the predetermined range. A block diagram of the proposed SoC control is shown in Figure 3.3. This control is distributed into four parts: top to bottom, UCS, UL, PS, LL, and LCS. The UCS and LCS scenarios use PI control (K_{psoc} and K_{isoc}) to maintain the battery output at zero, resulting in a frequency shift with zero BES output power. Both the UL and LL scenarios only use simple mathematical operations because the frequency shift has been f^{crmax} or f^{crmin}. This block's result is a frequency shift passed on to the LFC block in Figure 3.3. Combining the advanced LFC block diagram in Figure 2.7, the completed control block diagram containing LFC and SoC control is shown in Figure 3.4. This figure shows that the SoC condition at one time affects the BES output power obtained from the LFC.

3.4 Detailed System Model

Same to the system in Chapter 2, the microgrid system model used in this study refers to [20]. According to the reference, the study modeled the microgrid system in the Philippines. Both source capacity and load size were obtained. It is assumed that
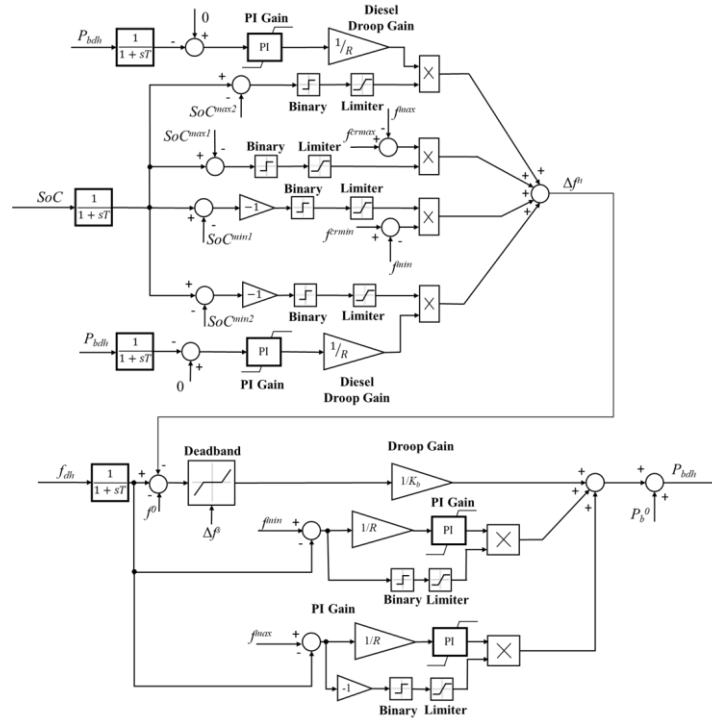
Figure 3.4 Completed SoC control with Advanced

LFC

the system mainly relies on diesel power generation, which implies high generation and operational costs due to varying fuel costs and transport costs. The load demand used in the study is based on the average load profile obtained from the actual data of 22 islands in the country. From these data, it is known that the load is never below 50% of the peak load. However, this study tries to demand a lower load than that obtained because the load characteristics are rural consumers. The data also states that the peak load is defined as 50% of the installed power generation capacity without a battery [56].

In this experiment, two types of experiments with different systems are carried out. The first system is used to verify the system at short notice, while the second system is used to verify the system when it is operating on one day and the system operation in one year. Thus, in this section, the three systems are introduced. The systems model must be explained because the size of the battery carried out at a short

time is different from that of the others. The software used is also different for short-term operations by one day and one year.

3.4.1 Short-term system model

In the short-term study, the proposed control is verified by applying a system model similar to the model used in Chapter 2. The system used is an islanded microgrid system consisting of a diesel generator, PV, BES, and load. The size of the system used is also the same as that used in Chapter 2. However, now the battery size is also determined to calculate the SoC of the battery each time. The measure used is a measure that makes it easier for SoC investigations that are not possible in the application. In
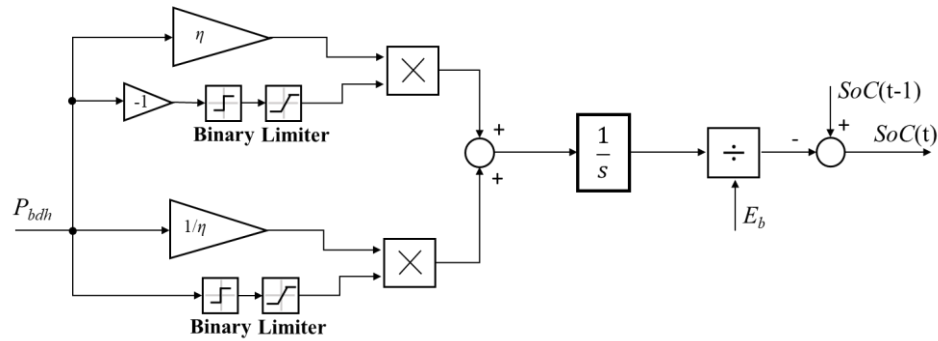
Figure 3.5 Battery SoC calculation model

this study, the battery model used in MATLAB / Simulink is the same as the model used in Chapter 2, but there are additional blocks for SoC calculations. Based on equations 3.2 and 3.4, the block diagram used is shown in Figure 3.5

Table 3.1 Short-term operation BES parameter

Description	Parameter	Value
BES Capacity	E_b	2 Ah
BES efficiency	η	85%
Deadband area	Δf^s	0.1 Hz
Maximum frequency	f^{max}	60.2 Hz
Minimum frequency	f^{min}	59.8 Hz
Shifted frequency max limit	f^{crmax}	60.3 Hz
Shifted frequency min limit	f^{crmin}	59.7 Hz

SOC control proportional gain	K_{Psoc}	0.1
SOC Control integrator gain	K_{Isoc}	0.1
Initial SOC	$SOC^{initial}$	60.00%
	SOC^{max2}	75.00%
	SOC^{max1}	70.00%
BESS SOC level	SOC^{min1}	50.00%
	SOC^{min2}	45.00%

The proposed control SoC has a function to shift the LFC curve according to the battery SoC information. The limit values of SoC, SoC^{max2}, SoC^{max1}, SoC^{min1}, and SoC^{min2}, are predefined. The steps that can be taken to determine the limit value determine UCS and LCS's parameter values. This value determines which area BES can work so that BES stops working when the SOC is lower than SoC^{min2} or greater than SoC^{max2}. Then SoC^{max1} and SoC^{min1} are determined in the area where BES can work optimally. Some studies say that it is good to operate between 40-80% for some types of batteries. This range can be used as a reference for verifying control performance. However, in this experiment, verification is not yet an application, so that all tests carried out only based on the control can read the SoC value and convert it into a command to change the output power. The BES model and control parameter is represented in Table 3.1.
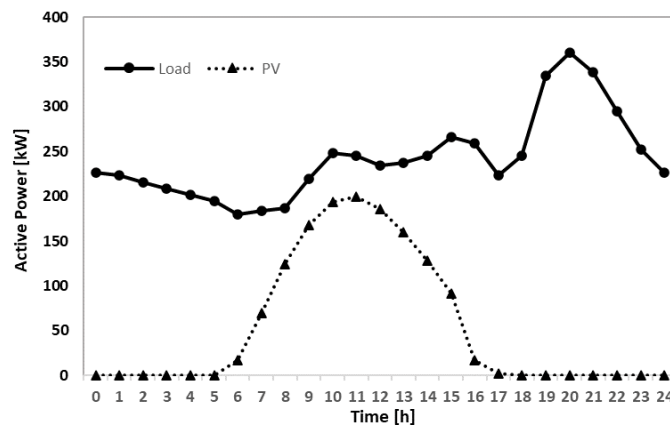
Figure 3.6 Load & PV output profile for one-day operation [20],[70]

3.4.2 One-day & one-year operation system model
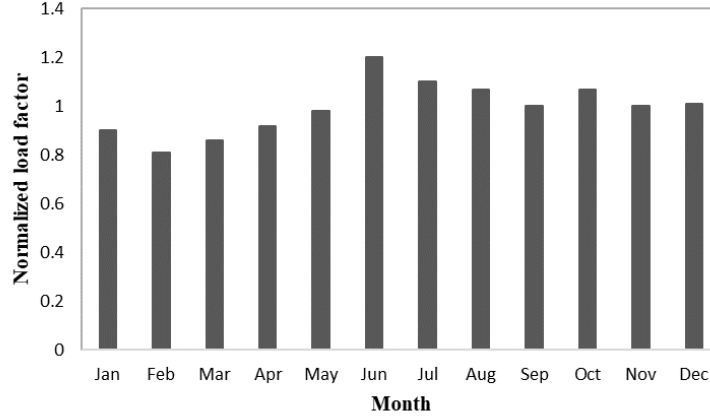
Figure 3.7 Load factor for one-year operation [20]

In this operation, the system considered is a microgrid composed of a combination of PV, BES system, and conventional droop-controlled units (in this study diesel generator is utilized). Each of these units is connected to the microgrid AC bus, as discussed in the previous section. This configuration is obtained by combining the systems described in [69]. The microgrid that contains a diesel generator with a rating is 390 kW, a PV array with maximum output power is 200 kW, and BES with a capacity of 65 MWh/50 kW is utilized to investigate the proposed BES control. The hourly data of renewable DER (PV) and loads are obtained from [70] and [20], shown in Figure 3.6, respectively. In this study, the load factor is also obtained from [20] to represent load variation in the 1-year operation shown in Figure 3.7. By using this model, one-day operation and one-year operation experiments are conducted.

Table 3.2 One-day & one-year operation BES parameter

Description	Parameter	Value
BES capacity	E_b	65 MWh
Deadband area	Δf^s	±0.1 Hz
Maximum frequency	f^{max}	60.2 Hz
Minimum frequency	f^{min}	59.8 Hz
Shifted operation limit	f^{crmax}	60.3 Hz
	f^{crmin}	59.7 Hz

Description	Parameter	Value
Generator droop gain	R	0.03 pu
BES droop gain	K_b	0.05 pu
Battery efficiency	η	85%
Initial SoC	SoC^{initia}_l	50%
	SoC^{max1}	90%
	SoC^{max1}	70%
BES SoC level	SoC^{min1}	40%
	SoC^{min1}	30%

This simulation is carried out using Microsoft Excel so that the calculation of output power, frequency, and SoC is based on the mathematical calculations that have been described (both this chapter and the previous chapter for other controls). Thus, the generator swing characteristics are not reflected in this operation, likewise with the battery model. The battery model is based on the battery equation described in this chapter. By borrowing the battery data from [71], the battery control parameters are given in Table 3.2, along with the operating limits. As the control parameter SOC^{max2}, SOC^{max1}, SOC^{min1} and SOC^{min2} respectively are set to 90%,70%, 40%, and 30%.

Deadband droop control, the traditional LFC, and advanced LFC are also simulated to evaluate the proposed control's performance. Both traditional and advanced LFC are used as a comparison to the proposed control. The traditional LFC is a droop control that has a deadband function. It is similar to advanced LFC but is only composed of Region 1. On the other hand, as described in the previous section, the advanced LFC is a deadband droop control with a frequency limit.

3.5 Results and Discussion

3.5.1 Short-term operation

3.5.1.1 Case 1 – Load increasing

In this case, the load increases from 200 kW to 295 kW. The system is initiated at 60.02 Hz and SoC at 60%. Figure 3.8(a)–(c) illustrates the BES active power, system frequency, and SoC. At t = 10 s, the load increases to 295 kW. It causes the system
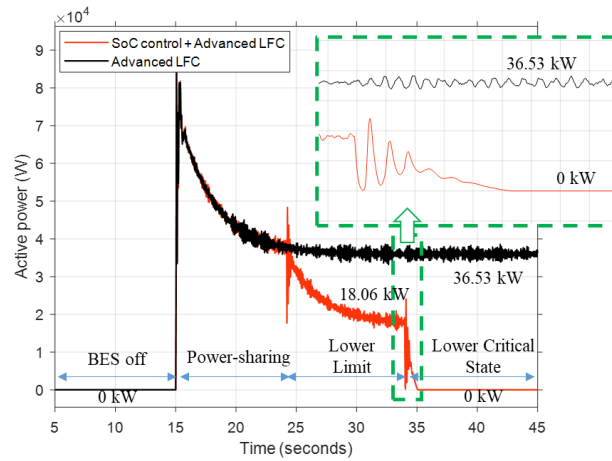
(a)
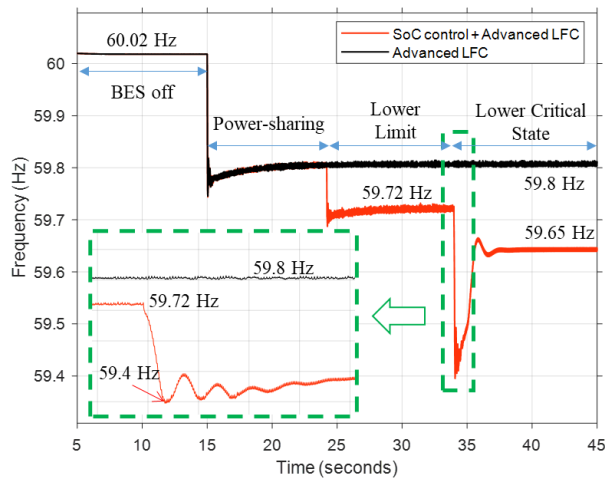
(b)
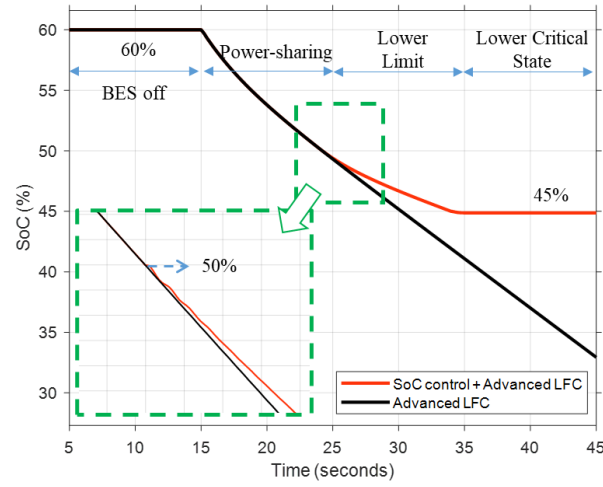
(c)

Figure 3.8 Short-term operation - load increasing; (a) BES
active power, (b) frequency, (c) BES Soc

frequency to drop from 60.02 Hz to around 59.78 Hz as the generator reaction. The
reaction triggers the BES to operate, shown in Figure 3.8(a) and Figure 3.8(b).

When the battery participates in the system, both generator and BES start
finding the load sharing point to keep the power balance. The point is achieved at 59.8
Hz while the BES supplies 29.2 kW. The power supplied by the BES results in a
decrease in SoC. It causes the SoC is decreasing to $SoC^{min1,}$ as shown in Figure 3.8(c).
At t = 20 s, the SoC operation changes from PS to LL, where the minimum frequency
limit changes to f^{crmin}, which puts the system frequency to 59.72 Hz. Changes in the
minimum frequency limit unnecessarily make the frequency at f^{crmin}, yet the frequency
still depends on the LFC curve. Now, the BES power drops to 18.06 kW, resulting in
a less sharp drop in SoC than the PS scenario. With the same load demand, the declining
SoC continues until it reaches SoC^{min2}. The SoC operation changes to LCS where BES
stops operating (returns to standby mode) and puts the SoC maintained at 45%. It
causes the frequency to drop to 59.65 Hz, which comes from the generator's governor
system. In contrast, without implementing SoC control, the frequency is maintained at

59.8 Hz. However, a continuously decreasing SoC may cause the SOC to be outside its operating limits or the battery to be undercharged.

3.5.1.2 Case 2 – Load decreasing

In this case, the load decreases from 200 to 110 kW. The system is initiated the same with the SoC control Case 1. Figures 3.9(a)-(c) illustrates the BES active power, system frequency, and the BES SOC, respectively. At t = 10 s, the load decreases to 110 kW. It causes the system frequency to rise to around 60.25 Hz as the system reaction. The reaction triggers the battery to operate, as shown in Figure 3.9(a),(b).
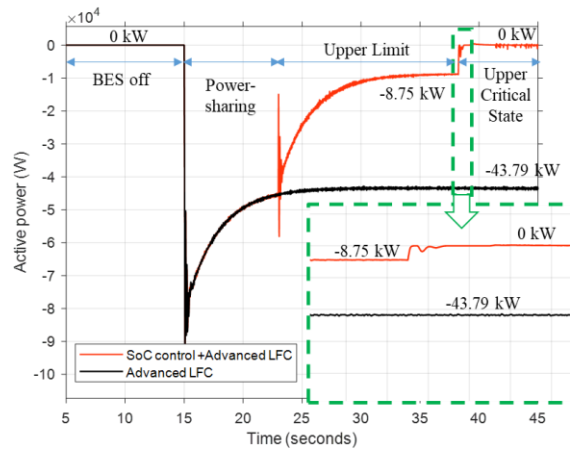
(a)
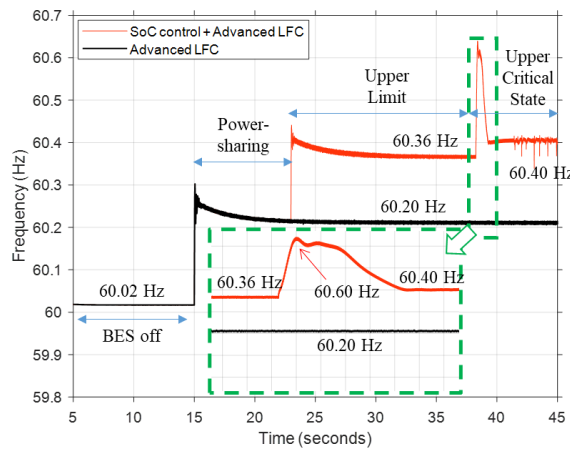
(b)
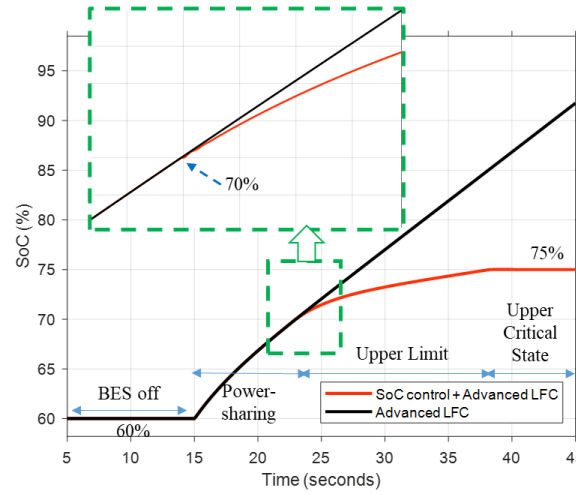
(c)

Figure 3.9 Short-term operation - load decreasing; (a)
BES active power, (b) frequency, (c) BES SoC

Once the battery participates in the system, both generator and battery start finding the load sharing point to keep the power balance. The point is achieved at 60.20 Hz when the battery delivers -43.79 kW. The power absorbed by BES increases SoC. It causes the SoC to increase to $SoC^{max1,}$ as shown in Figure 3.9(c). At t = 20 s, the SoC operation changes from PS to UL, where the maximum frequency limit changes to f^{crmax}, which puts the system frequency to 60.36 Hz. Changes in the maximum frequency limit unnecessarily make the frequency at f^{crmax}, yet the frequency still depends on the LFC curve. Now, the BESS charging power has dropped to -8.75 kW, resulting in a less sharp rise in SoC than the PS scenario. With the same load demand, the incline in SoC continues until it reaches SoC^{max2}. The SoC operation changes to UCS, where BESS stops operating (returns to standby mode) and puts the SoC maintained at 75%. It causes the frequency to rise to 60.40 Hz, which comes from the governor's system owned by the generator. In contrast, without implementing SoC control, the frequency is maintained at 60.20 Hz. However, a continuously increasing SoC may cause the SOC to be outside its operating limits or the battery to be overcharged.

3.5.1.3 Case 3 – PV output increasing

In this case, the load is maintained at 200 kW, while the PV power increases from 100 to 190 kW. The system is initiated at 60.02 Hz and SOC at 60%. Figure 3.10(a),(b),(c) illustrate the battery active power, system frequency, and the SoC, respectively. At t = 15 s, the PV increases to 190 kW. It causes the system frequency to rise to around 60.3 Hz as the system reaction against surplus power. The reaction triggers the battery to operate, shown in Figure 3.10(a) and (b).

(a)

(b)
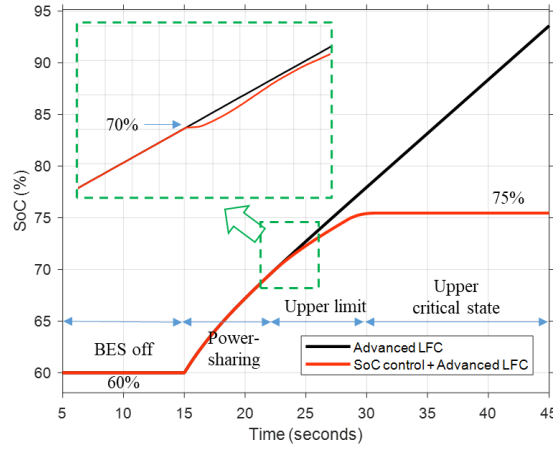
(c)

Figure 3.10 Short-term operation – PV output increasing; (a)
BES active power, (b) frequency, (c) BES SoC

Once the battery participates in the system, both generator and battery start finding the load sharing point to keep the power balance. The point is achieved at 60.30 Hz when the battery tries to deliver −45.92 kW, increasing BES SoC. It causes the SoC to reach $SoC^{max1,}$ as shown in Figure 3.10(c). At t = 20 s, the SoC operation changes from PS to UL, where the maximum frequency limit changes to f^{crmax}. It puts the system frequency to 60.3 Hz. However, changing the maximum frequency limit unnecessarily makes the system operates at f^{crmax}, yet the frequency still depends on the load-sharing point.

Now, the BESS charging power has dropped to −30.62 kW, resulting in a less intense rise in SoC than the PS scenario. With the same load demand, the incline in SoC continues until it reaches SoC^{max2}. The SoC operation changes to UCS, where BES stops operating (returns to standby mode) and puts the SoC maintained at 75%. It causes the frequency to rise to 60.42 Hz, which comes from the governor's system owned by the generator. In contrast, without implementing SoC control, the frequency

was maintained at 60.30 Hz. However, a continuously increasing SoC may cause the SoC to be outside its operating limits or the battery to be overcharged.

3.5.1.4 Case 4 – PV output decreasing

In this case, the load is maintained at 200 kW, while the PV power decreases from 100 to 20 kW. The system is initiated the same with the SoC control Case 3.
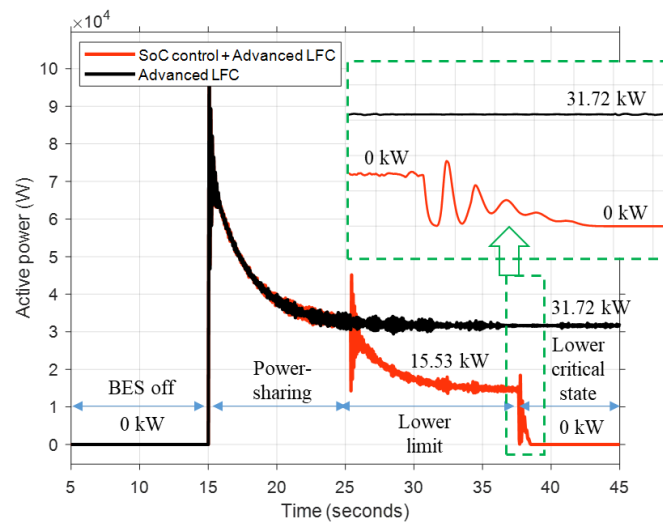
(a)
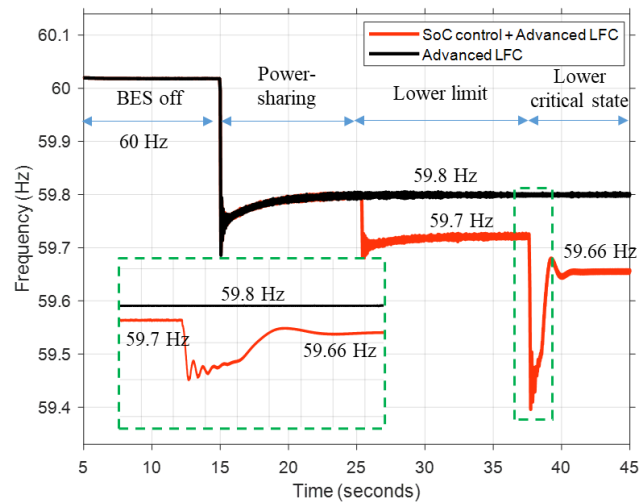
(b)
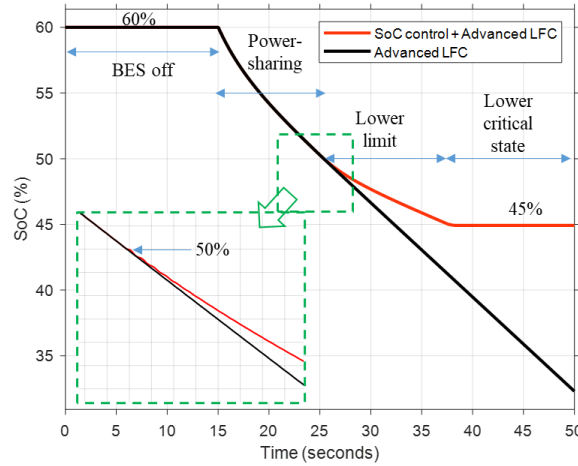
(c)

Figure 3.11 Short-term operation – PV output decreasing; (a)
BES active power, (b) frequency, (c) BES SoC

Figure 3.11(a),(b), and (c) illustrate the BES active power, system frequency, and the SoC, respectively. At t = 10 s, the PV decreases to 20 kW. It causes the system frequency to drop to around 59.7 Hz as the system reaction. The reaction triggers the battery to operate, as shown in Figure 3.11(a),(b).
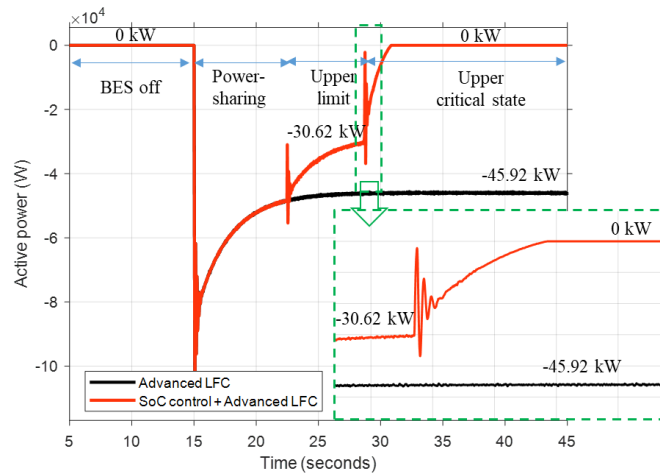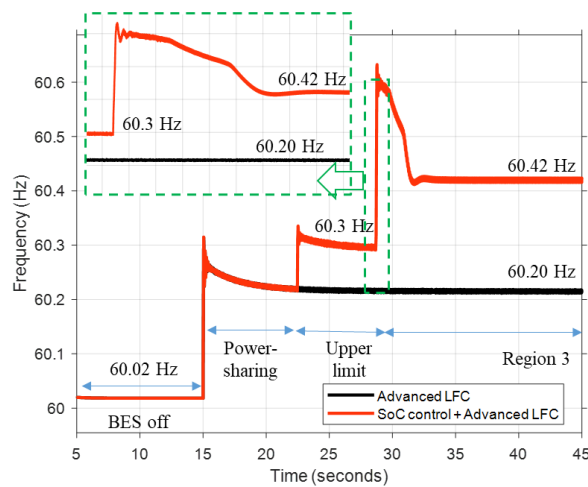
Once the battery participates in the system, both generator and battery start finding the load sharing point to keep the power balance. The point is achieved at 59.8 Hz when the battery tries to deliver 31.72 kW. The power delivered by the battery causes the SoC to drop. When the SoC reaches SOC^{min1}, the SoC control works and shifts the LFC curve of the battery. Now the operation changes from PS to LL, where the maximum frequency is shifted to f^{crmin}. This shift causes the system to operate at 59.7 Hz, which causes a slight reduction in the power delivered by the battery to 15.53 kW. Participation from the battery still makes the SoC move down until it finally reached SoC^{min2}. Now the operation has changed to LCS, so the battery must now stop operating. The battery that has not participated makes the generator compensate for the lack of power. As a result, the system frequency drops to 59.66 Hz. Stopping battery

operation is also synonymous with stopping the SoC drop at 45%. It can be seen that the proposed control keeps the SoC at a predetermined range by manipulating the output power of the battery. Compared to traditional LFC, the battery SoC steadily drops and causes the battery to be unable to participate when needed.

3.5.2 One-day operation

(a)

(b)

(c)
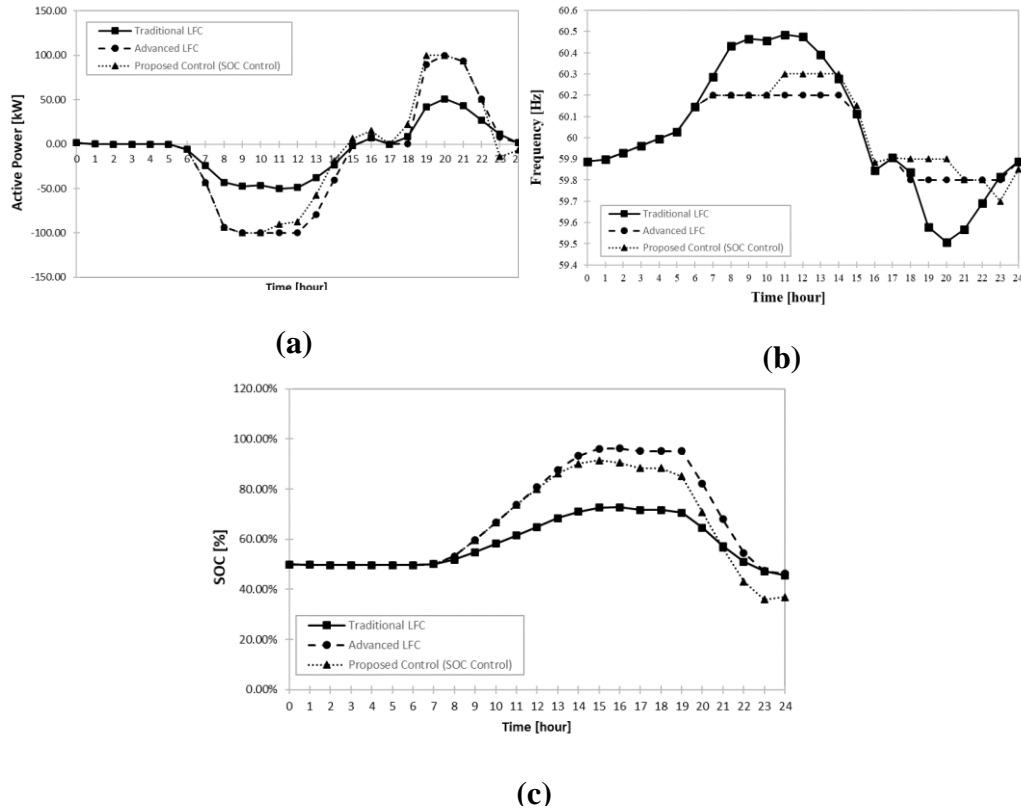
Figure 3. 12 One-day operation result; (a) BES active power, (b) frequency, (c) BES SoC

In this case, a one-day operation is conducted to investigate the proposed control operation. Figures 3.12(a)-(c) illustrates the BES active power, system frequency, and the BES SoC, respectively. When BES is operated using traditional LFC for one-day operation, the system frequency fluctuates between 59.48 – 60.46 Hz shown in Figure 3.12(b). It is achieved since the droop control allows BES to do load

sharing with the generator. An LFC control is introduced to improve the grid performance. The result shows LFC's use can improve the frequency value to be between 59.8 – 60.2 Hz. By applying this control, the system frequency can be suppressed at a specific value and put the diesel generator output indirectly suppressed by BES. The suppression causes BES to compensate for all the system changes where directly causes rapid SoC changes. Without operation restrictions on BES, the SoC may exceed 100% or less than 0%. Figure 3.12(c). shows that although the system frequency is maintained, the SoC level nearly exceeds 100%. In an actual application, it is impossible to put the battery SoC exceeds 100%, which the battery is overcharged. After the system frequency problem is resolved, the SoC problem with BES itself should not be left.

The proposed control, named advanced LFC with SoC control, is implemented to overcome this problem. By implementing shifted-droop control, BES regulates its output power while maintaining its SoC. In Figure 3.12 (a), there is a change in the power supplied by BES. This change is also in line with changes in the system frequency shown in Figure 3.12 (b). This change occurs when the SoC level touches the control parameter values shown in Figure 3.12 (c). It is achieved by the BES droop curve, which often changes depending on the level of SoC. At first, the results of this control are similar to the LFC result. However, at $t = 10$ h, when the SoC starts to reach SoC^{max}, the SoC control starts operating the Upper Limit. In this state, the BES charging power decreases to slow the SoC increasing rate represented in Fig. 3.12(c). Lower Limit operation is also encountered in this case. At t = 22 h, the SoC of the battery touches 40%, the lower limit or SoC^{min}. This event leads to change the operation to Lower Limit so that a shift in the Advanced LFC curve occurs. This shift led to different BES participation when compared to other controls. BES reduces the amount of power that must be supplied by it. This shift causes the BES operation to absorb power to avoid SoC^{min}. When applying the proposed control, the system frequency maintains

within the allowed range. Furthermore, BES SoC during operation can be maintained within the range of 50 – 90%.

3.5.3 One-year operation

The last verification is a one-year operation test. Figure 3.13(a) shows the system frequency result from all the controls, while Figure 3.13(b) shows the battery
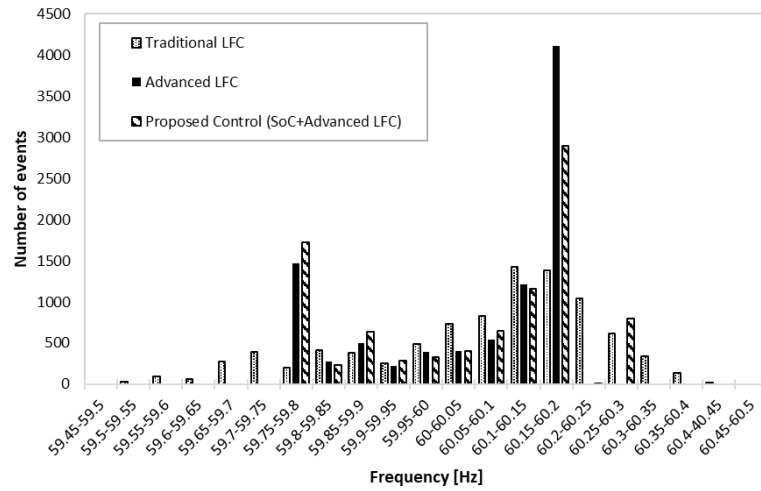
(a)
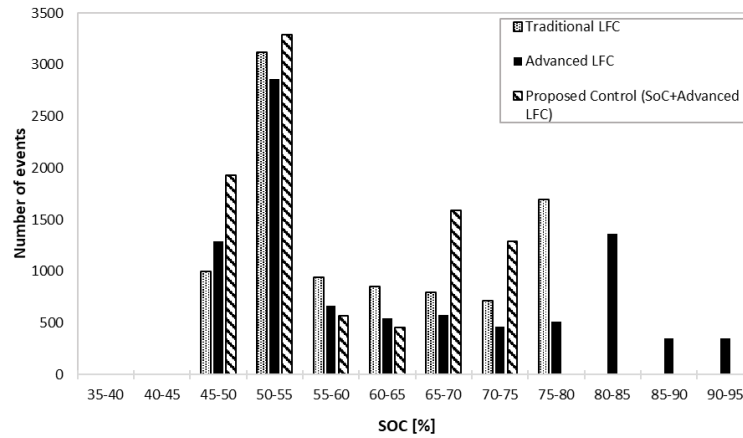
(b)

Figure 3.13 One-year operation result; (a) Number of
frequency events, (b) Number of SoC events

SoC. The frequency fluctuates between 59.5 – 60.4 Hz in a one-year operation when traditional LFC is performed. The advanced LFC implementation offers a frequency suppression that allows the frequency to fluctuate around 59.8 – 60.2 Hz. Compared to the traditional LFC result, the advanced LFC suppresses the frequency around the described range, which leads to around 4,000 events on 60.15 – 60.2 Hz. It means the battery regulating its output power to keep the frequency suppress at 60.2 Hz. The same result appears at the lower frequency side, roughly 1,500 events on 59.75 – 59.8 Hz. However, this participation brings a drawback to the battery. A considerable fluctuation in the SoC appears as the battery's participation, as shown in Figure 3.13(b). The SoC exceeds the limitation roughly 2,200 times, which does not apply to the implementation.

By using the proposed control, the SoC control is done by slightly relaxing the battery control frequency limitation (f^{max} -> f^{crmax}; f^{min} -> f^{crmin}). It leads the battery to reduce its output power when the SoC is outside of the desired range. Compared to the LFC, the proposed control brings a similar performance. The control allows the frequency is suppressed at f^{max} and f^{min} and shift to f^{crmax} and f^{crmin} if the SoC touches the control parameter. Figure 3.13(a) shows the proposed control allows the frequency to shift. The control puts the system frequency be 59.7 – 60.3 Hz when the SoC is outside the desired range. The frequency fluctuates around 60.25 – 60.3 Hz around 750 times. It means the frequency shifts to suppress the SoC while maintaining the power balance. It brings some differences to the SoC result, as shown in Fig. 3. The proposed control keeps the SoC to be around 45 – 75%.

The number of events in one frequency range on the LFC result is relatively high because the control suppresses the frequency at the f^{max} or f^{min}. However, this results in a wide SoC range in the battery (up to about 95%). On the other hand, the SoC control allows the frequency to become slightly wider than the LFC. The SoC control shifts f^{max} to f^{crmax} and f^{min} to f^{crmin}. This shift causes the battery SoC to fluctuate over a narrower area and within a predetermined range.

3.6 Conclusion

In this chapter, further application of advanced LFC is carried out by adding an SoC control feature based on the droop shift method. The proposed SoC control applies five control scenarios. Each control scenario provides a different BES operation based on the current SoC level. When the SoC level is outside the desired area, a shift in the LFC curve occurs so that BES changes its output power to maintain the SoC level. Control is verified through three operation cases, short-term operation, one-day operation, and one-year operation. The results show that by utilizing the proposed control, the BES can keep its SoC in the desired range by changing its output power, resulting in a slightly "relaxed" system frequency.

Chapter 4

4   Optimal Battery Energy Storage Sizing with Advanced Load-Frequency Control

4.1   Chapter Introduction

Electrical energy storage is recognized as underpinning technologies to have great potential to meet system stability challenges. As one of its kind, the deployment of battery energy storage (BES) is proposed. During the decision-making process of planning, information regarding the effect of BES on power system stability and economics is required before it can be introduced as a decision variable in the power system model. Using BES for frequency regulation, the system response to load variations is extremely fast because BES is a device based on power electronics containing a battery and inverter. Besides, many studies on BES have been carried out, so its ability to regulate frequency is more robust with greater capacity and lower self-discharge rates. In [72], a technical overview of battery energy storage systems and illustration of various operation modes for BES is introduced. Moreover, research related to BES frequency regulation is becoming an emerging research line due to increasing research in microgrid systems and RES fields [26], [72]–[74].

When discussing the advantages of BES, the significant issue of the battery must also be discussed. One of the main issues is the high price of BES equipment. This high cost is due to several things such as capital, operation, and maintenance costs so that BES can operate during its lifetime. Designers often overestimate battery sizes to guarantee reliability in the system. The designers are also afraid that if the BES size

is too tiny, the BES cannot operate according to its function. However, if the installed BES is too large, the BES can still operate, but the costs incurred to install the BES are too large. Therefore, many studies on BES sizing were conducted. Several studies have conducted sizing of BES by implementing frequency regulation [52], [71]–[77].

An emergency resistor is used to optimize BES with frequency regulation when over-frequency occurs. This method considers the state-of-charge (SoC) limits [75]. Research by [71] proposes a comprehensive BES sizing. This method is tested on a microgrid system by applying several operation scenarios. A control scheme using the optimal sizing of BES-based particle swarm optimization (PSO) with a load shedding scheme to improve the grid frequency after islanding occurred is proposed in [76]. In [52], a BES sizing strategy for primary frequency regulation is proposed. This method proposed a penalty function that depends on SoC. A paper investigating the impact of energy storage systems on low-inertia microgrids' frequency and voltage stability is conducted [77]. However, factors related to BES unit cost have to be considered, including an economic evaluation of its performance characteristics.

As discussed in the previous chapter, the problem of frequency stability can be resolved by implementing BES into the system. By implementing deadband droop control with frequency limits, advanced load-frequency control (LFC) performs better than traditional LFC. However, the proposed control study cannot stop at the technical discussion stage alone. Need further discussion to find out the system performance while the battery is operating. Moreover, the controls should be tested for a more extended period and a more pronounced system condition to describe the BES performance comprehensively.

Further investigation is needed whether, in a long period and more real system conditions, BES can fulfill its role in regulating frequency. Not only that, if an economic analysis is carried out, it is also necessary to investigate whether the proposed control has an economic advantage, namely lower costs than traditional LFCs. This

advantage can be realized if the BES size optimization is performed while the advanced LFC is implemented.

This chapter proposes a BES sizing that applies a frequency regulation function. The optimization model or expansion planning cost in this chapter covers the battery's investment costs as often done by many researchers and the microgrid operation cost. The microgrid operation cost consists of the fuel cost generated by the generator and the load curtailment. Active-frequency power control is applied to improve BES performance. An advanced LFC is used in BES as a function of power regulation. The control implements the droop control method that allows BES to supply power based on the system's frequency deviation. Also, a frequency limitation control is applied to LFC to maintain the system frequency within a specific range. This chapter discusses how the proposed control affects the battery size and the battery technology selection according to the expansion cost and the battery limitation, such as cycle life.

The rest of the paper is organized as follows: Section 2 describes the installation of BES. Section 3 describes the optimization model to find the optimal battery capacity. Section 4 outlines the optimization approach. The system model is explained in Section 5. The optimization results and the discussion on the proposed model are provided in Section 6 to demonstrate the proposed LFC benefits and validate its applicability. The conclusion is provided in Section 7.

4.2 Battery Energy Storage Installation

4.2.1 Battery Energy Storage Technology

Battery energy storage consists of several components: the battery bank, the DC-AC converter, the DC and AC filters, the protection circuits, and the step-up transformer [78]. The battery bank becomes the primary unit of BES. A significant development in battery technology is performed. Different types of batteries are being developed, of which some are available commercially while some are still in the

experimental stage [19]. There are some types such as lead-acid, lithium-ion (Li-ion), sodium-sulfur (NaS), nickel-cadmium (NiCd), and vanadium redox (VR). The lead-acid battery is the most mature technology, which has been employed for a majority of power system applications. Meanwhile, the Li-ion, NaS, and NiCd batteries represent the leading technologies in high-power-density applications [39].

In BES sizing terms, the battery capital cost is composed of power rating cost in $/kW and energy rating cost in $/kWh. Each technology offers different capital costs based on its characteristics. When choosing a battery technology, the low capital cost is not a critical factor [79]. It should also be noted other factors, such as life cycle, maintenance cost. Each technology has a different life cycle, high maintenance costs, and different operating temperatures, affecting the BES application in the system [80].

4.2.2 Battery Energy Storage Size

The BES capital cost mainly depends on battery size, both power, and energy rating. This cost positively affects the expansion planning cost. Figure 4.1 shows the expansion cost as a function of BES size [81]. Expansion planning costs consist of the battery capital cost and the microgrid operation cost. These two variables are key components to determine whether a BES can be implemented or not. The two of them
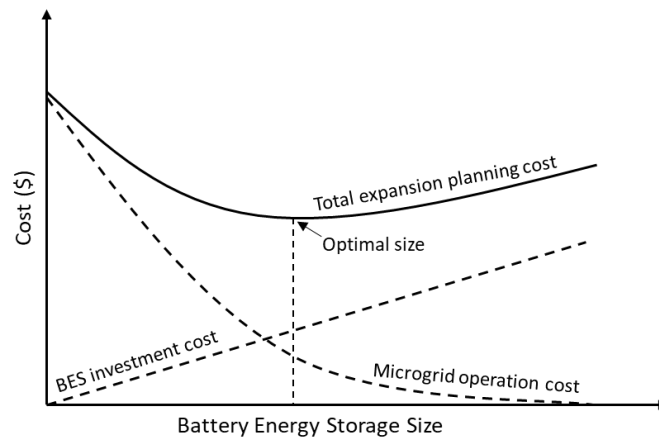
Figure 4. 1 Total expansion planning cost against BES size [81]

have different properties. When referring to Figure 4.1, the summation between the two variables shows the microgrid expansion plan curve or the BES installation plan cost.

Microgrid operation cost is the cost generated due to the operation of the generator in the system. This cost is broadly the fuel incurred by the operator to operate all generators in the system. These costs are based on the main driving force of the generator, also called the cost function. There are many types of prime movers, each of which has a different function. Generally, the cost function is represented by a second-order polynomial equation. This equation is not provided directly by the manufacturer. Manufacturers only provide prime mover operation reports from no load to full load. From these data, the cost function can be determined. There have been many studies conducted to model the cost function of a prime mover. Many studies write that each prime mover also has its uniqueness and operating characteristics that can affect cost functions. For expansion planning using BES in the islanded system, the greater the installed BES capacity, the cheaper the microgrid operating costs. It is because the greater the capacity of BES, the more significant the contribution made by BES. It impacts the lower the generator's power and the less fuel required to operate the generator.

The battery investment cost is proportionally linear with the battery size. Battery investment costs consist of battery capital costs, operation and maintenance costs. Often operating costs and battery capital costs only apply to one battery lifetime while maintenance costs are calculated annually. It is intended to maintain battery performance and ensure the battery can work in one project time. All of these costs depend on the size of the battery installed. In battery planning, size is often discussed. Apart from the economic side that must be considered, there is also a technical side that becomes the basis for planning the battery installation. Too small a battery size cannot participate in the system.

In contrast, an oversize BES is economically unattractive. Therefore, there is a confluence between microgrid operating costs and battery investment costs. However, as the battery size is increased, the microgrid operation is reduced. The lowest point of the expansion planning cost is the optimal point. This point shows the highest BES capital cost and the cheapest operation cost that can be achieved together. A mixed-integer programming (MIP) model is used to formulate the optimal BES sizing problem [82].

4.2.3 Battery Energy Storage Degradation

In BES operation, the degradation problem is often encountered. It is mainly caused by two factors: calendric aging and cyclic aging. The calendric aging is encountered even if the BES is not operated. Meanwhile, the cycle aging mainly comes from BES depth of discharge (DoD) and the number of cycles [83], [84]. The number of cycles and DoD determines whether the BES might need to be replaced before the end of the considered project lifetime or not. They are neglecting those matters in expansion planning results in an inaccurate economic assessment. Figure 4.2 shows the typical battery life cycle model versus DoD that the manufacturers usually provide [71],
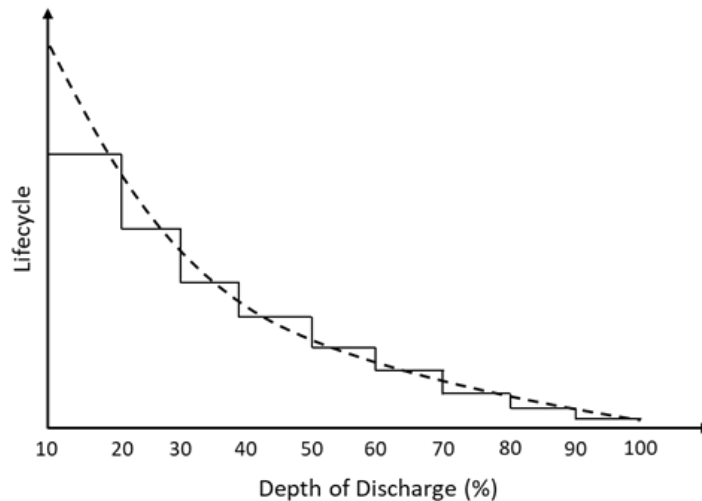
Figure 4. 2 Linearization of the lifecycle as a function of the depth of discharge [85]

[85]. Several studies to estimate the battery lifecycle have already been proposed. Those studies exhibit an exponential form of the relationship [86]–[88].

4.3 Optimization Approaches

4.3.1 Mathematical Programming

A battery energy storage system's operation can be modeled into an optimization problem with a cost function defined by a mathematical grid calculation, a financial mathematical calculation, or both. In modeling, some limitations must be defined so that optimization problems can be resolved. Several approaches can be used in modeling these problems and solving them, such as; mathematical programming, Stochastic programming, dynamic programming, and optimal control. One that is widely used in modeling electric power systems is mathematical programming. This programming has several examples, such as linear programming (LP) and mixed-integer programming (MIP). The modeling of each is discussed below.

Linear program

$$
\begin{aligned}
\text{minimize} \quad & c^T x \\
\text{subject to} \quad & Ax \le b \\
\text{and} \quad & 0 \le x \le \bar{x}
\end{aligned}
$$

For linear programming, the cost function is defined as a combination of the decision variable, x, which is limited by linear constraints. Then, the decision variable must be between zero and the upper bound of x [89]–[91]. Another example that is often used to model expansion planning problems is MIP. Similar to LP. Generally, the objective function in MIP is to minimize or maximize.

Mixed-integer program

$$\begin{aligned}
\text{minimize} \quad & c^T x + o^T y \\
\text{subject to} \quad & Ax + Gy \le b \\
& 0 \le x \le \bar{x} \\
\text{and} \quad & 0 \le y \le \bar{y}, \ \ y \in \mathbb{Z}
\end{aligned}$$

For MIP, the cost function is defined as a combination of the x and y decision variables. This programming is widely used in cases involving a component's working status [92]–[94]. Furthermore, MIP is widely used to resolve unit commitment generator problems. Considering the many changes in generator operation during the active life and the BES operation that may fluctuate, MIP was chosen to model the problem.

The approach that is often used in MIP problems is the branch and bound algorithm. This approach is divided into two stages of completion [95], [96].

1. *Bounding process*: At this stage, the mixed-integer problem is simplified, or the problem relaxes by removing the integral limitation so that it becomes an LP problem. This process often happens because, in electrical system modeling, this kind of thing cannot be avoided.
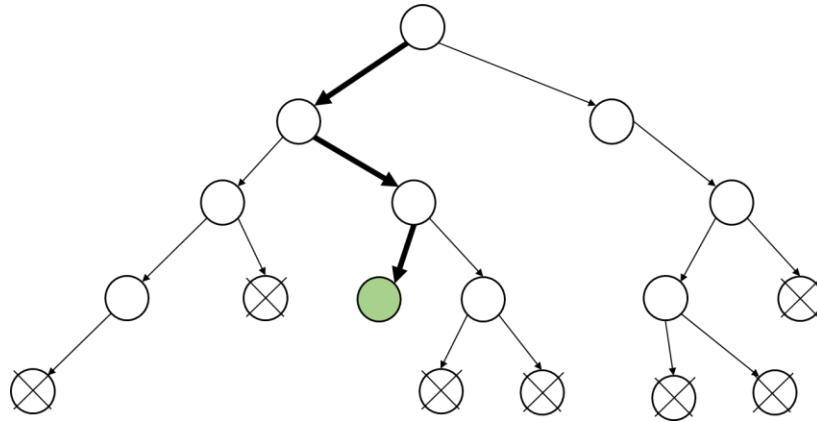
Figure 4.3 Bound and branch algorithm

2. *Branching process*: At this stage, the problem is broken down into several smaller sub-problems. This process is done to facilitate problem-solving.

Several software tools are available to solve MIP problems, such as CPLEX, Xpress-MP, and SYMPHONEY. These tools are potent solvers that utilize a combination of branch and bound techniques and cutting-plane techniques to speed up the time for solving MIP problems by computers. It results in solving problems in the electrical system or expansion planning problems in MIP that can be solved using a personal computer [81], [95], [96]. In this thesis, the software used to solve expansion planning problems is the IBM ILOG CPLEX Optimization Studio or CPLEX.

4.4 Optimization Model

The BES investment cost mainly depends on its size, both power rating and energy rating. The oversized BES is unattractive for investment. On the other hand, the undersized BES may not satisfy the demand. This section discusses in detail the objective function and constraints associated with the implementation of BES LFC. The proposed BES optimal selection and sizing problem's objective is to minimize the planning and operating cost subject to operational constraint.

$$\min \sum_d \sum_h Q\left(aP_{gdh}^2 + bP_{gdh} + c\right) + V \sum_d \sum_h LL_{dh} + \left[P_b^R\left(CP + CM\right) + E_b^R\left(CE + CI\right)\right] \quad (4.1)$$

The terms in equation (4.1) represent the expansion planning cost. It consists of microgrid operation cost, the value of lost load (VOLL), and the BES investment cost. The microgrid operation cost is composed of the fuel needed by the generator during its operation. The energy is determined according to the power supplied by the generator to the system. The generator is assumed to be a thermal unit generator that transforms the fuel-based energy source into electricity. Hence, the fuel needed is a quadratic function of the generated power. The process is imposed by the cost coefficients that determine the fuel cost.

The VOLL is used to quantify the economic loss associated with unserved energy. It is represented by the willingness of the customer to pay for reliable electricity service. Power rating and energy rating capital costs, annual maintenance cost, and installation cost are the components of the BES investment cost. The power conversion system is assumed embedded in the power rating capital cost. Usually, the annual maintenance cost is given in terms of the BES power rating. On the other hand, the installation cost is calculated according to the BES energy rating. Both the capital costs and installation costs are annualized using equation (4.2).

$$\text{Annualized cost} = \frac{r(1+r)^T}{(1+r)^T - 1} \times \text{one time cost} \tag{4.2}$$

4.4.1 Microgrid Constraints

Microgrid constraints include the power balance, and grid limitation is shown in (4.3)-(4.5).

$$\sum_{i \in \{G\}} P_{gidh} + P_{bidh} + \sum_{i \in \{W\}} P_{ridh} + LL_{dh} = P_{Ldh} \qquad \forall d, \forall h \tag{4.3}$$

$$f_{dh} = R\left[\frac{\left(P_{gidh} - P_g^0\right)}{P^{pu}}\right] f^{pu} + f^0 \qquad \forall i \in G, \forall d, \forall h \tag{4.4}$$

$$f^{\min} \leq f_{dh} \leq f^{\max} \qquad \forall d, \forall h \tag{4.5}$$

The power balance (4.3) ensures that the power generated from all generators, RESs, and BES equals the load demand at one time. The BES power and generator power are determined based on the LFC calculation. BES is discharging when the power is positive and charging when negative. The linear equation model is necessary to solve the model without introducing non-linear equations. Hence, the power losses, as well as the bus voltage magnitude and angle, are ignored. The generator acts as the

system backbone. Both the grid voltage and frequency are determined based on the generator output. In islanded microgrid systems, droop control applications are widely used. It allows the system to operate outside the nominal frequency. By applying the droop control, the grid frequency is determined based on the droop slope and the generator output power at each time interval in equation (4.4). The frequency is limited by maximum and minimum value. It is represented by equation (4.5).

4.4.2 Generator Constraints

The generator power is limited by maximum and minimum capacities illustrated in equation (4.6). Moreover, the ramp-up and ramp-down limitations, (4.7) and (4.8), are also included in the constraints.

$$P_{gi}^{\min} \leq P_{gidh} \leq P_{gi}^{\max} \qquad\qquad \forall i \in G, \forall d, \forall h \qquad (4.6)$$

$$P_{gidh} - P_{gid(h-1)} \leq RU_i \qquad\qquad \forall i \in G, \forall d, \forall h \qquad (4.7)$$

$$P_{gid(h-1)} - P_{gidh} \leq RD_i \qquad\qquad \forall i \in G, \forall d, \forall h \qquad (4.8)$$

4.4.3 BES Constraints

In this study, as the proposed LFC is installed on BES, the BES constraints must be included in the optimization model. The following equations model the constraint.

$$\rho^{\max} = \frac{\left(f^{\max} - f^0\right)P^{pu}}{f^{pu}R} + P_g^0 \qquad (4.9)$$

$$\rho^{\min} = \frac{\left(f^{\min} - f^0\right)P^{pu}}{f^{pu}R} + P_g^0 \qquad (4.10)$$

$$P_{bdh} = \max\left(P_{Ldh} - P_{ridh} - \rho^{\min}, \max\left(0, \frac{\left(K_b P_{Ldh} - K_b P_{ridh} + RP_g^0 - K_b LL_{dh}\right)}{R + K_b} - \frac{\left(\frac{\Delta f^s}{f^{pu}}\right)P^{pu}}{R + K_b} \right) \right)$$

$$+ \min\left(P_{Ldh} - P_{ridh} - \rho^{\max}, \min\left(0, \frac{\left(K_b P_{Ldh} - K_b P_{ridh} + RP_g^0 - K_b LL_{dh}\right)}{R + K_b} + \frac{\left(\frac{\Delta f^s}{f^{pu}}\right)P^{pu}}{R + K_b} \right) \right) \qquad \forall i \in W, \forall d, \forall h \quad (4.11)$$

$$-P_b^R \le P_{bdh} \le P_b^R \qquad\qquad \forall d, \forall h \qquad (4.12)$$

$$\alpha^{\min} P_b^R \le E_b^R \le \alpha^{\max} P_b^R \qquad\qquad \forall d, \forall h \qquad (4.13)$$

$$E_{bdh} = E_{bd(h-1)} - \frac{P_{bdh}^{dch} h}{\eta^{dch}} - P_{bdh}^{ch} \eta^{ch} h \qquad\qquad \forall d, \forall h \qquad (4.14)$$

$$(1-\beta) E_b^R \le E_{bdh} \le E_b^R \qquad\qquad \forall d, \forall h \qquad (4.15)$$

$$\zeta_{bdh} = \left(u_{dh} - u_{d(h-1)}\right) u_{dh} \qquad\qquad \forall d, \forall h \qquad (4.16)$$

$$\sum_d \sum_h \zeta_{dh} \le \frac{1}{T} e \qquad\qquad \forall d, \forall h \qquad (4.17)$$

By recalling the advanced LFC concept in Chapter 2, when BES is in Region 2, the output power compensates for the difference between the load demand, the RES output power, and generator power at f^{max}. This power is represented by the equation ρ^{max} (4.9). In charging mode, the output power is determined according to Region 1 and Region 3. In Region 3, the output power comes from the load demand, the RES power, and the generator power at f^{min}. This power is represented by the equation ρ^{min} (4.10).

Equation (4.11) represents the output power of BES. This equation is represented in two parts to determine the BES charging/discharging mode. The first

part of the equation illustrates the discharging mode, and the second one illustrates the charging mode. When BES is in discharge mode, the output power is determined based on Region 1, representing the deadband droop, and Region 2, representing the lower frequency saturation area. In Region 1, when BES operates in the deadband area, the output power is zero.

The charging/discharging powers of BES are limited by its power rating, in which the negative power illustrates the charging mode and positive power illustrates the discharging mode. The charging/discharging powers are illustrated in (4.12). The energy rating is correlated to the power rating and cannot be sized independently. The correlation is illustrated with a ratio that determines the maximum discharge time at rated power (4.13). Equation (4.14) describes the stored energy in BES at each time interval. It equals to the preceding stored energy minus the discharged or charged energy. The stored energy cannot exceed the maximum value. Also, the stored energy cannot be less than the minimum value. The minimum and maximum values are defined by the determined maximum depth of discharge and charge to keep the stored energy or SoC within a determined range (4.15). This equation leads to the depth of discharge estimation of the battery, which β respectively describe the maximum depth of discharge. Equation (4.16) is used to describe the BES cycles. The binary variable u_{dh} represents the BES operation status. The BES discharges when u_{dh} equals 1 and charges when u_{dh} equals 0. The BES cycle's summation cannot exceed the determined lifecycle associated with the desired maximum depth of discharge and desired project lifetime (4.17).

4.5 System Model

The system implemented to run BES, which utilizes advanced LFC, is an island microgrid system. This system consists of a diesel generator, a renewable energy source for PV, BES, and consumers. Each component will be discussed in this section to provide an overview of the simulation carried out. The generator and BES parameters

are shown in Table 4.1. Most of the parameters are the same as the parameter in previous chapters. Four battery technologies are used in this study. The VOLL is assumed to be 50 $/MWh borrowed from [71].

Table 4.1 System parameter

Parameter		Value
Generator droop gain	R	-0.0298 pu
Generator droop power reference	P_g^0	200 kW
Droop frequency reference	f^0	60 Hz
Base power	P^{pu}	400 kW
Base frequency	f^{pu}	60 Hz
BES droop gain	K_b	-0.015 pu
BES droop power reference	P_b^0	0 kW
LFC maximum frequency	f^{max}	60.2 Hz
LFC minimum frequency	f^{min}	59.8 Hz
Maximum depth of discharge	β	80%

4.5.1 Diesel generator

One of the machines that are widely used in power generation applications is the diesel engine. In this study, calculating the fuel used by the generator is very important. The calculation of the fuel used is closely related to the required microgrid operating costs. As a thermal power plant, the function of a diesel engine fuel cost can be expressed as:

$$Y\left(P_{gdh}\right) = aP_{gdh}^{2} + bP_{gdh} + c \tag{4.18}$$

In engine fuel cost modeling, the coefficients a, b, and c are not given directly by the manufacturer. It should be noted that the fuel cost function of an engine is a model that

reflects the engine operation. Hence, to determine the coefficient value, calculating the engine's amount of fuel is necessary.

In this study, the generator is assumed to have a capacity of 500 kVA / 400 kW. So, it can be said that the engine can run entirely or full-load at 400 kW. Fuel consumption needs to be known because this is where the cost function of diesel is obtained. However, this determination can only be made through accurate field testing. Several references provide a table of diesel fuel consumption based on the loading level, shown in Table 4.2 [97]–[100]. Each reference shows different results. However, the numbers shown do not differ much, as each machine can give different results.

Table 4.2 Comparison of fuel consumption [97] – [100]

Source	Consumption fuel (L/hr)			
	25% load	50% load	75% load	100% load
generatorsource.com [98]	33.69	56.40	80.63	108.27
Mechatornics.by [99]	-	59.85	89.78	119.7
Krugerpower.com.au[97]	36	62.4	90	120
globalpwr.com[100]	32.56	55.27	80.63	107.88
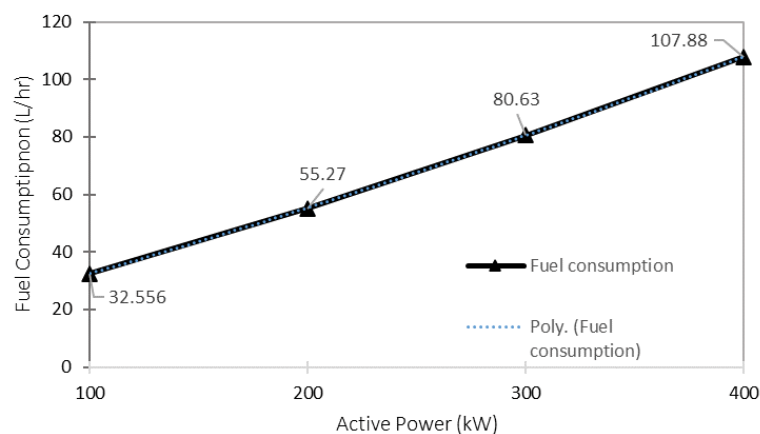
Figure 4.4 Diesel fuel consumption curve

We can draw the diesel fuel consumption curve from the obtained fuel consumption values shown in Figure 4.4. Each loading level can be drawn a line which is denoted by a dashed blue line. By using a quadratic approach, it is found that the fuel consumption function becomes:

$$Y\left(P_{gdh}\right) = 0.0001134P_{gdh}^{2} + 0.19463P_{gdh} + 11.921 \text{ L/hr}$$
(4.19)

Hence, the coefficients *a*, *b*, and *c* are written in Table 4.3. The fuel cost is assumed 0.9 $ / L borrowed from [101].

Table 4. 3 Diesel generator fuel coefficients

Type	Cost Coefficient		
	a (L/kWh²)	*b* (L/kWh)	*c* (L)
Diesel unit	0.0001134	0.19463	11.921

4.5.2 Photovoltaic array

In this study, photovoltaics are used as an installed renewable energy source. This study focuses on installing batteries in an islanded microgrid system so that neither the PV installation costs nor the other PV-related costs are taken into account. However,
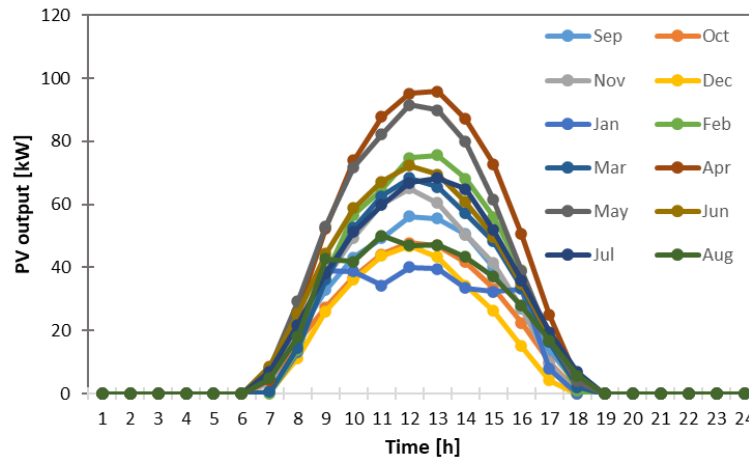
Figure 4.5 Average hourly PV output power per month [70]

the PV operation is taken into account, so data regarding the PV output is required. The PV output power for one year can be found at [70]. The selected location is similar to the location shown in [102]. Therefore, by assuming the installed PV is 200 kWp, PV data can be obtained. On average, the daily PV output can be illustrated in Figure 4.5, which shows the daily average PV output power in 2019.

4.5.3 Load

As discussed in the previous chapter, the load used is the same as the one-year operation load. This load is obtained from the load demand on the small island provided on [20], [102]. The data obtained are the average load curve each day and the load factor that applies every month. Thus, one year of the system operation can be carried out. Figure 4.6 shows the load per day curve for one year. Each month, the load curve changes due to the weather and season's influence, thus slightly changing the consumer's lifestyle.
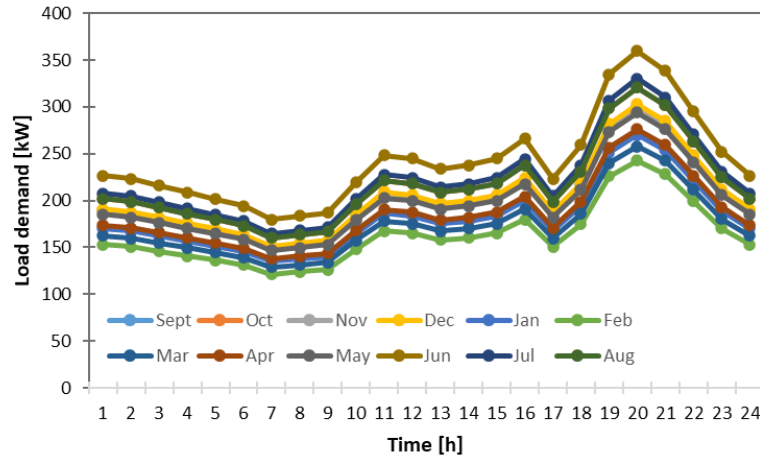
Figure 4.6 Average hourly load profile [20]

4.5.4 Battery energy storage

In this study, the main objective is to determine the size of the battery used. As explained in the previous section, the battery's objective function depends on variable

capital costs, operating and maintenance costs, and battery installation costs. The characteristics of BES used are borrowed from [71] and shown in Table 4.4.

Table 4.4 List of BES technology investment costs [71]

Technology	Power Rating Cost ($/kW)	Energy Rating Cost ($/kWh)	Maintenance Cost ($/kW/yr)	Installation Cost ($/kWh)	η (%)
Lead-acid	200	200	50	20	70
NiCd	500	400	20	12	85
Li-ion	950	600	–	3.6	98
NaS	350	300	80	8	95

Table 4. 5 BES lifecycle for various depth of discharge value [103] – [106]

Depth of Discharge (%)	Number of cycles			
	Lead-acid	NiCd	Li-ion	Nas
10	8000	7900	–	100000
20	2500	5800	–	60000
30	1500	3400	–	30000
40	950	2000	–	15000
50	700	1200	8000	10000
55	645	1050	7500	9500
60	590	900	6900	9000
65	545	950	6200	8000
70	500	800	5800	7000
75	475	850	5000	6500
80	450	700	4500	6000
85	420	650	4100	5500
90	390	600	3700	5000
100	350	500	3000	4000

In this study, the selection of a battery technology that utilizes advanced LFC was also carried out. The main parameter in battery technology choice is the number

of cycles performed by a battery during its lifetime. Table 4.5 that borrowed from [103]–[106], shows the number of cycles that apply to each battery technology with various DoD.

4.6 Results and Discussions

4.6.1 Implementation of Advanced LFC

In order to show the effect of the proposed control in the system, three scenarios are studied in this paper:

Case 1: Microgrid system optimal scheduling without BES installation.

Case 2: BES installation in microgrid system with traditional LFC.

Case 3: BES installation in microgrid system with the advanced LFC.

Case 1: Table 4.6 shows the operating system's results without using a battery where the generator compensates for all changes in the load and PV power. The absence of a battery makes expansion costs equal to microgrid operating costs. When the frequency cap is not in place, frequencies operate between 59.28-60.63 Hz at an expansion cost of $ 484,591 / year. However, when the system imposes frequency limits, the expansion costs are even higher. The tighter the frequency limit, the more expensive the operation cost is due to the generator's operation limits. Thus, the VOLL of the system is getting higher. This result shows that the lowest cost of expansion is obtained when the frequency limitation is neglected.

Case 2: Table 4.7 shows the operation of a system that implements the traditional LFC on the battery, with a considered project lifetime of 10 years and an interest rate *r 4%*. The optimization results with the droop gain variation are conducted to show their effect on expansion costs. Traditional LFC has no frequency limitation, so the system operates according to a load-sharing mechanism between the generator

and battery. The results show that the greater the battery's droop gain, the greater the frequency deviation from the nominal value. Even with -0.08, the system operates in the 59.45-60.34 Hz range, outside the value recommended by the manual. The choice of droop gain affects the amount of power capacity and battery energy, causing changes in the cost of expansion to the droop gain. The greater the droop gain, the lower the expansion costs required. Due to the battery's small participation, the generator must compensate for any changes in the system. This operation causes the battery's cost to be smaller, and the system frequency deviates from the nominal value.

Table 4.6 Optimization result for case 1

Operating frequency (Hz)	Microgrid operation cost ($/year)	Total expansion cost ($/year)
59.28-60.63	484,591	484,591
59.5-60.5	759,188	759,188
59.6-60.4	1,641,050	1,641,050
59.7-60.3	3,556,352	3,556,352
59.8-60.2	7,075,788	7,075,788
59.85-60.15	9,696,305	9,696,305

Case 3: Table 4.8 shows the results of operating a system that implements advanced LFC on the battery. Optimization with droop gain variation is carried out in order to show its effect on expansion costs. Besides, investigations are also carried out by varying the operating ranges of f^{max} and f^{min}. In general, the larger the droop gain contributes to lower expansion costs. The frequency limitation contributes to holding the generator from operating outside the specified range. It causes the diesel operation to be suppressed so that the battery's power compensation increases the size of the battery. The large size of the battery can be confirmed in the table showing the low cost of expansion. However, the limit of frequency should be kept in mind because a broader range tends to provide lower costs than a narrow range (59.85-60.15 Hz). It is closely related to VOLL, which is getting higher.

Table 4.7 Optimization result for case 2

Droop gain	Operation range (Hz)	Battery capacity (MWh/kW)	Microgrid operation cost ($/year)	BES Investment Cost ($/year)	Expansion cost ($/year)
-0.015	59.69-60.21	22.57/130.78	4,668,919	621,868	5,290,787
-0.02	59.65-60.23	20.3/117.65	4,668,990	559,431	5,228,422
-0.03	59.59-60.26	16.9/97.98	4,669,107	465,881	5,134,988
-0.04	59.55-60.29	14.45/83.94	4,669,198	399,136	5,068,334
-0.06	59.49-60.31	11.26/65.25	4,669,330	310,242	4,979,571
-0.08	59.45-60.34	9.21/53.61	4,669,419	253,731	4,923,150

Table 4.8 Optimization result for case 3

Droop gain	Operation range (Hz)	Battery capacity (MWh/kW)	Microgrid operation cost ($/year)	BES Investment Cost ($/year)	Expansion cost ($/year)
-0.015	59.8-60.2	104.73/164.65	1,060,442	2,852,941	3,913,383
	59.85-60.15	50.19/180.63	3,040,992	1,374,837	4,415,829
-0.02	59.8-60.2	81.86/164.65	1,524,755	2,232,710	3,757,465
	59.85-60.15	27.79/180.63	3,600,879	767,340	4,368,219
-0.03	59.8-60.2	50.71/164.65	2,163,021	1,387,708	3,350,729
	59.85-60.15	13.9/94.87	4,875,732	384,112	5,259,844
-0.04	59.8-60.2	31.77/164.65	2,560,896	873,942	3,434,838
	59.85-60.15	9.175/94.35	5,762,704	255,924	6,018,627
-0.06	59.7-60.3	49.81/132.69	1,048,955	1,361,071	2,410,026
	59.8-60.2	14.57/95.43	3,338,498	402,203	3,740,701
	59.85-60.15	131.80/180.63	466,105	3,588,302	4,054,407
-0.08	59.7-60.3	36.25/132.69	1,261,462	993,057	2,254,519
	59.8-60.2	10.44/65.99	4,050,660	287,974	4,338,635
	59.85-60.15	130.88/180.63	465,976	3,563,400	4,029,376

In general, Case 1, the diesel-only operation, offers the cheapest expansion cost. However, the resulted grid frequency is found to be outside the allowed range. The second-cheapest expansion cost is found to be Case 3 for every droop gain. Besides, Case 3 results the grid operates on the allowed frequency range. The proposed control can lower the expansion cost without violating the power quality. It is realized because the control can maintain the generator output, impacting the amount of fuel needed.

Figure 4.7 shows the comparison of operations for each case for 1 week. This figure illustrates that when the battery is not implemented, the grid frequency fluctuates within 59.8 Hz – 60.63 Hz. In terms of power quality, this result is still outside the allowed range in [107]. Thus, the use of a battery with deadband droop is introduced. The utilization of deadband droop control keeps the frequency within 59.69 Hz – 60.28 Hz due to the load sharing between the generator and the battery. It reduces the grid operation cost. The proposed control introduces a broader range of active-frequency control capabilities. This control ensures that the frequency is maintained within 59.69 Hz – 60.2 Hz. This control expands the battery ability to regulate the grid frequency in the desired range. Hence, it causes the generator output to be maintained at these points affecting the grid operation cost.
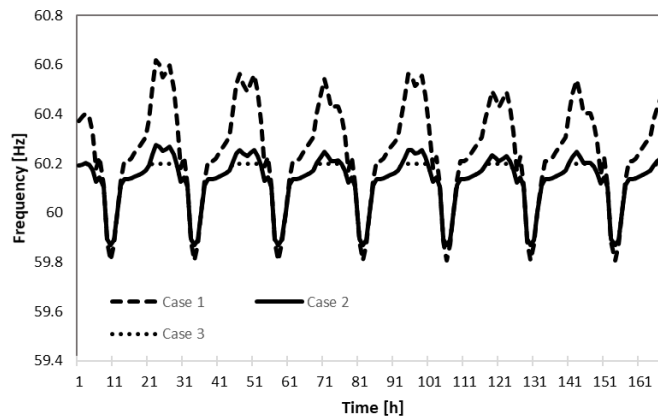
Figure 4.7 Frequency result comparison for each case in 1-week operation

4.6.2 Selection of BES technology installed advanced LFC

The previous subsection estimates that the maximum DoD of BES using LFC is found to be 80% in a one-year operation. It shows unrealistic results since the installed BES is estimated to display 621 cycles per year. By referring to Table 4.5, it can be estimated that the battery must be replaced in about 8.5 months or less than 1 year. The BES replacement certainly causes additional planning costs and is unattractive economically. Thus, a discussion of whether the proposed control is applicable for various battery types must be performed to draw the control capability. Each battery technology's simulation results are shown in Table 4.9, assuming each battery has a maximum DoD of 80%. These results indicate that the Li-ion battery can perform the proposed control. With an installed 2.5 MWh/59.44 kW, the total expansion cost becomes $4,630,710 per year. During one-year operation, BES is estimated to perform 1002 cycles per year. However, it is estimated the battery replacement still needs to be done after operating for about 4.5 years for a 10-year project.

Table 4.9 Optimization results based on BES technologies (same maximum DoD)

Battery Type	Total Cost ($/year)	Operation Cost ($/year)	BES investment Cost ($/year)	Energy Rating (MWh)	Power Rating (kW)	Maximum DoD (%)	Number of Cycles (Cycles/year)
Lead acid	3,413,552	2,552,140	861,412	31.31	164.65	80	621
NiCd	4,377,500	3,973,638	403,862	7.81	89.71	80	870
Li-ion	4,630,710	4,435,223	195,488	2.54	59.45	80	1002
NaS	4,195,552	2,567,113	1,628,439	42.49	121.32	80	636

Table 4. 10 Optimization results based on BES technologies (different maximum DoD)

Type	Total Expansion Cost	Operation Cost	BES investment Cost	Energy Rating	Power Rating	Maximum DoD	Number of Cycles	Expected end of lifetime
	($/year)	($/year)	($/year)	(MWh)	(kW)	(%)	(Cycles/year)	(Years)
Lead acid	3,689,075	2,827,663	861,412	31.31	164.65	50	688	1
NiCd	4,406,673	3,606,274	800,399	15.61	89.71	65	848	1
Li-ion	4,630,710	4,435,223	195,488	2.54	59.45	80	1002	4.5
NaS	4,180,408	2,552,140	1,628,268	42.89	120.18	75	628	10

The optimal results for each battery type are described in Table 4.10, where each maximum DoD for each battery is distinguished. The lead-acid battery delivers the total expansion cost of $3,689,075 per year at a 31.31 MWh/164.65 kW with a maximum DoD of 50%. Compared with the DoD calculation result of 80%, the expansion cost increases due to the battery operation restriction. Hence, the power difference must be satisfied by the grid. It increases the microgrid operation cost.

In one year, the lead-acid battery operates 688 cycles. However, after a 1-year operation, the battery replacement must be carried out due to the cycle limitation. A similar result is also found in the NiCd battery. At a total cost of $4,406,673 per year, size of 15.61 MWh/89.71 kW, and a maximum DoD of 65%, the battery performs 848 cycles per year. The battery can operate for 1 year without a replacement. However, assuming a 10-year project, around 9 replacements are required, leading to the additional cost of battery replacement. Li-ion battery shows an installed battery of 2.54 MWh/59.45 kW, a total expansion cost of $4,630,710 per year, and a maximum DoD of 80%. The battery is estimated to operate for 4.5 years without a battery replacement. By assuming a 10-year project, battery replacements are required. The best result is obtained with a NaS battery.

The operation cost incurred is $4,194,552 per year, with a 42.89 MWh/120.18 kW and a maximum DoD of 75%. In one year of operation, the battery operates 628 cycles, where a replacement battery is not needed. Assuming the project period is 10 years, the battery cycle is still below the operating cycle limit. It shows the NaS battery can perform the proposed control. Moreover, NaS battery offers the second cheapest after lead acid when compared to other technologies. It shows that selecting a suitable battery and the proposed control can reduce the expansion cost without relinquishing the system power quality.
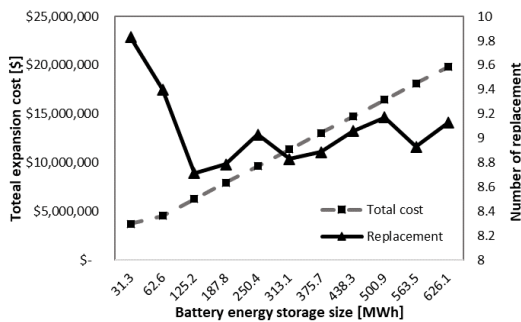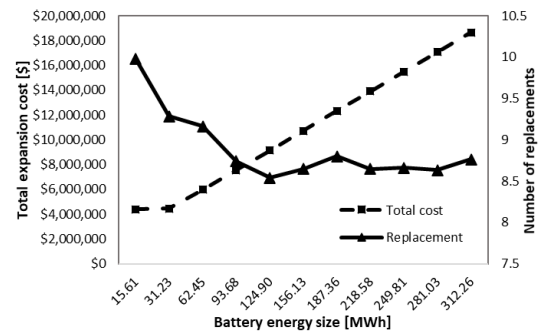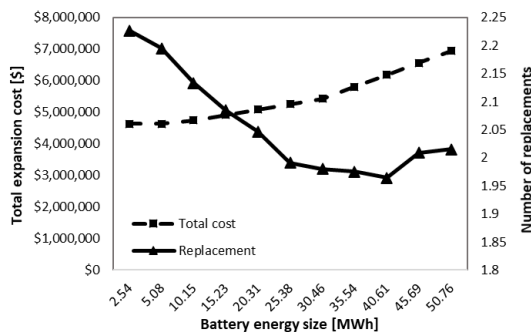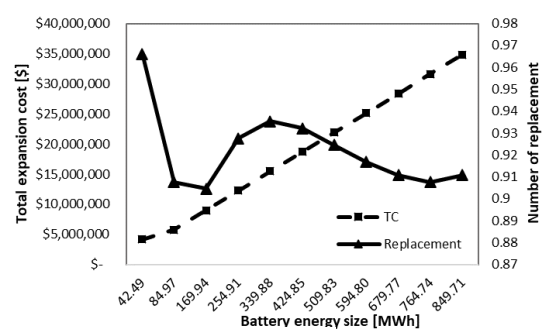
Figure 4.8 Battery size against number of replacements: (a) Lead-acid, (b) NiCd, (c) Li-ion, (d) NaS

These results indicate the proposed method has limitations that must be satisfied for battery implementation. This method only applies to a battery technology that has a high energy density or high capacity. A sensitivity analysis of battery size for each type is performed, shown in Figure 4.8(a)-(d). The relation between battery capacity, expansion cost, and some battery replacements can be seen by varying the battery energy capacity.

The number of battery replacements tends to decrease for all battery technologies as the battery capacity is increasing. The higher capacity causes lower DoD, which leads to a higher operation cycle. Thus, the higher capacity battery can operate much longer due to the allowed operating cycles. However, it leads to an increasing expansion cost which is the objective function of this study due to the higher BES investment cost.

4.7 Conclusion

It is found that the proposed LFC reduces the expansion planning cost. The frequency limitations in the LFC cause the operation of the generator to be restricted. The operation restrictions ultimately lead to reduced grid operation costs. Hence, it is concluded that the proposed LFC can reduce the expansion cost and keep the grid power quality.

In choosing a battery to implement, it is necessary to consider the degradation factor or battery life cycle. The factor illustrates that the BES operation affects the lifetime of the BES itself. By comparing the four battery types, it is found that the proposed control applies only to high-density or high-capacity batteries. Hence, this is the limitation in implementing the proposed control.

Chapter 5

5 Conclusion and Future Works

5.1 Conclusion

This thesis defines one control method used in BES, namely advanced load-frequency control (LFC). To elaborate on battery participation to regulate system frequency, advanced LFC can participate in regulating system frequency. The proposed control utilizes three control areas, each of which determines the battery operation of the system. The three regions include Region 1 deadband droop, Region 2 Lower-frequency saturation, and Region 3 Upper-frequency saturation. The proposed control is proven to have the ability to regulate the frequency to stay in the desired area. Thus, further deviations from the nominal value can be avoided.

The active participation of the battery to continuously regulate the system has an obvious drawback. This participation often makes the battery SoC touch critical numbers. As a result, this operation can result in the battery performing more cycles and impacting battery life. SoC control is proposed to solve this problem. The proposed control adopts an LFC curve reference change so that the power supplied by the battery can change depending on the SoC level. The proposed control can keep the battery SoC in the desired range without sacrificing frequency values that deviate too far from their nominal values.

Advanced LFC has technical advantages but not yet proven economic advantages. In order to address the problem of how advanced LFCs impact microgrid operation from an economic point of view, an economic analysis based on the performance of the proposed controls is carried out. Expansion planning costs hit the

cheapest when advanced LFC is employed. It occurs because the proposed control suppresses the generator operation at a certain point so that the required fuel costs do not soar. Furthermore, a discussion of battery type selection is also included to show that the proposed control may not be suitable for all battery types and is only effective for some battery types.

5.2 Future Works

The proposed LFC has tested its performance under one example system. One of the future works that can be done is investigating SoC control's impact on battery size optimization. If this is done, a new perspective will open up regarding battery operation in microgrid systems, particularly the islanded microgrid. Next, it will be interesting to test the proposed control on other systems. A test system such as the IEEE microgrid testbed poses an appropriate challenge for testing the proposed control. After the technical test is carried out, an investigation of the battery size can be carried out to see the advanced LFC effects.

References

[1] "History of the greenhouse effect and global warming." https://www.lenntech.com/greenhouse-effect/global-warming-history.htm (accessed Mar. 22, 2021).

[2] "EDGAR - Fossil CO2 and GHG emissions of all world countries, 2019 report - European Commission." https://edgar.jrc.ec.europa.eu/overview.php?v=booklet2019 (accessed Mar. 25, 2021).

[3] "CO₂ and Greenhouse Gas Emissions - Our World in Data." https://ourworldindata.org/co2-and-other-greenhouse-gas-emissions (accessed Mar. 22, 2021).

[4] "Greenhouse Effect and Historical Emissions." https://clintonwhitehouse5.archives.gov/Initiatives/Climate/greenhouse.html (accessed Mar. 22, 2021).

[5] "greenhouse gas | Definition, Emissions, & Greenhouse Effect | Britannica." https://www.britannica.com/science/greenhouse-gas (accessed Mar. 22, 2021).

[6] P. Moriarty and D. Honnery, "What is the global potential for renewable energy?," *Renew. Sustain. Energy Rev.*, vol. 16, no. 1, pp. 244–252, Jan. 2012, doi: 10.1016/j.rser.2011.07.151.

[7] "Renewables – Global Energy Review 2020 – Analysis - IEA." https://www.iea.org/reports/global-energy-review-2020/renewables (accessed Jun. 15, 2021).

[8] A. Llaria, O. Curea, J. Jiménez, and H. Camblong, "Survey on microgrids: Unplanned islanding and related inverter control techniques," *Renew. Energy*, vol. 36, no. 8, pp. 2052–2061, Aug. 2011, doi: 10.1016/j.renene.2011.01.010.

[9] H.-J. Moon, Y. J. Kim, J. W. Chang, and S.-I. Moon, "Decentralised Active Power Control Strategy for Real-Time Power Balance in an Isolated Microgrid with an Energy Storage System and Diesel Generators," *Energies*, vol. 12, no. 3, p. 511, Feb. 2019, doi: 10.3390/en12030511.

[10] M. Ahmed, L. Meegahapola, A. Vahidnia, and M. Datta, "Stability and Control Aspects of Microgrid Architectures–A Comprehensive Review," *IEEE Access*, vol. 8, pp. 144730–144766, 2020, doi: 10.1109/ACCESS.2020.3014977.

[11] H. Mahmood and J. Jiang, "Decentralized Power Management of Multiple PV, Battery, and Droop Units in an Islanded Microgrid," *IEEE Trans. Smart Grid*, vol. 10, no. 2, pp. 1898–1906, Mar. 2019, doi: 10.1109/TSG.2017.2781468.

[12] W. Gu, W. Liu, Z. Wu, B. Zhao, and W. Chen, "Cooperative Control to Enhance the Frequency Stability of Islanded Microgrids with DFIG-SMES," *Energies*, vol. 6, no. 8, pp. 3951–3971, Aug. 2013, doi: 10.3390/en6083951.

[13] R. Shah, N. Mithulananthan, and R. C. Bansal, "Oscillatory stability analysis with high penetrations of large-scale photovoltaic generation," *Energy Convers. Manag.*, vol. 65, pp. 420–429, Jan. 2013, doi: 10.1016/j.enconman.2012.08.004.

[14] Y. Song, D. J. Hill, and T. Liu, "Impact of DG Connection Topology on the Stability of Inverter-Based Microgrids," *IEEE Trans. Power Syst.*, vol. 34, no. 5, pp. 3970–3972, Sep. 2019, doi: 10.1109/TPWRS.2019.2917624.

[15] Liu, Wang, and Wang, "Research on Frequency Control of Islanded Microgrid with Multiple Distributed Power Sources," *Processes*, vol. 8, no. 2, p. 193, Feb. 2020, doi: 10.3390/pr8020193.

[16] K. Lai, Y. Wang, D. Shi, M. S. Illindala, Y. Jin, and Z. Wang, "Sizing battery storage for islanded microgrid systems to enhance robustness against attacks on energy sources," *J. Mod. Power Syst. Clean Energy*, vol. 7, no. 5, pp. 1177–1188, Sep. 2019, doi: 10.1007/s40565-019-0501-1.

[17] Y.-Y. Hong, Y.-Z. Lai, Y.-R. Chang, Y.-D. Lee, and C.-H. Lin, "Optimizing Energy Storage Capacity in Islanded Microgrids Using Immunity-Based Multiobjective Planning," *Energies*, vol. 11, no. 3, p. 585, Mar. 2018, doi: 10.3390/en11030585.

[18] X. Tan, Q. Li, and H. Wang, "Advances and trends of energy storage technology in Microgrid," *Int. J. Electr. Power Energy Syst.*, vol. 44, no. 1, pp. 179–191, Jan. 2013, doi: 10.1016/j.ijepes.2012.07.015.

[19] M. R. Aghamohammadi and H. Abdolahinia, "A new approach for optimal sizing of battery energy storage system for primary frequency control of islanded Microgrid," *Int. J. Electr. Power Energy Syst.*, vol. 54, pp. 325–333, Jan. 2014, doi: 10.1016/j.ijepes.2013.07.005.

[20] J. D. Ocon and P. Bertheau, "Energy Transition from Diesel-based to Solar Photovoltaics-Battery-Diesel Hybrid System-based Island Grids in the Philippines – Techno-Economic Potential and Policy Implication on Missionary

Electrification," *J. Sustain. Dev. Energy Water Environ. Syst.*, vol. 7, no. 1, pp. 139–154, Mar. 2019, doi: 10.13044/j.sdewes.d6.0230.

[21] S. Eftekharnejad, V. Vittal, G. T. Heydt, B. Keel, and J. Loehr, "Small Signal Stability Assessment of Power Systems With Increased Penetration of Photovoltaic Generation: A Case Study," *IEEE Trans. Sustain. Energy*, vol. 4, no. 4, pp. 960–967, Oct. 2013, doi: 10.1109/TSTE.2013.2259602.

[22] S. You *et al.*, "Impact of High PV Penetration on the Inter-Area Oscillations in the U.S. Eastern Interconnection," *IEEE Access*, vol. 5, pp. 4361–4369, 2017, doi: 10.1109/ACCESS.2017.2682260.

[23] T. Li, B. Wen, and H. Wang, "A Self-Adaptive Damping Control Strategy of Virtual Synchronous Generator to Improve Frequency Stability," *Processes*, vol. 8, no. 3, p. 291, Mar. 2020, doi: 10.3390/pr8030291.

[24] M. Tucci and G. Ferrari-Trecate, "A scalable, line-independent control design algorithm for voltage and frequency stabilization in AC islanded microgrids," *Automatica*, vol. 111, p. 108577, Jan. 2020, doi: 10.1016/j.automatica.2019.108577.

[25] M. Parvizimosaed and W. Zhuang, "Enhanced Active and Reactive Power Sharing in Islanded Microgrids," *IEEE Syst. J.*, pp. 1–12, 2020, doi: 10.1109/JSYST.2020.2967374.

[26] W. Pinthurat and B. Hredzak, "Decentralized Frequency Control of Battery Energy Storage Systems Distributed in Isolated Microgrid," *Energies*, vol. 13, no. 11, p. 3026, Jun. 2020, doi: 10.3390/en13113026.

[27] R. R. Kolluri, I. Mareels, T. Alpcan, M. Brazil, J. de Hoog, and D. A. Thomas, "Power Sharing in Angle Droop Controlled Microgrids," *IEEE Trans. Power Syst.*, vol. 32, no. 6, pp. 4743–4751, Nov. 2017, doi: 10.1109/TPWRS.2017.2672569.

[28] S. Aminzadeh, M. Tarafdar Hagh, and H. Seyedi, "Reactive power management for microgrid frequency control," *Int. J. Electr. Power Energy Syst.*, vol. 120, p. 105959, Sep. 2020, doi: 10.1016/j.ijepes.2020.105959.

[29] W. Pinthurat and B. Hredzak, "Decentralized Frequency Control of Battery Energy Storage Systems Distributed in Isolated Microgrid," *Energies*, vol. 13, no. 11, p. 3026, Jun. 2020, doi: 10.3390/en13113026.

[30] K. C. Divya and J. Østergaard, "Battery energy storage technology for power systems—An overview," *Electr. Power Syst. Res.*, vol. 79, no. 4, pp. 511–520, Apr. 2009, doi: 10.1016/j.epsr.2008.09.017.

[31] N. Kawakami and Y. Iijima, "Overview of battery energy storage systems for stabilization of renewable energy in Japan," in *2012 International Conference on Renewable Energy Research and Applications (ICRERA)*, Nagasaki, Japan, Nov. 2012, pp. 1–5. doi: 10.1109/ICRERA.2012.6477391.

[32] J. Choi, H. Jo, and S. Han, "BESS life span evaluation in terms of battery wear through operation examples of BESS for frequency regulation," in *2017 IEEE Innovative Smart Grid Technologies - Asia (ISGT-Asia)*, Auckland, Dec. 2017, pp. 1–5. doi: 10.1109/ISGT-Asia.2017.8378432.

[33] P.-H. Huang, J.-K. Kuo, and C.-Y. Huang, "A new application of the UltraBattery to hybrid fuel cell vehicles: Novel UltraBattery on fuel cell vehicles for the hybrid system," *Int. J. Energy Res.*, vol. 40, no. 2, pp. 146–159, Feb. 2016, doi: 10.1002/er.3426.

[34] S.-L. Lin *et al.*, "Characterization of spent nickel–metal hydride batteries and a preliminary economic evaluation of the recovery processes," *J. Air Waste Manag. Assoc.*, vol. 66, no. 3, pp. 296–306, Mar. 2016, doi: 10.1080/10962247.2015.1131206.

[35] C. Liu, Z. G. Neale, and G. Cao, "Understanding electrochemical potentials of cathode materials in rechargeable batteries," *Mater. Today*, vol. 19, no. 2, pp. 109–123, Mar. 2016, doi: 10.1016/j.mattod.2015.10.009.

[36] P. Breeze, "Power System Energy Storage Technologies," in *Power Generation Technologies*, Elsevier, 2019, pp. 219–249. doi: 10.1016/B978-0-08-102631-1.00010-9.

[37] C. L. Chen, H. K. Yeoh, and M. H. Chakrabarti, "An enhanced one-dimensional stationary model for the all-vanadium redox flow battery," p. 7.

[38] R. H. Byrne, T. A. Nguyen, D. A. Copp, B. R. Chalamala, and I. Gyuk, "Energy Management and Optimization Methods for Grid Energy Storage Systems," *IEEE Access*, vol. 6, pp. 13231–13260, 2018, doi: 10.1109/ACCESS.2017.2741578.

[39] S. Vazquez, S. M. Lukic, E. Galvan, L. G. Franquelo, and J. M. Carrasco, "Energy Storage Systems for Transport and Grid Applications," *IEEE Trans. Ind. Electron.*, vol. 57, no. 12, pp. 3881–3895, Dec. 2010, doi: 10.1109/TIE.2010.2076414.

[40] M. T. Lawder *et al.*, "Battery Energy Storage System (BESS) and Battery Management System (BMS) for Grid-Scale Applications," *Proc. IEEE*, vol. 102, no. 6, pp. 1014–1030, Jun. 2014, doi: 10.1109/JPROC.2014.2317451.

[41] A. Zeh, M. Müller, M. Naumann, H. Hesse, A. Jossen, and R. Witzmann, "Fundamentals of Using Battery Energy Storage Systems to Provide Primary Control Reserves in Germany," *Batteries*, vol. 2, no. 3, p. 29, Sep. 2016, doi: 10.3390/batteries2030029.

[42] U. Datta, A. Kalam, and J. Shi, "Battery Energy Storage System for Aggregated Inertia-Droop Control and a Novel Frequency Dependent State-of-Charge Recovery," *Energies*, vol. 13, no. 8, p. 2003, Apr. 2020, doi: 10.3390/en13082003.

[43] J. Glover and F. Schweppe, "Advanced Load Frequency Control," *IEEE Trans. Power Appar. Syst.*, vol. PAS-91, no. 5, pp. 2095–2103, Sep. 1972, doi: 10.1109/TPAS.1972.293542.

[44] O. P. Malik, A. Kumar, and G. S. Hope, "A load frequency control algorithm based on a generalized approach," *IEEE Trans. Power Syst.*, vol. 3, no. 2, pp. 375–382, May 1988, doi: 10.1109/59.192887.

[45] V. Gholamrezaie, M. G. Dozein, H. Monsef, and B. Wu, "An Optimal Frequency Control Method Through a Dynamic Load Frequency Control (LFC) Model Incorporating Wind Farm," *IEEE Syst. J.*, vol. 12, no. 1, pp. 392–401, Mar. 2018, doi: 10.1109/JSYST.2016.2563979.

[46] G. Lalor, A. Mullane, and M. O'Malley, "Frequency Control and Wind Turbine Technologies," *IEEE Trans. Power Syst.*, vol. 20, no. 4, pp. 1905–1913, Nov. 2005, doi: 10.1109/TPWRS.2005.857393.

[47] Y. Xu, C. Li, Z. Wang, N. Zhang, and B. Peng, "Load Frequency Control of a Novel Renewable Energy Integrated Micro-Grid Containing Pumped Hydropower Energy Storage," *IEEE Access*, vol. 6, pp. 29067–29077, 2018, doi: 10.1109/ACCESS.2018.2826015.

[48] J. W. Shim, G. Verbic, H. Kim, and K. Hur, "On Droop Control of Energy-Constrained Battery Energy Storage Systems for Grid Frequency Regulation," *IEEE Access*, vol. 7, pp. 166353–166364, 2019, doi: 10.1109/ACCESS.2019.2953479.

[49] K. Das, M. Altin, A. D. Hansen, and P. E. Sørensen, "Inertia Dependent Droop Based Frequency Containment Process," *Energies*, vol. 12, no. 9, p. 1648, Apr. 2019, doi: 10.3390/en12091648.

[50] S.-J. Ahn, J.-W. Park, I.-Y. Chung, S.-I. Moon, S.-H. Kang, and S.-R. Nam, "Power-Sharing Method of Multiple Distributed Generators Considering Control Modes and Configurations of a Microgrid," *IEEE Trans. Power Deliv.*, vol. 25, no. 3, pp. 2007–2016, Jul. 2010, doi: 10.1109/TPWRD.2010.2047736.

[51] "IEEE Guide for Design, Operation, and Integration of Distributed Resource Island Systems with Electric Power Systems," IEEE. doi: 10.1109/IEEESTD.2011.5960751.

[52] D. Mejía-Giraldo, G. Velásquez-Gomez, N. Muñoz-Galeano, J. Cano-Quintero, and S. Lemos-Cano, "A BESS Sizing Strategy for Primary Frequency Regulation Support of Solar Photovoltaic Plants," *Energies*, vol. 12, no. 2, p. 317, Jan. 2019, doi: 10.3390/en12020317.

[53] F. Arrigo, E. Bompard, M. Merlo, and F. Milano, "Assessment of primary frequency control through battery energy storage systems," *Int. J. Electr. Power Energy Syst.*, vol. 115, p. 105428, Feb. 2020, doi: 10.1016/j.ijepes.2019.105428.

[54] Mathukumalli Vidyasagar, *Nonlinear Systems Analysis*, Second edition. New York, NY: Prentice Hall.

[55] J.-J. E. Slotine and W. Li, *Applied nonlinear control*. Englewood Cliffs, N.J: Prentice Hall, 1991.

[56] Silver Navarro, Jr., "Hybrid Opportunities in SPUG Areas Using Homer." [Online]. Available: https://www.asiacleanenergyforum.org/wp-content/uploads/2016/03/Silver-Navarro-Hybrid-Opportunities-in-SPUG-Areas-using-HOMER-final.pdf

[57] G. S. Stavrakakis and G. N. Kariniotakis, "A general simulation algorithm for the accurate assessment of isolated diesel-wind turbines systems interaction. I. A general multimachine power system model," *IEEE Trans. Energy Convers.*, vol. 10, no. 3, pp. 577–583, Sep. 1995, doi: 10.1109/60.464885.

[58] K. E. Yeager and J. R. Willis, "Modeling of emergency diesel generators in an 800 megawatt nuclear power plant," *IEEE Trans. Energy Convers.*, vol. 8, no. 3, pp. 433–441, Sep. 1993, doi: 10.1109/60.257056.

[59] NEPLAN AG, "Turbine-Governor Models." NEPLAN AG.

[60] Woodward, "Speed Droop and Power Generation." Woodward, 1991.

[61] "Implement three-phase transmission line section with lumped parameters - Simulink."
https://www.mathworks.com/help/physmod/sps/powersys/ref/threephasepisecti online.html (accessed Mar. 25, 2021).

[62] A. Adrees, H. Andami, and J. V. Milanovic, "Comparison of dynamic models of battery energy storage for frequency regulation in power system," in *2016 18th Mediterranean Electrotechnical Conference (MELECON)*, Lemesos, Cyprus, Apr. 2016, pp. 1–6. doi: 10.1109/MELCON.2016.7495314.

[63] D. Pattabiraman, R. H. Lasseter., and T. M. Jahns, "Comparison of Grid Following and Grid Forming Control for a High Inverter Penetration Power System," in *2018 IEEE Power & Energy Society General Meeting (PESGM)*, Portland, OR, Aug. 2018, pp. 1–5. doi: 10.1109/PESGM.2018.8586162.

[64] Mathworks, "Simplified Model of a Small Scale Micro-Grid." [Online]. Available: https://www.mathworks.com/help/physmod/sps/ug/simplified-model-of-a-small-scale-micro-grid.html

[65] B. Mantar Gundogdu, S. Nejad, D. T. Gladwin, M. P. Foster, and D. A. Stone, "A Battery Energy Management Strategy for U.K. Enhanced Frequency Response and Triad Avoidance," *IEEE Trans. Ind. Electron.*, vol. 65, no. 12, pp. 9509–9517, Dec. 2018, doi: 10.1109/TIE.2018.2818642.

[66] R. Sebastián, "Application of a battery energy storage for frequency regulation and peak shaving in a wind diesel power system," *IET Gener. Transm. Distrib.*, vol. 10, no. 3, pp. 764–770, Feb. 2016, doi: 10.1049/iet-gtd.2015.0435.

[67] C. A. Hill, M. C. Such, D. Chen, J. Gonzalez, and W. M. K. Grady, "Battery energy storage for enabling integration of distributed solar power generation," *IEEE Trans. Smart Grid*, vol. 3, no. 2, pp. 850–857, 2012, doi: 10.1109/TSG.2012.2190113.

[68] Senjyu T., Kikunaga Y., Yona A., and Funabashi T., "Study on Optimum Capacity of Battery Energy Storage System for Wind Power Generator," *IEEJ Trans. Power Energy*, vol. 128, no. 1, pp. 321–327, 2008, doi: 10.1541/ieejpes.128.321.

[69] Liu, Wang, and Wang, "Research on Frequency Control of Islanded Microgrid with Multiple Distributed Power Sources," *Processes*, vol. 8, no. 2, p. 193, Feb. 2020, doi: 10.3390/pr8020193.

[70] "PVWatts Calculator." https://pvwatts.nrel.gov/ (accessed Feb. 17, 2021).

[71] I. Alsaidan, A. Khodaei, and W. Gao, "A Comprehensive Battery Energy Storage Optimal Sizing Model for Microgrid Applications," *IEEE Trans. Power Syst.*, vol. 33, no. 4, pp. 3968–3980, Jul. 2018, doi: 10.1109/TPWRS.2017.2769639.

[72] C. A. Hill, M. C. Such, D. Chen, J. Gonzalez, and W. M. Grady, "Battery Energy Storage for Enabling Integration of Distributed Solar Power Generation," *IEEE Trans. Smart Grid*, vol. 3, no. 2, pp. 850–857, Jun. 2012, doi: 10.1109/TSG.2012.2190113.

[73] D.-I. Stroe, V. Knap, M. Swierczynski, A.-I. Stroe, and R. Teodorescu, "Operation of a Grid-Connected Lithium-Ion Battery Energy Storage System for Primary Frequency Regulation: A Battery Lifetime Perspective," *IEEE Trans. Ind. Appl.*, vol. 53, no. 1, pp. 430–438, Jan. 2017, doi: 10.1109/TIA.2016.2616319.

[74] H. Jo, J. Choi, K. A. Agyeman, and S. Han, "Development of frequency control performance evaluation criteria of BESS for ancillary service: A case study of frequency regulation by KEPCO," in *2017 IEEE Innovative Smart Grid Technologies - Asia (ISGT-Asia)*, Auckland, Dec. 2017, pp. 1–5. doi: 10.1109/ISGT-Asia.2017.8378437.

[75] P. Mercier, R. Cherkaoui, and A. Oudalov, "Optimizing a Battery Energy Storage System for Frequency Control Application in an Isolated Power System," *IEEE Trans. Power Syst.*, vol. 24, no. 3, pp. 1469–1477, Aug. 2009, doi: 10.1109/TPWRS.2009.2022997.

[76] T. Kerdphol, Y. Qudaih, and Y. Mitani, "Battery energy storage system size optimization in microgrid using particle swarm optimization," in *IEEE PES Innovative Smart Grid Technologies, Europe*, Istanbul, Turkey, Oct. 2014, pp. 1–6. doi: 10.1109/ISGTEurope.2014.7028895.

[77] A. Toliyat and A. Kwasinski, "Energy storage sizing for effective primary and secondary control of low-inertia microgrids," in *2015 IEEE 6th International Symposium on Power Electronics for Distributed Generation Systems (PEDG)*, Aachen, Germany, Jun. 2015, pp. 1–7. doi: 10.1109/PEDG.2015.7223077.

[78] M. Stecca, L. Ramirez Elizondo, T. Batista Soeiro, P. Bauer, and P. Palensky, "A Comprehensive Review of the Integration of Battery Energy Storage Systems into Distribution Networks," *IEEE Open J. Ind. Electron. Soc.*, pp. 1–1, 2020, doi: 10.1109/OJIES.2020.2981832.

[79] X. Luo, J. Wang, M. Dooner, and J. Clarke, "Overview of current development in electrical energy storage technologies and the application potential in power

system operation," *Appl. Energy*, vol. 137, pp. 511–536, Jan. 2015, doi: 10.1016/j.apenergy.2014.09.081.

[80] H. Chen, T. N. Cong, W. Yang, C. Tan, Y. Li, and Y. Ding, "Progress in electrical energy storage system: A critical review," *Prog. Nat. Sci.*, vol. 19, no. 3, pp. 291–312, Mar. 2009, doi: 10.1016/j.pnsc.2008.07.014.

[81] S. X. Chen, H. B. Gooi, and M. Q. Wang, "Sizing of Energy Storage for Microgrids," *IEEE Trans. Smart Grid*, vol. 3, no. 1, pp. 142–151, Mar. 2012, doi: 10.1109/TSG.2011.2160745.

[82] S. Bahramirad, W. Reder, and A. Khodaei, "Reliability-Constrained Optimal Sizing of Energy Storage System in a Microgrid," *IEEE Trans. Smart Grid*, vol. 3, no. 4, pp. 2056–2062, Dec. 2012, doi: 10.1109/TSG.2012.2217991.

[83] R. E. MacDougall, J. D. Bertolino, K. L. Rodden, and E. T. Alger, "Lab testing of battery charge management systems for electric and hybrid electric vehicle battery packs to evaluate cycle life improvement," in *Fifteenth Annual Battery Conference on Applications and Advances (Cat. No.00TH8490)*, Long Beach, CA, USA, 1999, pp. 237–242. doi: 10.1109/BCAA.2000.838410.

[84] F. Vellucci, V. Sglavo, G. Pede, E. Pasca, V. Malvaldi, and S. Scalari, "Life cycles test on a lithium battery system," in *IECON 2014 - 40th Annual Conference of the IEEE Industrial Electronics Society*, Dallas, TX, USA, Oct. 2014, pp. 3129–3134. doi: 10.1109/IECON.2014.7048957.

[85] E. Karanasios, M. Ampatzis, P. H. Nguyen, W. L. Kling, and A. van Zwam, "A model for the estimation of the cost of use of Li-Ion batteries in residential storage applications integrated with PV panels," in *2014 49th International Universities Power Engineering Conference (UPEC)*, Cluj-Napoca, Romania, Sep. 2014, pp. 1–6. doi: 10.1109/UPEC.2014.6934739.

[86] T. M. Masaud and E. F. El-Saadany, "Correlating Optimal Size, Cycle Life Estimation, and Technology Selection of Batteries: A Two-Stage Approach for Microgrid Applications," *IEEE Trans. Sustain. Energy*, vol. 11, no. 3, pp. 1257–1267, Jul. 2020, doi: 10.1109/TSTE.2019.2921804.

[87] L. H. Thaller, "Expected Cycle Life vs. Depth of Discharge Relationships of Well-Behaved Single Cells and Cell Strings," *J. Electrochem. Soc.*, vol. 130, no. 5, pp. 986–990, May 1983, doi: 10.1149/1.2119928.

[88] A. Bocca, A. Sassone, D. Shin, A. Macii, E. Macii, and M. Poncino, "An equation-based battery cycle life model for various battery chemistries," in *2015 IFIP/IEEE International Conference on Very Large Scale Integration*

(VLSI-SoC), Daejeon, South Korea, Oct. 2015, pp. 57–62. doi: 10.1109/VLSI-SoC.2015.7314392.

[89] R. H. Byrne, S. Hamilton, D. R. Borneo, T. Olinsky-Paul, and I. Gyuk, "The value proposition for energy storage at the sterling municipal light department," in *2017 IEEE Power & Energy Society General Meeting*, Chicago, IL, Jul. 2017, pp. 1–5. doi: 10.1109/PESGM.2017.8274631.

[90] R. H. Byrne and C. A. Silva-Monroy, "Potential revenue from electrical energy storage in the Electricity Reliability Council of Texas (ERCOT)," in *2014 IEEE PES General Meeting | Conference & Exposition*, National Harbor, MD, USA, Jul. 2014, pp. 1–5. doi: 10.1109/PESGM.2014.6939886.

[91] R. H. Byrne, R. J. Concepcion, and C. A. Silva-Monroy, "Estimating potential revenue from electrical energy storage in PJM," in *2016 IEEE Power and Energy Society General Meeting (PESGM)*, Boston, MA, USA, Jul. 2016, pp. 1–5. doi: 10.1109/PESGM.2016.7741915.

[92] S. de la Torre, A. J. Conejo, and J. Contreras, "Transmission Expansion Planning in Electricity Markets," *IEEE Trans. Power Syst.*, vol. 23, no. 1, pp. 238–248, Feb. 2008, doi: 10.1109/TPWRS.2007.913717.

[93] H. Haghighat and B. Zeng, "Bilevel Mixed Integer Transmission Expansion Planning," *IEEE Trans. Power Syst.*, vol. 33, no. 6, pp. 7309–7312, Nov. 2018, doi: 10.1109/TPWRS.2018.2865189.

[94] G. Munoz-Delgado, J. Contreras, and J. M. Arroyo, "Joint Expansion Planning of Distributed Generation and Distribution Networks," *IEEE Trans. Power Syst.*, vol. 30, no. 5, pp. 2579–2590, Sep. 2015, doi: 10.1109/TPWRS.2014.2364960.

[95] A. Soroudi, *Power system optimization modeling in gams*. New York, NY: Springer Science+Business Media, 2017.

[96] "Mixed-Integer Programming (MIP) - A Primer on the Basics - Gurobi." https://www.gurobi.com/resource/mip-basics/ (accessed Mar. 23, 2021).

[97] "Diesel Generator Fuel Consumption Formula | Diesel Generator Fuel Calculator." https://krugerpower.com.au/generator-fuel-calculator (accessed Feb. 24, 2021).

[98] "Approximate Diesel Generator Fuel Consumption Chart." https://www.generatorsource.com/Diesel_Fuel_Consumption.aspx (accessed Mar. 23, 2021).

[99] "Diesel genset fuel consumption calculator – Mechatronics." https://mechatronics.by/en/service/utilities/diesel-genset-fuel-consumption/ (accessed Mar. 23, 2021).

[100] "Power Calculator: kVA to kW, kW to kVA, Diesel Fuel Consumption by kW." https://www.globalpwr.com/power-calculator/ (accessed Mar. 23, 2021).

[101] "Diesel prices around the world, 22-Feb-2021 | GlobalPetrolPrices.com." https://www.globalpetrolprices.com/diesel_prices/ (accessed Feb. 24, 2021).

[102] Asian Development Bank, "Guidebook for Deploying Distributed Renewable Energy Systems:: A Case Study on the Cobrador Hybrid Solar PV Mini-Grid," Asian Development Bank, Manila, Philippines, Aug. 2019. doi: 10.22617/TIM190342-2.

[103] "Performance Series Battery Specifications | ODYSSEY® Battery." https://www.odysseybattery.com/performance-series-battery-specifications/ (accessed Feb. 22, 2021).

[104] "Our Products - C&D Technologies, Inc." https://cdtechno.com/our-products/ (accessed Feb. 22, 2021).

[105] "Batteries." https://www.alphaindustrialpower.com/products/industrial-power-equipment/batteries (accessed Feb. 22, 2021).

[106] N. Lu, M. R. Weimar, Y. V. Makarov, and C. Loutan, "An evaluation of the NaS battery storage potential for providing regulation service in California," in *2011 IEEE/PES Power Systems Conference and Exposition*, Phoenix, AZ, USA, Mar. 2011, pp. 1–9. doi: 10.1109/PSCE.2011.5772494.

[107] "IEEE Guide for Design, Operation, and Integration of Distributed Resource Island Systems with Electric Power Systems," IEEE. doi: 10.1109/IEEESTD.2011.5960751.

Research Achievements

Research achievements during the doctoral degree course at Shibaura Institute of Technology, as of September 2021.

Journal Articles

[P.1] S. Sitompul, G. Fujita, "Impact of Advanced Load-Frequency Control on Optimal Size of Battery Energy Storage in Islanded Microgrid System," *Energies,* vol. 14, no.8, pp 2213, April 2021.

[P.2] S. Sitompul, Y. Hanawa, V. Bupphaves, and G. Fujita, "State of Charge Control Integrated with Load Frequency Control for BESS in Islanded Microgrid," *Energies*, vol. 13, no. 18, pp 4657, Sep. 2020**.**

International Conference Proceedings

[P.1] S. Sitompul, G. Fujita, "Impact of State-of-Charge Control Integrated with Load-Frequency Control on Battery Energy Storage System in Islanded Microgrid System," *Energy Conversion Congress and Exposition – Asia (ECCE Asia) 2021*, Singapore, May 2021.

[P.2] S. Sitompul, G. Fujita, "Implementation of Shifted-Droop Method as State-of-Charge Control on Battery Energy Storage System Load-Frequency Control," *15th South East Asian Technical University Consortium (SEATUC)*, Bandung, Indonesia, February 2021.

[P.3] S. Sitompul, G. Fujita, "Implementation of BESS Load-Frequency Control in Islanded Microgrid by Considering State-of-Charge," *IEEE PES Innovative Smart Grid Technology (ISGT) Europe,* The Haag, Netherlands, 2020.

[P.4] S. Sitompul, G. Fujita, "Sizing of Battery Energy Storage System in Islanded Microgrid by Considering a Short-term operation," *14th South East Asian Technical University Consortium (SEATUC),* Bangkok, Thailand, February 2020.

[P.5] S. Sitompul, G. Fujita, "Reducing Self-discharge Rates Effects of Flywheel Energy Storage System in Power System Application," *13th South East Asian Technical University Consortium (SEATUC),* Hanoi, Vietnam, February 2019.